Slow Motions in the Tropical Troposphere

By
John R. Anderson

Department of Atmospheric Science
Colorado State University
Fort Collins, Colorado

Colorado State University

Department of Atmospheric Science

Paper No. 381

SLOW MOTIONS IN THE TROPICAL TROPOSPHERE

by

John R. Anderson

Department of Atmospheric Science

Colorado State University

Fort Collins, Colorado 80523

July 1984

Atmospheric Science Paper No. 381

ABSTRACT OF THESIS

SLOW MOTIONS IN THE TROPICAL TROPOSPHERE

Quasi periodic variations with periods of 40-50 days have been observed in several tropical meteorological parameters. In this work we examine possible mechanisms for the oscillation time scale. An observational study of the seasonal variation of the observed oscillation period is presented which indicates that it is unlikely that a Doppler shifted traveling wave mechanism is responsible for the 40-50 day period. A new possible mechanism is proposed where the time scale results from the advection of perturbation quantities by a "Hadley" cell basic state circulation. The results of a forced calculation with this basic state indicate the possibility that the slow motions couple to the cumulus convection through a modulation of the basic state static stability. A non-zonally symmetric forced calculation produces wind fields in good agreement with observations.

John R. Anderson
Atmospheric Science Department
Colorado State University
Fort Collins, Colorado 80523
Summer 1984

ACKNOWLEDGEMENTS

I would like to thank my advisor, Prof. Duane Stevens for his guidance and encouragement throughout this work . I would also like to thank my committee members, Prof. W. Gray, Dr. P. Julian, Prof. W. Schubert, and Prof. J. Thomas for their helpful advice and Dr. R. Madden for several useful conversations. I appreciate the assistance of Judy Sorbie for preparing the figures and Machel Sandfort for typing the manuscript. Finally, I would like to thank my family, Sharon Gould-Stewart and Jesse Rosenstock, for their encouragement and assistance. Support for this work was provided by the National Science Foundation under grant ATM-8305759 and National Aeronautics and Space Administration under grant NAG 5-136. Computing support was provided by the National Center for Atmospheric Research.

TABLE OF CONTENTS

1. INTRODUCTION

The presence of quasi-periodic fluctuations in the tropical troposphere with periods ranging from 40-50 days were first reported by Madden and Julian (1971). Since then, observations of these variations have been reported in a large number of observed tropical meteorological parameters including winds, surface pressure and observed convective cloud cover. Recent diagnostic studies have also reported evidence for a mid-latitude component of the phenomenon. The existence of the mid-latitude component provides new incentive for studying the oscillation because of its possible role in understanding tropical-midlatitude interations on these and longer time scales.

In spite of the rather lengthy observational history of the 40-50 day oscillation there have been relatively few dynamical explanations proposed for the time scale of the motion. The source of the oscillation period remains a topic of considerable interest and uncertainty.

In the first report of the oscillation Madden and Julian (1971) detected the presence of a relatively narrow-band signal with periods of 40-50 days in 850 mb level zonal wind, 150 mb level zonal wind and surface pressure observations which were taken at Canton Island in the West Pacific. The 850 mb winds were observed to be essentially out of phase with the winds at 150 mb. An interesting aspect of the Madden and Julian report is that there was no detectable signal in the 850 mb mixing ratio field at Canton Island which suggests that the oscillation

was not locally forced by variations in the water vapor content, although it is possible that the oscillation could be forced further west in the Indonesian region. This would seem to argue against a mechanism forced from the surface by effects such as variations in sea surface temperature.

Madden and Julian (1972) reported the results of a study designed to determine the spatial structure of the 40-50 day oscillation. In this study they computed the surface pressure cross-spectra of Canton Island with the other available tropical stations. Their results, which are summarized in Fig. 1-1, indicate that the surface pressure effects of the phenomena involve most of the tropics with the possible exception of the Atlantic region. The surface pressure phase analysis shows a strong tendency for the disturbance to propagate away from the equator towards both poles and eastward phase propagation in the Indonesia/Borneo "maritime continent" region. The longitudinal variation of the oscillation is consistent with that of a motion having both zonally symmetric (wavenumber 0) and zonal wavenumber 1 components. Based on the evidence of the observed winds and 700 mb mixing ratio values Madden and Julian proposed an observational description of the phenomenon which consisted of a modulated, eastward traveling convective disturbance in the Indonesia/western Pacific areas. Although they did not detect any extratropical evidence for the oscillation they noted that since the average tropical surface pressure varied with the oscillation phase that the net change in the mass of the tropical atmosphere must be reflected in other regions.

A study similar to the work by Madden and Julian was performed by Parker (1973). Parker, who was apparently unaware of the Madden and

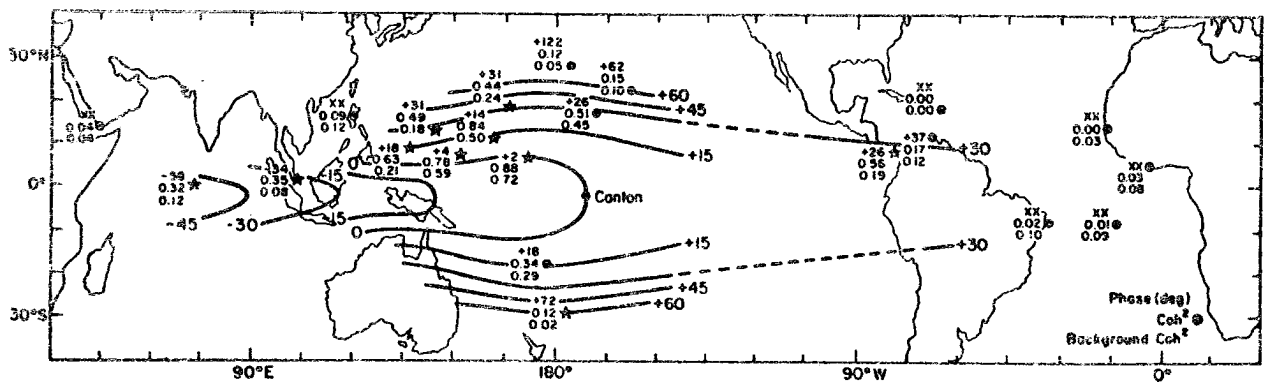

Fig. 1-1. Mean phase angles, coherence-squares, and background coherence-squares for approximately the 36-50 day period range of cross spectra between all stations and Canton. The plotting model is given in lower right-hand corner. Positive phase angles at a station means the Canton series leads that of the station. Stations indicated by a star have coherence-squares above the background at the 95% level. Mean coherence-squares at Shemya (52°43'N, 174°6'E) and Campbell I (52°33'S, 169°9'E) (not shown) are 0.08 and 0.02, respectively. Both are below their average background coherence-squares (from Madden and Julian, 1972).

Julian work, studied the 100 mb winds in an equatorial band from 10°S to 10°N. A longitude-height cross section of Parker's results is given in Fig. 1-2. This figure shows the basic character of the motion to be a mostly standing wave-like pattern with a very sharp phase transition in the region from 120°E to the dateline. Parker proposed an explanation for the motion in terms of an equatorial Kelvin wave. A major difficulty with this explanation, as noted by Chang (1977), is that the observed slow meridional propagation of the motion, particulary in the region of the steep phase transition, is inconsistent with the observed large vertical wavelength of the motion when examined using the Kelvin wave dispersion relation.

Chang (1977) attempted to resolve the problem of the apparent disagreement with the Kelvin wave dispersion relation by including the effects of cumulus cloud momentum transport and radiative thermal damping. One difficulty with this explanation which was pointed out by Stevens and White (1979) is that the result is very dependent on the values chosen for the damping coefficients. In particular the inclusion of strong Newtonian cooling, which is necessary to slow the Kelvin modes, is questionable in the tropical troposphere. Another concern for any explanation involving a Doppler-shifted traveling wave is that the mean zonal wind changes with season so that one would expect the frequency of the oscillation to also change with season. The observations of the oscillation periods as reported by Parker (1973) and Anderson and Rosen (1983) do not appear to show this effect. This topic will be discussed in some detail in Chapter 5 where a new analysis of the oscillation seasonality based on a 25 year data set will be presented.

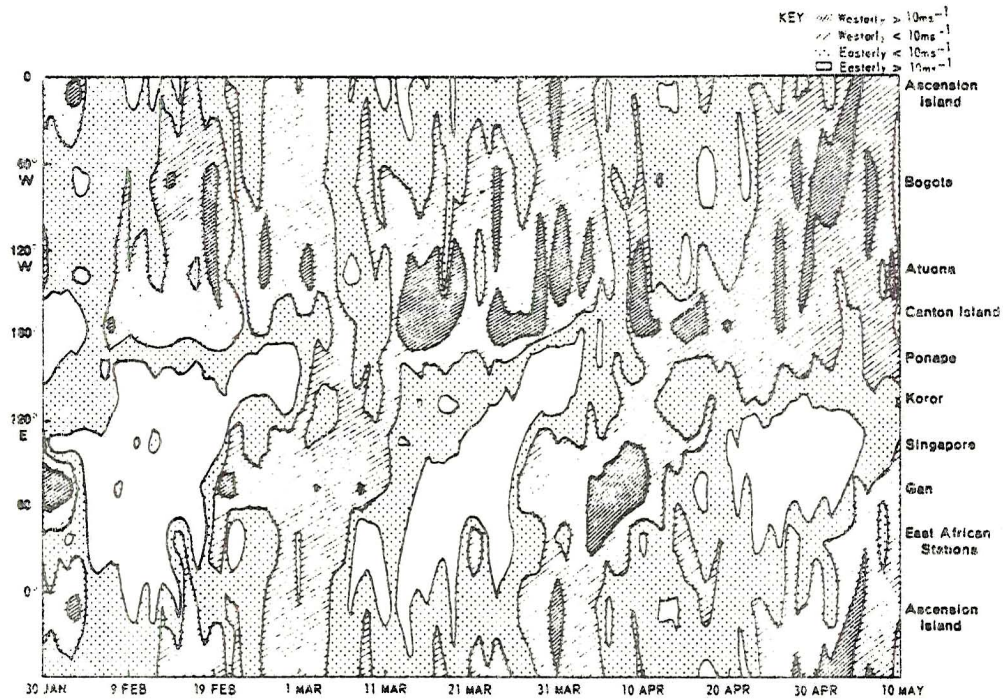

Fig. 1-2. Longitude-time cross section of 100 mb equatorial zonal winds (from Parker, 1973).

Yasanari (1980) and Julian and Madden (1981) have studied variations in tropical cloud cover and have confirmed the Madden and Julian hypothesis that the eastward propagating surface lows are associated with enhanced cumulus convection.

Langley et al. (1981) studied the relationship between the total atmospheric relative angular momentum and the rotation rate of the Earth. These quantities are related by the requirement that the total angular momentum of the earth-atmosphere system be conserved when solar and lunar tidal effects are accounted for. Langley et al. found that there were coherent quasi-periodic fluctuations in both quantities with periods in the 40-50 day range. Anderson and Rosen (1983) showed that these variations were due to the zonally symmetric component of the tropical motions. Their results, which are depicted in Fig. 1-3, show a spatial structure which has its maximum amplitude in equatorially symmetric maxima located at approximately 20°N and 20°S. The zonally symmetric motions propagate poleward and downward in phase from a phase center located in the equatorial upper troposphere. The observations of Anderson and Rosen also indicated the presence of a northern hemisphere mid-latitude component to the oscillation. This component, which also appears in a non-symmetric analysis by Weickmann (1983) is probably the response of the mid-latitude climate to changes in the tropical forcing.

The observations of a zonally symmetric oscillation raise the possibility that the basic source of the 40-50 day period may result from the symmetric rather than the wavenumber 1 component. This hypothesis was offered support by Goswami and Shukla (1984) who report the results

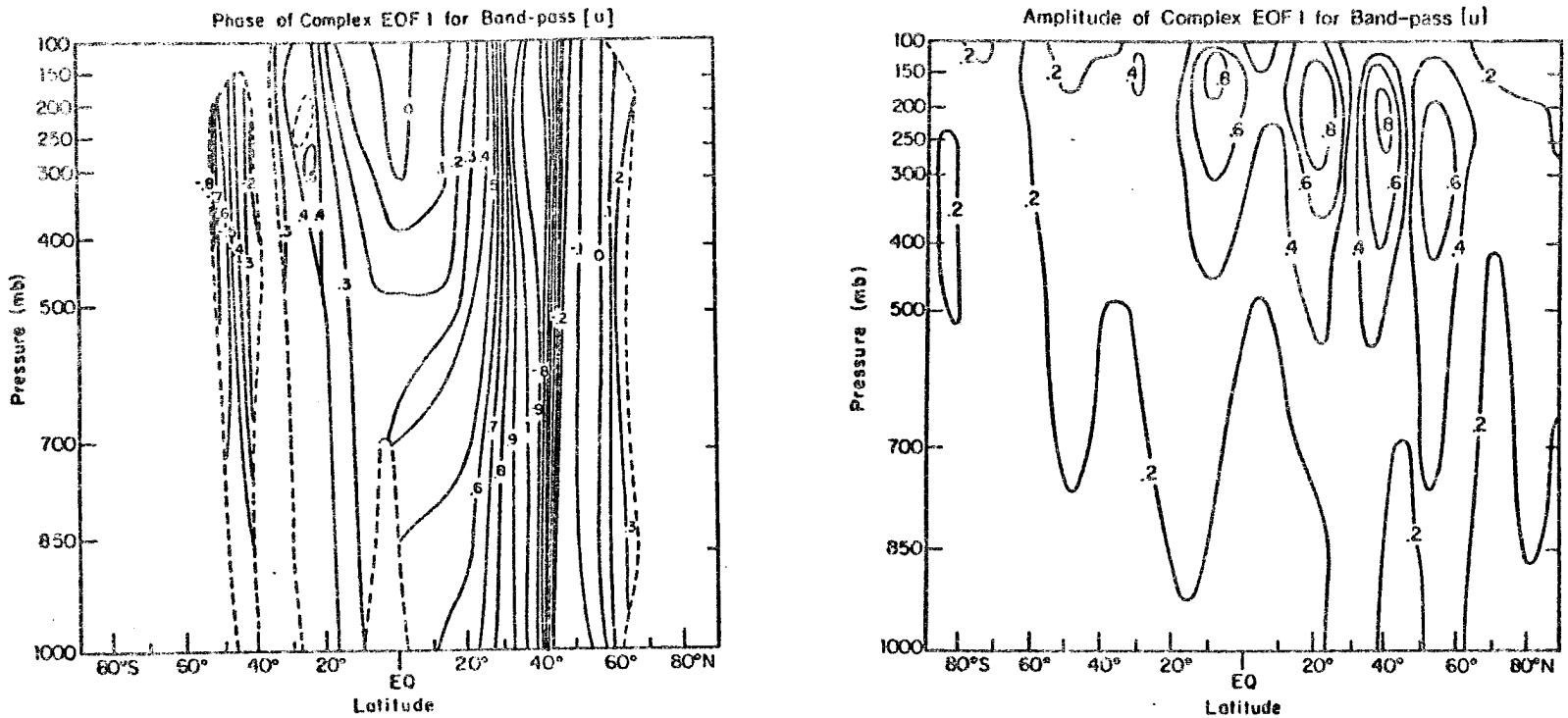

Fig. 1-3. Phase-amplitude analysis of the observed oscillation latitude-height structure (from Anderson and Rosen, 1983). Phase convention is from -1 to 1 with propagation direction from smaller to larger.

of a study using a zonally symmetric version of the GLAS general circulation model. They noted a tendency for the model circulation to oscillate with periods on the order of a month, however, the oscillations occurred in their model only when an explicit water budget and cumulus heating parameterization were included.

One of the critical questions in the explanation of the oscillation now appears to be the relationship between and the relative roles of the wavenumber 0 and non-symmetric motions in the oscillation. In a very recent paper, Yamagata and Hayashi (1984) report the results of using a simplified shallow water model, similar to the one developed by Gill (1980), to examine the effects of locally forcing an equatorial atmosphere with a heat source which has a 40 day periodicity. The results of this study show that the principal features of the observed non-symmetric components of the oscillation can be explained as a response to local forcing in the maritime continent region. Their analysis did not indicate any source for the time scale of the motion.

In this work the possibility that the time scale for the motion comes from symmetric processes is further examined. In particular, various calculations are made to determine the effects of a basic state consisting of a simple "Hadley" type circulation on the large scale tropical motions. It will be shown in Chapter 3 that the inclusion of these effects results in the formation of a new time scale for the dynamics which arises from the advection of perturbation quantities by the Hadley cell mass circulation. The existence of this time scale results in a new class of slowly oscillating linear normal modes, some of which have many similarities with the observed oscillation. The forced symmetric and non-symmetric response of the atmosphere are

discussed in Chapter 4 where the resting basic state shallow water analysis of Yamagata and Hayashi is extended to include the effects of a more realistic basic state. This study will be used to examine the possibility that the non-symmetric motion may result from the modulation of the strong western Pacific convection by the symmetric mode.

The results of the dynamical calculations are then compared with the available observational data to determine the plausibility for this explanation of the oscillation. In particular, comparison will be made with the symmetric study of Anderson and Rosen (1983) and the recent three dimensional study of the FGGE Summer MONEX by Murakami et al. (1983).

It is not the goal of this work to provide a comprehensive explanation for the origin of the tropical 40-50 day oscillation. Instead this report presents the results of several modeling and observational efforts which are each intended to shed some light on dynamical processes which may be involved in the phenomenon. It is hoped that this work will contribute to the eventual development of an explanation which can be considered a general description of the observed motions.

2. MODEL FORMULATION AND DERIVATION OF THE BASIC STATE

One of the goals of this work is to make an assessment of the effects of various dynamical processes on tropical motions with periods in the 40-50 day range. In order to be able to perform this assessment we must develop a complete system of equations for the tropical atmosphere within which the various problems can be posed.

The choice of an equation system is an important one as we are trying to develop as simple a framework as possible while retaining the physical processes which are important to provide a description of the various phenomena which is at least qualitatively correct. Since we are dealing with very slow motions our first simplifications will be to eliminate vertically propagating sound waves by making the hydrostatic and analastic (quasi-Bousinesq) approximations. This involves taking the total time derivatives of the vertical motion to be small and we will take the density of the atmosphere to be a time-independent function of height except where multiplied by gravity.

Since the hydrostatic primitive equation system has prognostic equations for three state variables - the westerly wind (u), the easterly wind (v), and a mass field variable (either potential temperature and surface pressure or geopotential) - the model has three eigenmodes for each spatial degree of freedom of the model. These three eigenmodes correspond to two inertia-gravity modes and one Rossby wave mode. For the zonally symmetric case with a resting basic state,

the Rossby modes become a degenerate set of motions in thermal wind balance with exactly zero frequency. Since the observed slow motions tend to have u-wind fields in near geostrophic balance, it would be desirable if the inertia-gravity modes could be eliminated with the use of a filtered system of equations. Such a simplification of the model to one eigenmode per degree of freedom would be quite desirable from a computational point of view since it would reduce the number of model state variables by a factor of three and would reduce the complexity of the linear matrix problems by a factor of 27. The principle difficulty of this approach is that many filtered systems seriously distort the wave modes. For example, the quasi-geostrophic (linear balance) system eliminates the Kelvin wave solutions. Solution of more accurate filtered systems generally involves the solution of one or more elliptic diagnostic equations for each time step during an integration which can be numerically quite complex. For these reasons we have chosen to stay with the primitive equation set although at some point in the future we plan to consider a possible generalization of the "long wave" approximation (Gill, 1980) to a fully stratified system.

In the interest of computational efficiency we have chosen to utilize the equatorial β-plane geometry proposed by Matsuno (1966) to take advantage of the fact that the eigenfunctions of the Laplacian operator in this geometry are sinusoids. This makes it possible to perform extremely efficient prognostic integrations using semi-implicit time differencing and fast Fourier transform (FFT) techniques.

In addition to the traditional primitive equations it is necessary to introduce parameterizations for the effects of cumulus convection on the model. We have taken the linearized representation of cumulus

momentum transport proposed by Schneider and Lindzen (1976), and we take the cloud induced heating field to be specified in the calculation of the basic state and parameterized using the simple scheme proposed by Stevens and Lindzen (1978) for the linear perturbation problem.

Starting with the primitive equations, using physical height as the vertical coordinate, and making the above assumptions we obtain the system of equations (2.1a) - (2.1e).

$$u_t = -(uu_x + vu_y + wu_z) + \beta yv - \frac{1}{\tilde{\rho}} p_x - \alpha(y,z)u + \mu u_{zz} + F_{cx} \qquad (2.1a)$$

$$v_t = -(uv_x + vv_y + wv_z) - \beta yu - \frac{1}{\tilde{\rho}} p_y - \alpha(y,z)v + \mu v_{zz} + F_{cy} \qquad (2.1b)$$

$$\theta_t = -(u\theta_x + v\theta_y + w(\tilde{\theta+\theta})_z) + Q - \gamma(y,z)\theta + \mu\theta_{zz} \qquad (2.1c)$$

$$-\frac{1}{\tilde{\rho}} (\tilde{\rho}w)_z = u_x + v_y \qquad (2.1d)$$

$$\left(\frac{p}{\rho}\right)_z = \frac{g}{\theta} \theta \qquad (2.1e)$$

where $\tilde{\rho}$, $\tilde{\theta}$, and $\tilde{p}$ represent a hydrostatically balanced mean height-dependent stratification and θ and p are the departures from this stratification. The symbols have the usual meaning and are defined in appendix I. In the derivation of the hydrostatic equation (2.1) the term

$$\frac{p'}{\tilde{p}} \quad g\left(H \frac{d\ell n\tilde{p}}{dz} - \frac{c_v}{c_p}\right)$$

has been ignored following Silva Dias (1979). This approximation is necessary to produce the correct equivalent depth for the model external mode when the system is linearized. The Rayleigh friction and

Newtonian cooling parameters $\alpha(y,z)$ and $\gamma(y,z)$ are included for the purpose of imposing the model boundary conditions and representing surface friction, mid-latitude cyclones and radiative cooling. Since cumulus momentum transport terms are included as F_{cx} and F_{cy}, these coefficients are small in the model interior.

The parameterization for cumulus momentum transport is taken from Stevens et al. (1977) and is given in Eqs. (2.2a) and (2.2b).

$$F_{cx} = \frac{1}{\tilde{\rho}} \left(M_c(u - u_c)\right)_z \tag{2.2a}$$

$$F_{cy} = \frac{1}{\tilde{\rho}} \left(M_c\ (v - v_c)\right)_z \quad , \tag{2.2b}$$

where M_c, the cloud mass transport, is given by

$$M_c(y,z) = M_c(y) \begin{cases} 1-\exp\left(\frac{p_t-\tilde{p}}{p_{dtr}}\right) & p_T \le \tilde{p} \le p_c \\ 0 & \text{otherwise} \end{cases} .$$

The cloud momentum variables u_c, v_c are taken to be independent of height and equal to u and v at the height where $\tilde{p}=p_c$ thus eliminating the apparent discontinity in the vertical flux derivatives. p_{dtr} represents the detrainment height scale of the clouds.

The formulation of the Rayleigh friction term $\alpha(y,z)$, includes terms for surface friction, mid-latitude cyclonic eddies, and a boundary sponge. The Newtonian cooling term represents the large radiative cooling effects in the stratosphere and helps absorb energy at the top of the model.

$$\alpha(y,z) = \alpha_{sp} + \alpha_{ce} + \alpha_{sp} \tag{2.2c}$$

$$\alpha_{sp} = 1/1.5 \cdot \mathrm{Exp}[-(z/1.275\ (\mathrm{km})^2] \qquad (1/\mathrm{days})$$

$$\alpha_{ce} = \begin{cases} 1/7 \cdot (\mathrm{lat} - 30°)/10° & \mathrm{lat} > 30° \\ & 30° > \mathrm{lat} > 20° \\ 0 & \mathrm{lat} < 20° \end{cases} \qquad (1/\mathrm{days})$$

$$\alpha_{sp} = \begin{cases} 1/2\ (\mathrm{lat} - 35°)/8° & \mathrm{lat} > 35° \\ 1/50 & \mathrm{lat} < 35° \end{cases} \qquad (1/\mathrm{days})$$

$$\gamma(z) = 1/2.3 \cdot \mathrm{Exp}[-((z_{top} - z)10.85(\mathrm{km}))^2] \qquad (1/\mathrm{days}) \quad (2.2d)$$

The diabatic heating term, Q, represents the effects of radiative processes and latent heat release. For the nonlinear basic state calculation we will take these effects to be specified. For the case of the linear perturbation calculation we will often ignore both of these effects, however we will study the sensitivity of the results to latent heat release by using the simple moisture convergence scheme proposed by Stevens and Lindzen (1976).

The system of equations given by (2.1) and (2.2) are a non-linear partial differential system; and, as such, it is extremely difficult to make analytic progress for any but the most simplified problems. Since the problem which we are addressing here does not appear to by analytically tractable, we will now discretize the system in the spatial coordinates to produce a system of ordinary differential equations in time. At this point it is necessary to consider the representation of the problem in somewhat more detail. One feature of the tropical 40-50 day oscillation is that it can be considered a relatively small perturbation when compared to such variations as the mean seasonal cycle. This would suggest that a linear model can probably yield at least a qualitative description of the dynamics. On the other hand with the

slow time scale of the oscillation one must be very cautious of the basic state which is used for the linear problem. For example, one effect which is significant for our problem is the advection of perturbation quantities by the basic state Hadley cell mass circulation. This can be seen if we take a typical observationally determined length scale of 10 degrees of latitude ($1.1 \cdot 10^6$ m) and a typical mean meridional velocity of 1 m/s. This yields an advective time scale of $1.1 \cdot 10^6$ s or ~13 days which is of the same order as the oscillatory scale of 45 days/2π = ~7 days. A similar analysis shows the vertical advection time scale to also be important and indicates the need to include the full effects of the Hadley cell mass circulation within the linearized model.

Now that we have decided to include a complete Hadley cell as the model basic state, the next problem is to determine what this circulation should be. The first requirement that we shall impose is that the basic state be zonally symmetric. This constraint allows the separation of the perturbation model into independent systems for each zonal wavenumber. While this restriction is one of the largest potential sources of quantitative error in our model, we have chosen to make it because of the vast simplification which it provides while still including the effects of the Hadley mass circulation in a zeroth order way.

One way of defining the zonally symmetric basic state is to use observed data. Another approach, which is taken here, is to find steady state solutions to the non-linear equations with a specified thermodynamic forcing. This approach has the formal advantage of producing a basic state which is a solution of the governing equations.

Thus our first step in producing a model will be the description of (2.1) and (2.2) in the zonally symmetric form where $\partial/\partial x = 0$.

The model is discretized by using a second order finite difference formulation in the vertical and a Fourier spectral representation in the meridional direction. The non-linear terms are calculated using the Fourier transform technique described by Machenhaur and Rasmussen (1972) and Orzag (1970). Since the natural boundary conditions for the Fourier basis functions are periodic, it is necessary to include a Rayleigh friction absorbing layer at the poleward boundaries to prevent the interaction of model motions across the boundaries. The vertical differencing scheme is shown schematically in Fig. 2-1 and employs a staggered variable spacing with the potential temperature being kept on full vertical levels and the u and v component winds represented on half levels. The model upper boundary condition is that the flow above the top level is non-divergent so that the surface pressure tendency can be computed by a vertical integration of the continuity equation from a w=0 lower boundary condition. Although this upper boundary condition allows local mass flux out of the domain, the total model mass is conserved due to the periodic horizontal boundary conditions. An important property of this scheme is that there are the same number of mass field variables (N_z-1 potential temperature, 1 surface pressure) as wind field variables (N_z), so that none of the linear vertical eigenmodes have zero eigenvalues (equivalent depths).

A plot of the reference stratification $\tilde{\theta}$ is shown in Fig. 2-2. The eigenvalues of the model linear vertical modes for N_z=20, Δz=850 m, are shown in Table 2.1. Plots of the vertical wind vertical structure functions for the five lowest order modes are shown in Fig. 2-3. The

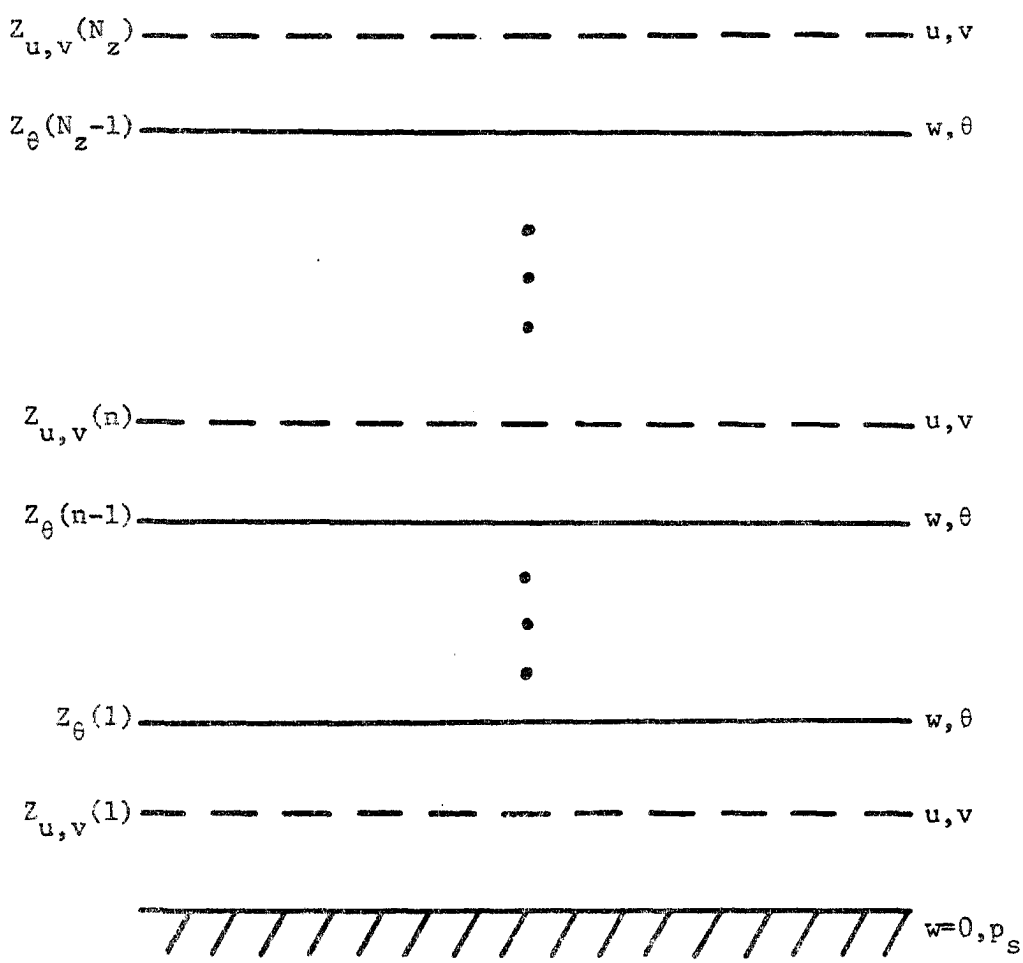

Fig. 2-1. Schematic representation of model vertical finite difference scheme.

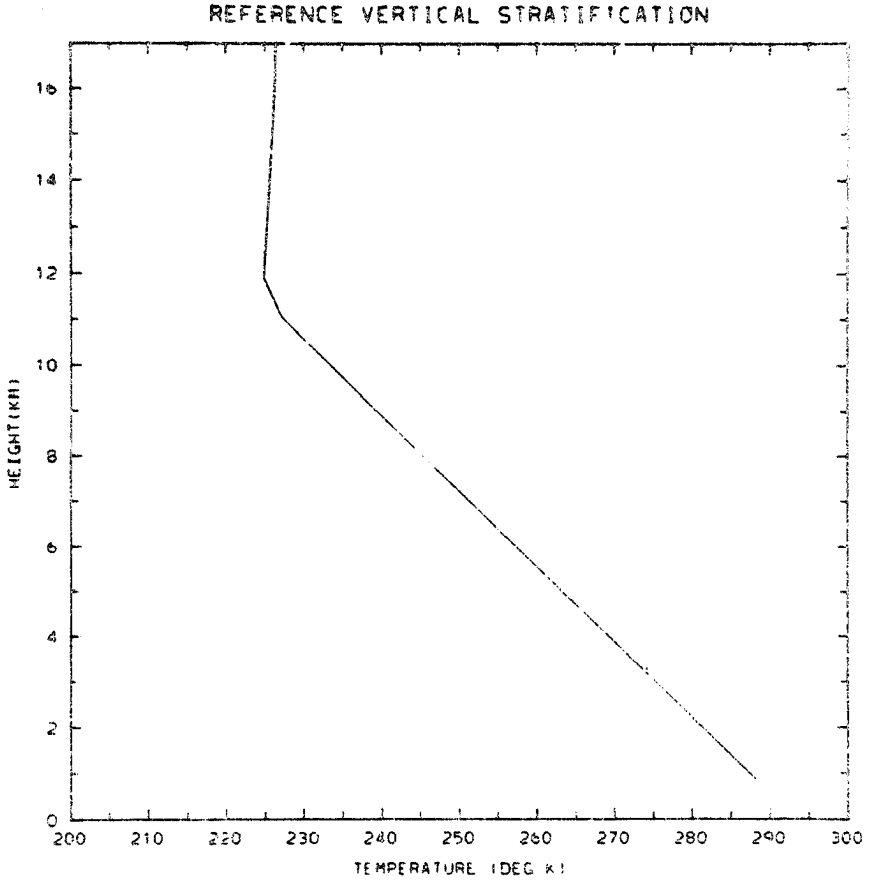

Fig. 2-2. Reference vertical stratification.

Table 2.1. Model vertical eigenmodes.

n	C(m/s)	n	C(m/s)
1	263.4	11	9.3
2	79.7	12	8.9
3	39.2	13	8.2
4	26.7	14	7.3
5	20.4	15	6.5
6	16.5	16	6.0
7	14.0	17	5.7
8	12.2	18	5.4
9	10.9	19	5.2
10	10.0	20	5.0

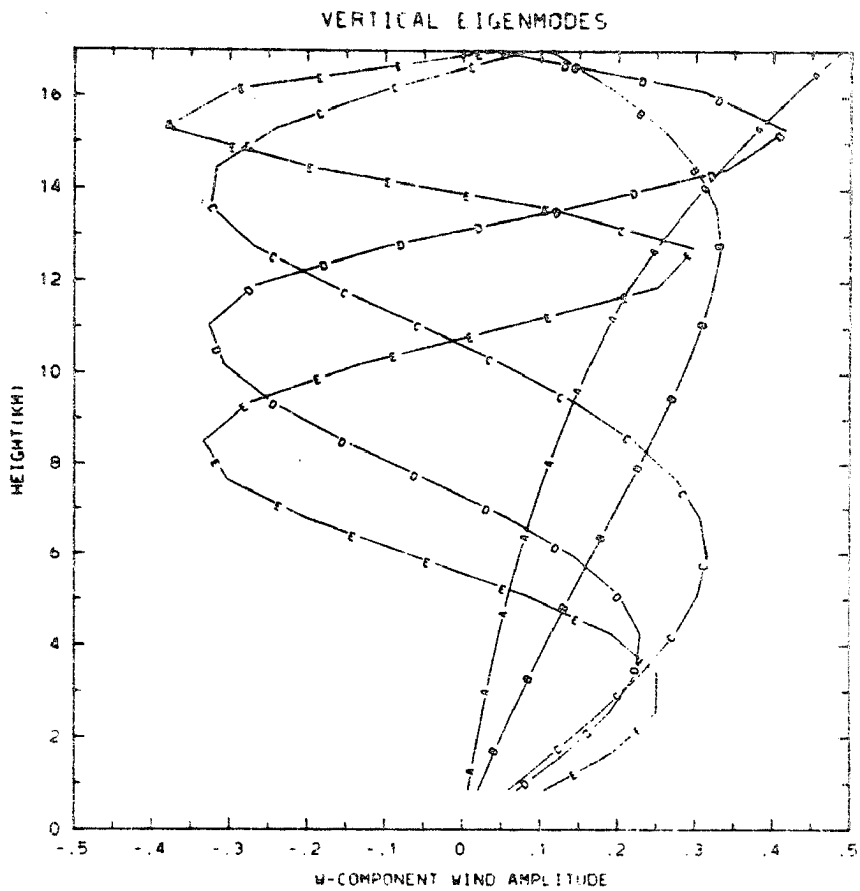

Fig. 2-3. Five lowest order vertical normal modes of model vertical differencing.

vertical modes appear to be typical for a model of this type with an accurate representation of the external mode and reasonable model internal modes.

As a check on the accuracy of the use of the Fourier horizontal representation we have reproduced the forced tropical problem originally solved by Gill (1980) using the model horizontal basis functions truncated at meridional wavenumber 20 and zonal wavenumber 10 to discretize the shallow water set. The Gill solution was constructed using an analytical solution for an approximate set of shallow water equations. The two solutions are presented in Fig. 2-4 and show essentially identical results, indicating the suitability of our model horizontal structure for tropical problems.

Once the spatial structure of the model has been set it is now necessary to deal with the temporal evolution of the model. The basic model resolution of 20 complex meridional wavenumbers and 20 vertical levels corresponds to 2400 total real degrees of freedom. This very large model order essentially precludes the use of techniques such as linear matrix eigensolvers. The solution adopted here is to use a prognostic model formulation for the full resolution model and use a more severely truncated model when direct linear solution techniques are required.

The time differencing is accomplished in spectral space by using a trapezoidal semi-implicit formulation for the gravity wave terms, a leap-frog scheme for the non-constant coefficient terms and a forward Euler scheme for the dissipation terms. In this form the model prognostic system is given by (2.3).

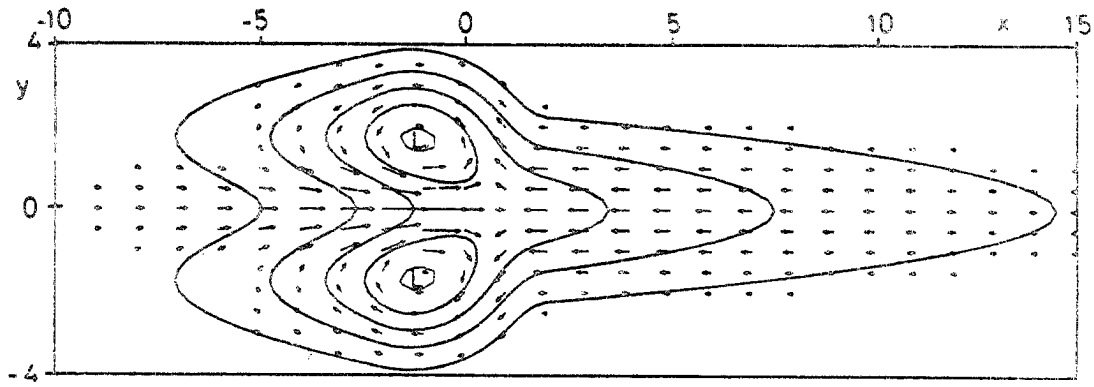

(a)

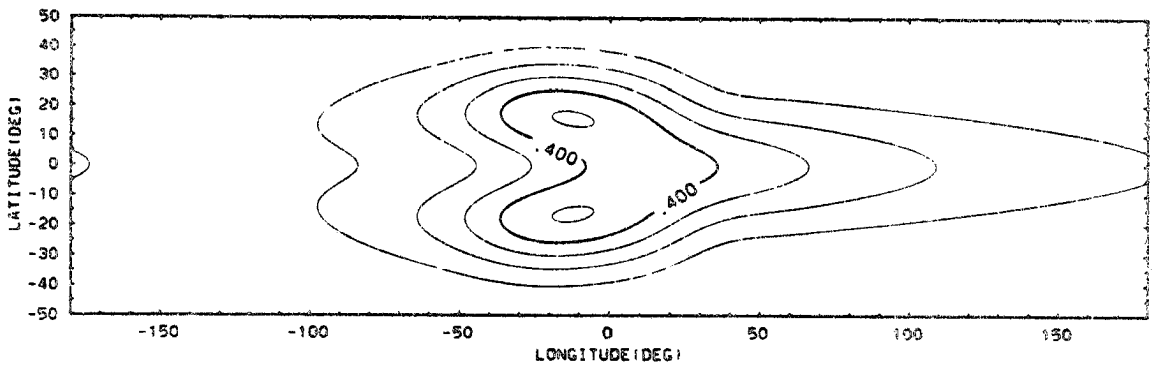

(b)

Fig. 2-4. Comparisons for forced tropical geopotential response as computed by Gill (1980) (a) and using the model horizontal discretization (b).

$$(\underline{\underline{I}}-\underline{\underline{A}}_\ell\Delta t)\ \hat{\underline{S}}_\ell^{t+1} = (\underline{\underline{I}}+\underline{\underline{A}}_\ell\Delta t)\ \hat{\underline{S}}_\ell^{t-1} + 2\Delta t(\underline{F}_\ell(\hat{\underline{S}}^t)+\hat{Q})+2\Delta t(\underline{D}_\ell(\hat{\underline{S}}^{t-1})) \quad (2.3)$$

Here $\hat{\underline{S}}_\ell$ is the state vector given by $(\hat{u}_\ell(z),\ \hat{v}_\ell(z),\ \hat{\theta}_\ell(z))$ describing the model state variables for meridional wavenumber ℓ, and $\underline{\underline{I}}$ is the identity matrix. The pressure gradient terms for the reference stratification are given by the constant matrix $\underline{\underline{A}}_\ell$, the non-linear and non-constant coefficient terms by the function $\underline{F}_\ell$ and the dissipation by the function $\underline{D}_\ell$. Here the surface pressure is considered to be a $\hat{\theta}$ variable. Following each time step a temporal filter (Asselin, 1972) is applied to damp the neutral computational mode of the leap-frog scheme. Each time step of the model requires solving the matrix problem (2.3) for each meridional wavenumber. The computational complexity of this problem is $O[9N_z^2]$ for the zonally asymmetric case and $O[4N_z^2]$ for the zonally symmetric (zonal wavenumber 0) case where $\underline{\underline{A}}_\ell\ \underline{S}_\ell$ does not project on $\underset{\sim}{u}_\ell$ since the zonally symmetric divergence does not involve u. The $(\underline{\underline{I}}-\underline{\underline{A}}_\ell\Delta t)$ is factored once at the beginning of the integration, thus yielding the $O[N_z^2]$ problem for each time step. This is equivalent to inverting that matrix before the integration but is somewhat more accurate. The term $(\underline{\underline{I}}+\underline{\underline{A}}_\ell\Delta t)\ \underline{S}_\ell^t$ is not calculated as a full matrix product but rather from a vertical integration of the discrete form of (2.1e) which is considerably more efficient. With the system described in (2.3), the maximum stable time step is defined by the deviation of the model stratification from $\tilde{\theta}(z)$ which results in some of the gravity wave terms appearing in $\underline{F}_\ell(\hat{\underline{S}})$ and by the explicit integration of terms involving the Coriolis force. For the integrations performed in this model a time step of 4000 seconds was required. On the NCAR Cray-1 computer each time step of the zonally symmetric

model requires ~0.04 seconds of CPU time for the baseline model with N_z=20 and N_ℓ=20 on a domain of 43°N to 43°S.

The full discrete problem for the nonlinear basic state system is defined by integrating (2.3) from rest with a Q field designed to represent the effects of cumulus heating and radiative cooling as shown in Fig. 2-5. The model domain is from 43°N to 43°S; however in this and other figures we display the fields to 30° latitude, thus eliminating the regions near the boundary sponges. For this system, the time derivative functions are given below as Eqs. (2.4) by defining the u, v, and θ components of the operators $\underline{\underline{A}}$, $\underline{F}$ and $\underline{D}$.

The discrete coordinates are given by

$$Z_{u,v}(n) = (n-\tfrac{1}{2})\cdot\Delta z$$

$$Z_{\theta}(n) = n\cdot\Delta z$$

$$Y(m) = m\cdot\Delta y.$$

The time derivative operators are defined by

$$\frac{d}{dt}\,\hat{u}_\ell(n) = \underline{\underline{A}}_\ell^{\hat{u}_\ell(n)}\,\underline{S}_\ell + \underline{F}_\ell^{\hat{u}_\ell(n)}(\underline{S}) + \underline{D}_\ell^{\hat{u}_\ell(n)}(\underline{S}) \tag{2.4a}$$

$$\underline{\underline{A}}_\ell^{\hat{u}_\ell(n)}\,\underline{S}_\ell = 0 \tag{2.4b}$$

$$\underline{F}^{\hat{u}_\ell(n)}(\underline{S}) = \mathcal{F}\{-v(m,n)\cdot\mathcal{F}^{-1}(i\ell\hat{u}_\ell(n)) - [w_{adv} - \frac{1}{\bar{\rho}(n)} M_c(m,n)]\cdot D_z u(m,n) + \beta y\, v(m,n)\} \tag{2.4c}$$

$$\underline{D}^{\hat{u}_\ell(n)}(\underline{S}) = \mathcal{F}\{-\alpha(m,n)\cdot u(m,n) + \mu D_{zz} u(m,n) - \frac{1}{\bar{\rho}(n)} D_z\, M_c(m,n)\cdot[u(m,n)-u(m,2)]\} \tag{2.4d}$$

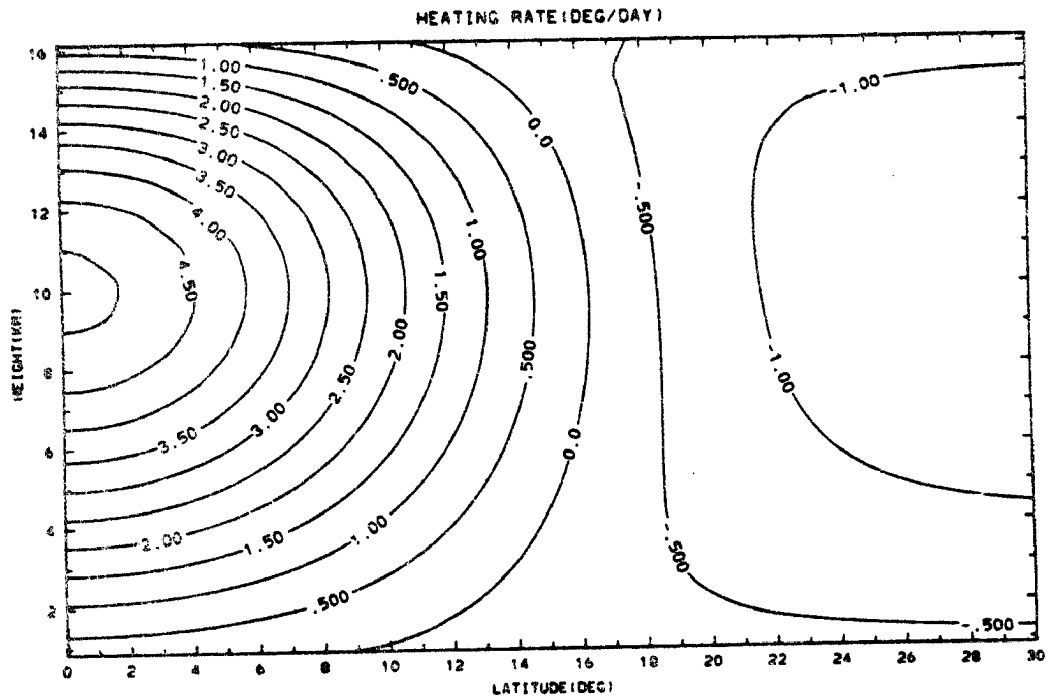

Fig. 2-5. Thermal forcing for model Hadley cell calculation.

$$\frac{d}{dt}\,\underline{\hat{v}}_{\ell}(n) = \underline{\underline{A}}_{\ell}^{\hat{v}_{\ell}(n)}\,\underline{S}_{\ell}t\;\underline{F}_{\ell}^{\hat{v}_{\ell}(n)}(\underline{S}) + \underline{D}_{\ell}^{\hat{v}_{\ell}(n)}(\underline{S}) \tag{2.4e}$$

$$\underline{\underline{A}}_{\ell}^{\hat{v}_{\ell}(n)}\,\underline{S}_{\ell} = i\ell\cdot\hat{PGF}_{\ell}(n) \tag{2.4f}$$

$$\text{where } \hat{PGF}_{\ell}(n) = \frac{1}{\bar{\rho}(n)}\,\hat{PS}_{\ell} + \sum_{j=1}^{n}\frac{g}{\theta(j)}\,\hat{\theta}_{\ell}(j)$$

$$\frac{d}{dt}\,\hat{PS}_{\ell} = \underline{\underline{A}}_{\ell}^{\hat{PS}_{\ell}}\,\underline{S}_{\ell} = -\sum_{j=1}^{N_z}\tilde{\rho}(n)\cdot i\ell\hat{v}_{\ell}(n) \tag{2.4g}$$

$$\underline{F}^{\hat{v}_{\ell}(n)}(\underline{S}) = \mathcal{F}\{-v(m,n)\cdot\mathcal{F}^{-1}(i\ell\hat{v}_{\ell}(n)) \tag{2.4h}$$

$$-[w_{adv} - \frac{1}{\bar{\rho}(n)}\,M_c(m,n)]\cdot D_z v(m,n)$$

$$-\beta y\,u(m,n)\}$$

$$\underline{D}^{\hat{v}_{\ell}(n)}(\underline{S}) = \mathcal{F}\{-\alpha(m,n)\cdot v(m,n) + \mu D_{zz}v(m,n) \tag{2.4i}$$

$$-\frac{1}{\bar{\rho}(n)}\,D_z\,M_c(m,n)\cdot[v(m,n)-v(m,2)]\}$$

$$\frac{d}{dt}\,\hat{\theta}_{\ell}(n) = \underline{\underline{A}}_{\ell}^{\hat{\theta}_{\ell}(n)}\,\underline{S}_{\ell} + \underline{F}_{\ell}^{\hat{\theta}_{\ell}(n)}(\underline{S}) + \underline{D}_{\ell}^{\hat{\theta}_{\ell}(n)}(\underline{S}) \tag{2.4j}$$

$$\underline{\underline{A}}_{\ell}^{\tilde{\theta}_{\ell}(n)}\,\underline{S}_{\ell} = -\,\hat{w}_{\ell}(n)\,\tilde{\theta}\,(n) \tag{2.4k}$$

$$\text{where } \tilde{\rho}(n)\,\hat{w}_{\ell}(n) = \sum_{j=1}^{n} -\,\tilde{\rho}(j)\cdot i\ell\hat{v}_{\ell}(j)$$

$$\underline{F}^{\tilde{\theta}_\ell(n)} = \mathcal{F}\{-v_{adv}\cdot\mathcal{F}^{-1}(i\ell\hat{\theta}(n)) - w(m,n)\cdot[D_z\theta(m,n)+\tilde{\theta}_z]\} \tag{2.41}$$

$$\underline{D}^{\tilde{\theta}_\ell(n)} = \mathcal{F}\{-\gamma(m,n)\cdot\theta(m,n)+\mu D_{zz}\theta(m,n)\} \tag{2.4m}$$

where $w_{adv} = \frac{1}{2}[w(m,n) + w(m,n-1)]$

$v_{adv} = \frac{1}{2}[v(m,n+1) + v(m,n)]$

$D_z a = \frac{1}{2\Delta z}\,[a(m,n+1) - a(m,n-1)]$

$D_{zz} a = \frac{1}{\Delta z^2}\,[a(m,n+1) + a(m,n-1) - 2a(m,n)]$

$\mathcal{F}$ is the discrete Fourier transform operator

$\mathcal{F}^{-1}$ is its inverse

i.e. $\hat{a}(n) = \mathcal{F}\{a(m,n)\}$

$a(m,n) = \mathcal{F}^{-1}\{\hat{a}(n)\}$

$$M_c(n) = M_{co}\cdot\left(1-\exp\left(\frac{p_T-\tilde{p}(n)}{p_{dtr}}\right)\right) \tag{2.4n}$$

$p_T = 1.34\cdot10^4$ Pa $p_{dtr} = 7.5\ 10^3\ p_a$

$$M_{co} = \frac{1}{r_c L_c}\int \tilde{\rho}\ c_p\ q_c\ dz$$

The nonlinear model is integrated for 100 days at which point the model is in a very nearly steady state. This state, which is shown in Fig. 2-6, is qualitatively similar to the winter hemisphere Hadley cells which are reproduced from Newell et al. (1974) as Fig. 2-7a. One feature which is not reproduced by the model is the layer of deep easterlies which is observed in the west Pacific (see Fig. 2-7b). This may be due to the equatorally symmetric model heating profile.

We can now formulate a linear perturbation model for the problem using the results of the integration as the basic state. The form of this system is the same as before and is given by Eq. (2.3) with the time derivative functions computed in a way analogous to Eq. (2.4).

The Stevens-Lindzen latent heating parameterization relates latent heat release to low level moisture convergence and uses a specified vertical heating profile.

$$Q'(y,z) = \begin{cases} \dfrac{\tilde{\theta}(z)}{\tilde{T}(z)} \cdot L \cdot W'_{cb}(y) \cdot \tilde{\rho}_{cb} q_{cb}(y) \cdot \eta(z) & \left| \; cb \leq z \leq ct \right. \\ 0 & \left| \; \text{otherwise} \right. \end{cases} \tag{2.5}$$

where $\eta(z) \alpha \sin\left[\frac{z}{\pi z_T}\right] \exp\left[\frac{z}{2z_T}\right]$

and $\int_{cb}^{ct} c_p \, \tilde{\rho} \, \eta(z) dz = 1$

Here cb and ct represent the cloud base and cloud top. The model cloud base is taken to be level 2 and the cloud top is at 130 mb. L is the latent heat of condensation and q_{cb} is the mixing ratio at cloud base. The integral constraint requires the heating to equal the latent heat associated with vapor crossing the cloud base.

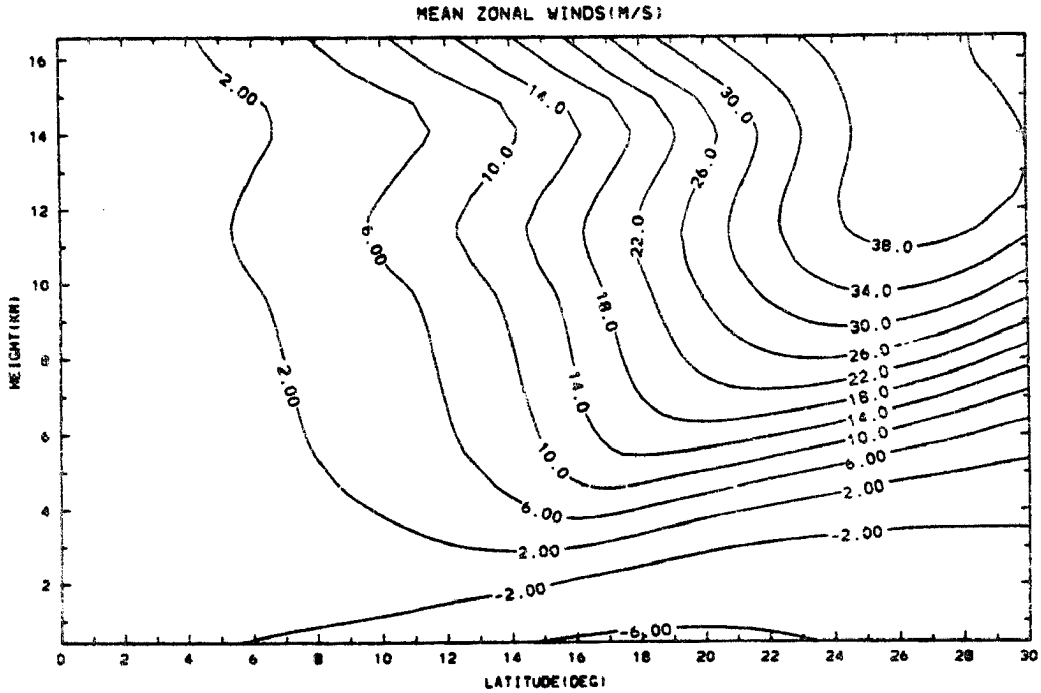

Fig. 2-6a. Model basic state u-wind field.

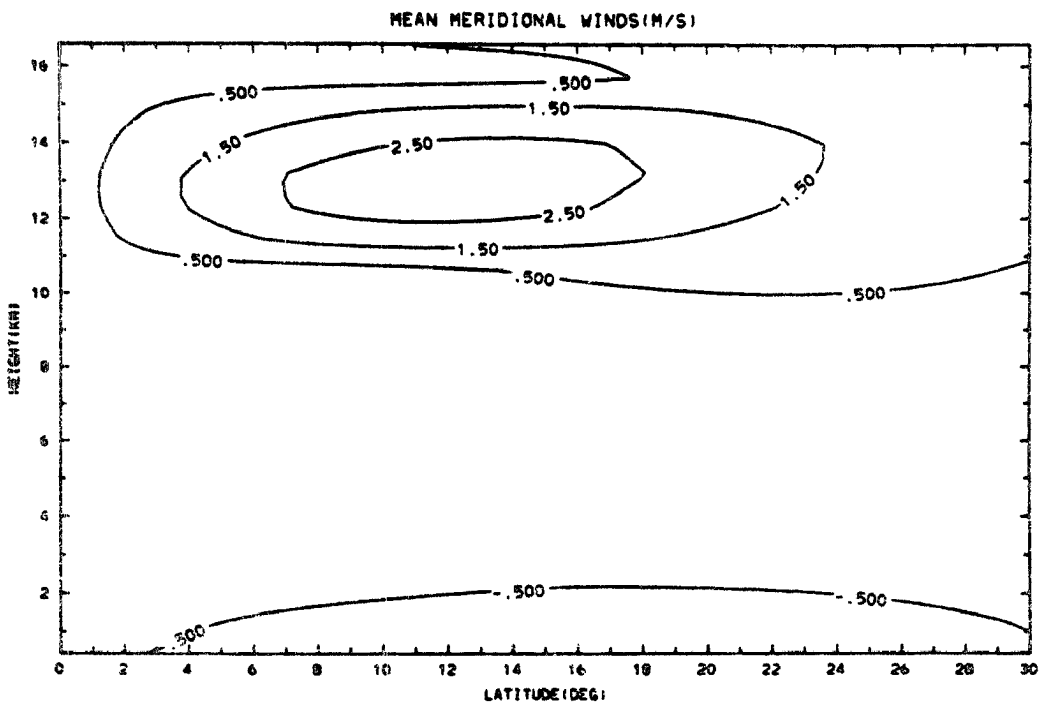

Fig. 2-6b. Model basic state v-wind field.

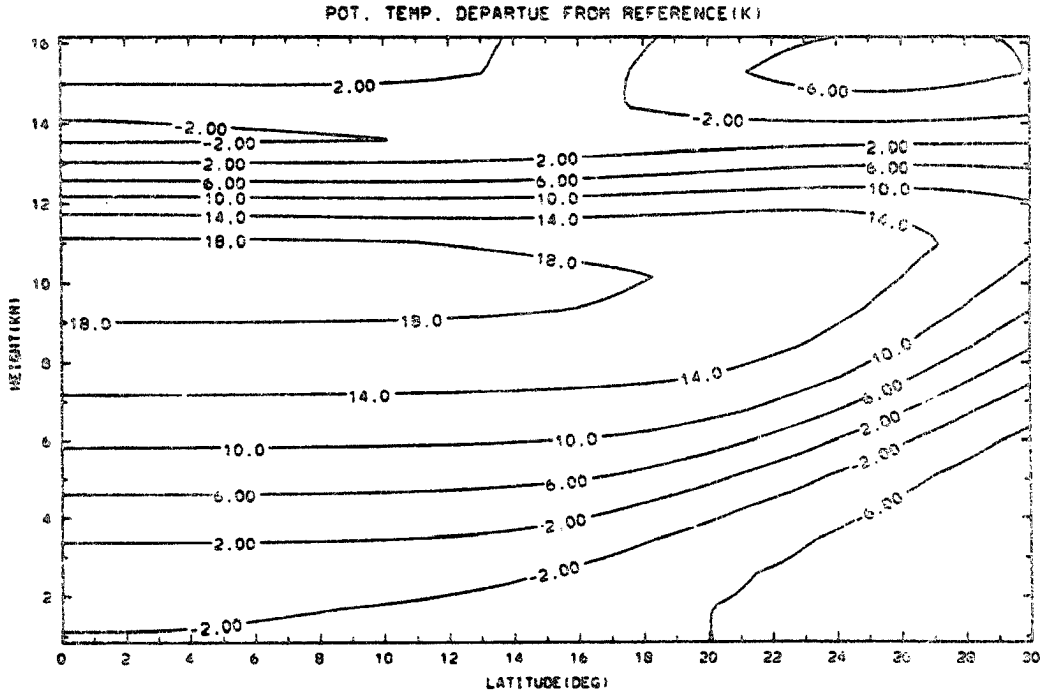

Fig. 2-6c. Model basic state potential temperature departure from reference.

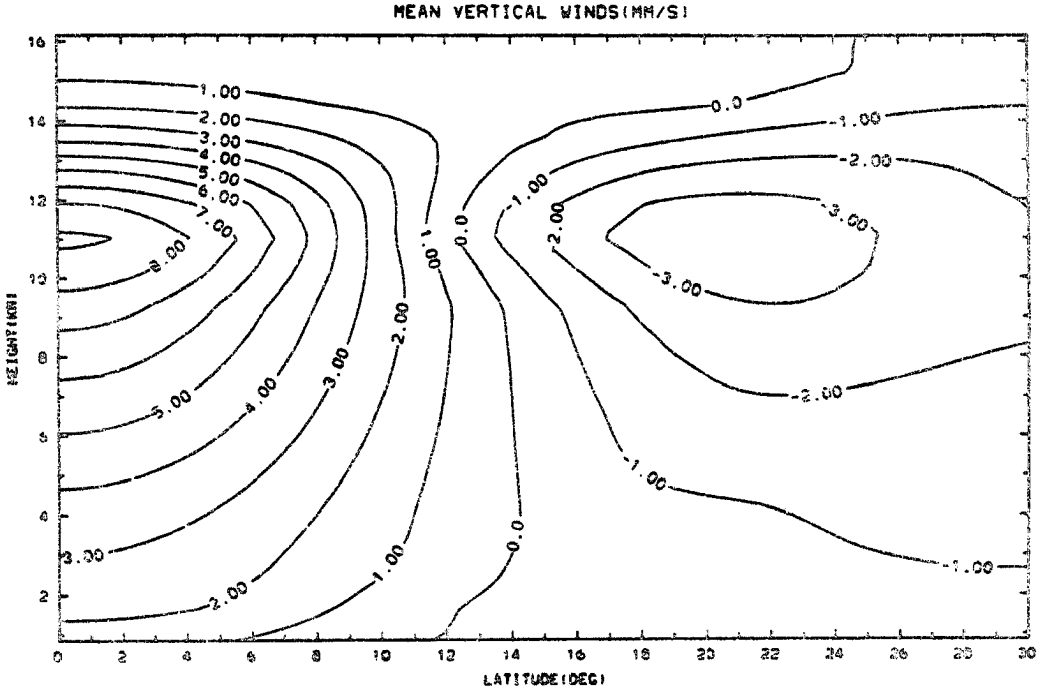

Fig. 2-6d. Model basic state w-wind field.

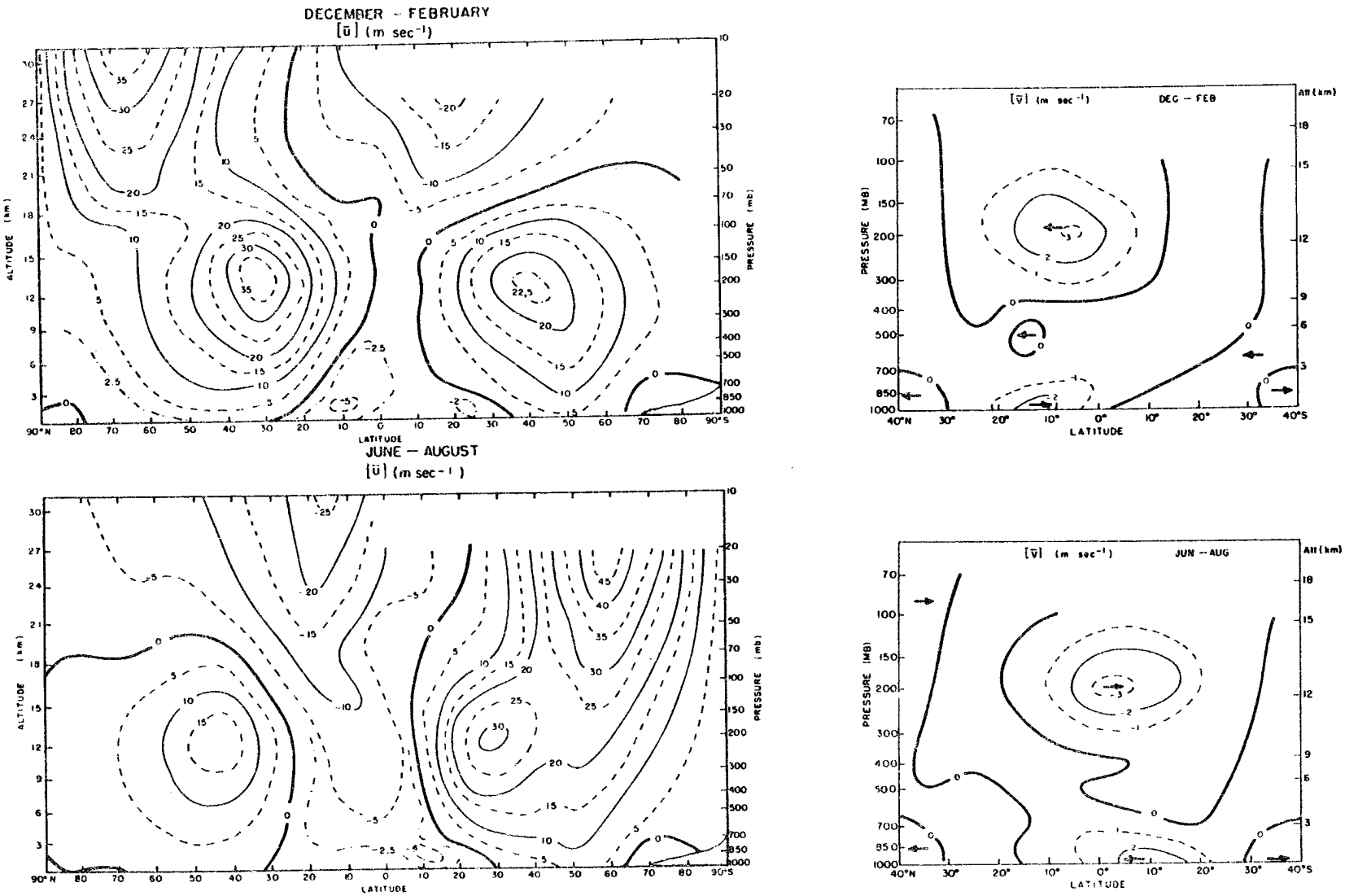

Fig. 2-7a. Zonally averaged observed circulation (from Newell et al., 1974).

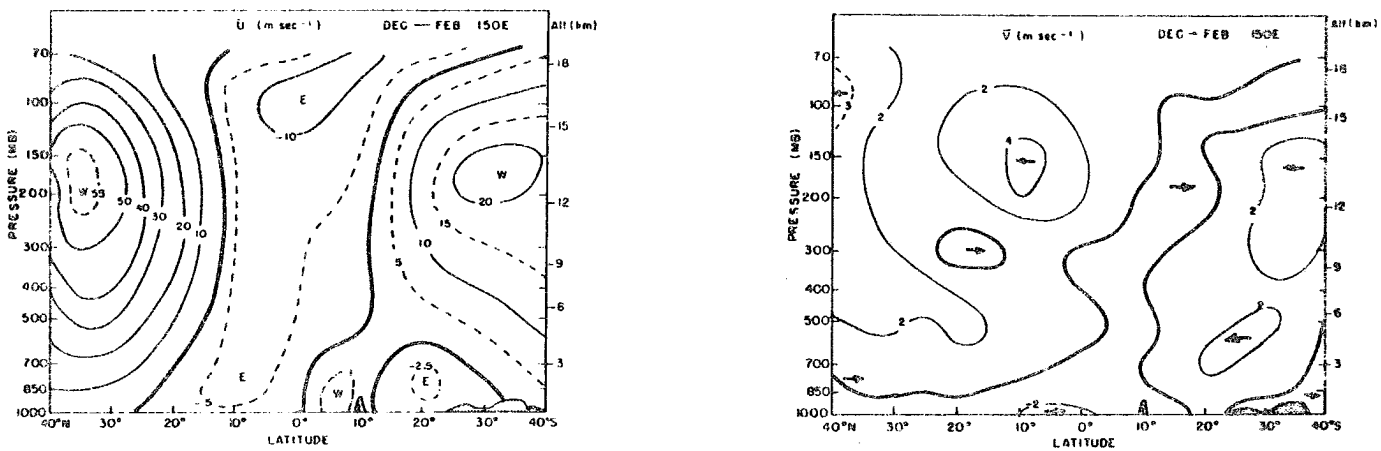

Fig. 2-7b. Mean circulation at 150°E (from Newell et al., 1974).

In the next chapter we will examine the dynamical properties of this linear system; in particular, we will examine the behavior of zonally symmetric, thermal-wind balanced circulations under the influence of the Hadley cell direct circulation.

3. THE ZONALLY SYMMETRIC LINEAR MODES

In this Chapter we will investigate the linear zonal wavenumber 0 modes of an atmosphere whose basic state is given by the Hadley cell which we derived in the previous section.

The first study to provide a complete description of the linear modes of an equatorial atmosphere was performed by Lindzen (1967). Lindzen derived the normal modes of a resting atmosphere on an equatorial β-plane by first taking the Fourier transform in the x-direction and then separating the problem into systems governing the y and z structure. When this has been done the equations governing the y-structure of the system are those generally known as the shallow water equations. The separation constant plays a role proportional to the depth of the shallow fluid layer depth and is referred to as the equivalent depth.

Matsuno (1966) and Lindzen (1967) solved the resulting horizontal structure equations by combining the system into a third order system for v and then transforming it to get a linear eigenmode problem with known quantized solutions. This yields a cubic dispersion relationship which has roots corresponding to eastward moving gravity waves, westward moving gravity waves, and a set of Rossby waves which move eastward in phase. There is also a special solution of the system which is an eastward propagating non-dispersive gravity wave with no v-component wind. This solution is generally referred to as the equatorial Kelvin

wave because of its similarity to the f-plane Kelvin wave; the change in sign of f at the equator plays the role of a boundary wall. A copy of the dispersion diagram for the Matsuno system is presented as Fig. 3-1.

When we consider the above solutions for zonal wavenumber 0 the two gravity roots combine to form a set of standing (in the y-direction) oscillatory waves and the Kelvin and Rossby modes collapse to form a degenerate set which consists of symmetric motions in thermal wind balance with exactly zero frequency and arbitrary horizontal structure. Here we are interested in what happens to this degenerate set when the advective effects of the basic state Hadley cell are added to the system and disturb the thermal wind balance. Using the discretization methods discussed in the previous chapter, we can now write the governing linear system for zonal wavenumber 0 as

$$\frac{d\underline{S}}{dt} = \underline{\underline{L}}(\bar{\underline{S}})\ \underline{S} \tag{3.1}$$

where $\bar{\underline{S}}$ is the basic state about which the system is linearized. $\underline{\underline{L}}$ is a linear matrix operator combining the gravity wave operator $\underline{\underline{A}}$ and the linearized effects of the operators $\underline{F}$ and $\underline{D}$.

The solution of an initial value problem for (3.1) has the form

$$\underline{S}(t) = \sum_{i=1}^{N} a_i \hat{\underline{S}}_i \exp(\lambda_i t) \tag{3.2}$$

where N is the total number of model degrees of freedom, a_i are complex mode amplitudes, the $\hat{\underline{S}}_i$'s are the eigenvectors of $\underline{\underline{L}}$ and the λ_i's are the associated eigenvalues. For the zonally symmetric case $\underline{\underline{L}}$ is real,

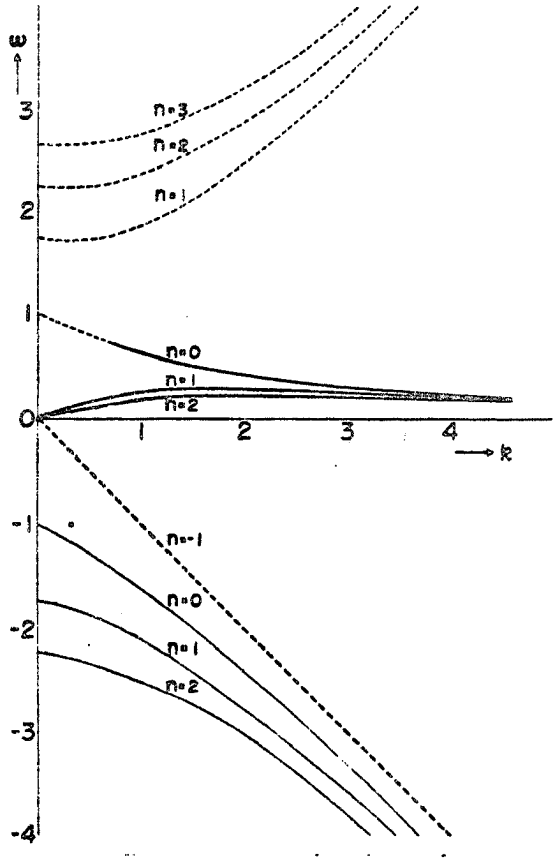

Fig. 3-1. Dispersion diagram for one vertical mode of an equatorial atmosphere. Thin solid line: eastward propagating inertia-gravity waves. Thin dashed line: westward propagating inertia-gravity waves. Thick solid line: Rossby (quasi-geostrophic) waves. Thick dashed line: The Kelvin wave (from Matsuno, 1966).

and the oscillating eigenmodes must therefore occur in complex conjugate pairs. Note that in this formulation the system is not formally degenerate, as in the Matsuno model, even for the resting basic state, due to the inclusion of the space dependent damping which splits the thermal wind motions into modes which decay at various rates.

Our problem has now been reduced to finding the eigenvectors of $\underline{\underline{L}}$. This is a conceptually straightforward task but is complicated by the large size of $\underline{\underline{L}}$ (N×N) which arises from the non-separable (in y and z) nature of the problem. For the resolution of our baseline run (20 wavenumbers, 20 vertical levels), N = 2400 when the problem is written such that $\underline{\underline{L}}$ is real. This is a factor of four larger than the eigenmode problems which can be solved directly on currently available super-computers. One approach is to truncate the problem more severely; this will be done later in this Chapter. However, before resorting to this rather brutal procedure, we wish to get some idea of the behavior of the baseline system.

If we consider the evolution of the initial value problem described by (3.1) we will note from (3.2) that the time evolution of any linear combination of model state variables, $j(t) = \underline{r}\cdot\underline{S}(t)$, where $\underline{r}$ is arbitrary, has the form

$$j(t) = \sum_{t=1}^{N} b_i \exp(\lambda_i t). \tag{3.3}$$

This indicates that we can learn something about the system behavior by merely studying a representative time series during a numerical integration of (3.1) which is computationally practical even for large N.

Here we will take the model initial condition to be resting u-wind and v-wind fields and an initial perturbation potential temperature

field which is randomly distributed in space, the intent being to project the initial condition approximately equally on all the model modes. The initial condition is constrained so that the value for meridional wavenumber 0 is exactly zero. This avoids exciting modes which have no associated wind fields. For a representative time series we will take the model potential temperature averaged within a box covering 13°N to 23°N latitude and 5 km to 10 km height. Potential temperature was chosen as a time series because it plays a first order role in both the gravity and thermal wind modes. The choice of averaging box is arbitrary; we have simply tried to represent the large scale behavior of the model.

The linear model was run for a number of cases which are summarized in Table 3.1. All prognostic runs are made with Q' and M_c' taken to be zero, ignoring the effects of perturbation cumulus clouds. This is necessary for the prognostic model to eliminate unstable, fast gravity wave modes. The effects of perturbation clouds on the slow modes will be studied later in this chapter using a direct eigensolver.

Table 3.1. Prognostic model runs.

Run	Basic State	Dissipation
1	rest	given by (2.2a-d), $\bar{M}_c=0$
2-Baseline	Hadley cell	given by (2.2a-d)
3	Hadley cell	$\bar{M}_c=0$
4	rest	$\gamma=\alpha_{sp}=\alpha_{ce}=0$
5	Hadley cell	$\gamma=\alpha_{sp}=\alpha_{ce}=0$

For our first run we will consider the case where $\bar{S}=0$ and $\bar{M}_c=0$. This case is essentially the same as the Lindzen problem except for our

inclusion of non-zero values for the damping. Following our discussion above, we would expect the model to display relatively fast oscillatory behavior about a mean thermal wind balance, both of which would exponentially decay. The box averaged temperature, which we will call θ_1, is plotted in Fig. 3-2a and generally agrees with our expectations.

One way to interpret an experiment of this type is as a forced problem with forcing which is impulsive in time. Since impulsive forcing is white in frequency, we can develop an estimate of the frequency response of the model for θ_1 and random spatial forcing by computing an estimate for the power spectrum of θ_1 using the techniques described in Chapter 5. Estimates of the system autocorrelation function and power spectral density are shown in Figs. 3-2b and 3-2c.

The next experiment (run 2) is run using a baseline system with the Hadley cell basic state and the same value for $\bar{M}_c$ used in Chapter 2. The results of run 2 where the initial condition is the same as before are shown in Fig. 3-3. This figure shows a dramatic difference in system behavior in that rather than decaying smoothly to 0, the system actually crosses 0 and continues to a positive value before decaying, indicating the presence of oscillatory slow modes. This tendency appears in the spectral response as a broadband peak at low frequencies (20-40 day periods). Note also the faster damping of the 1.8 day mode due to the presence of cumulus momentum mixing.

For the next run (run 3) we repeat the baseline experiment with $\bar{M}_c=0$ to investigate the system in the presence of less damping. This result, which is presented in Fig. 3-4 shows the presence of an oscillatory mode with a period of about 50 days quite clearly.

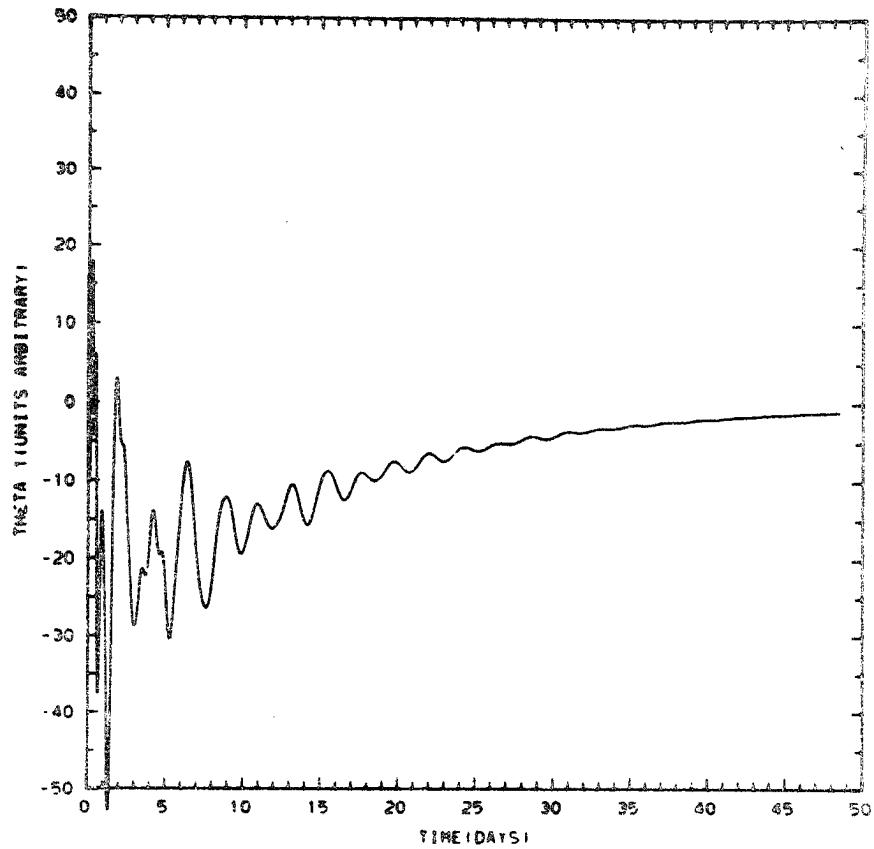

Fig. 3-2a. Time evolution of θ_1 from run 1. Basic state is rest, $\bar{M}_c$=0.

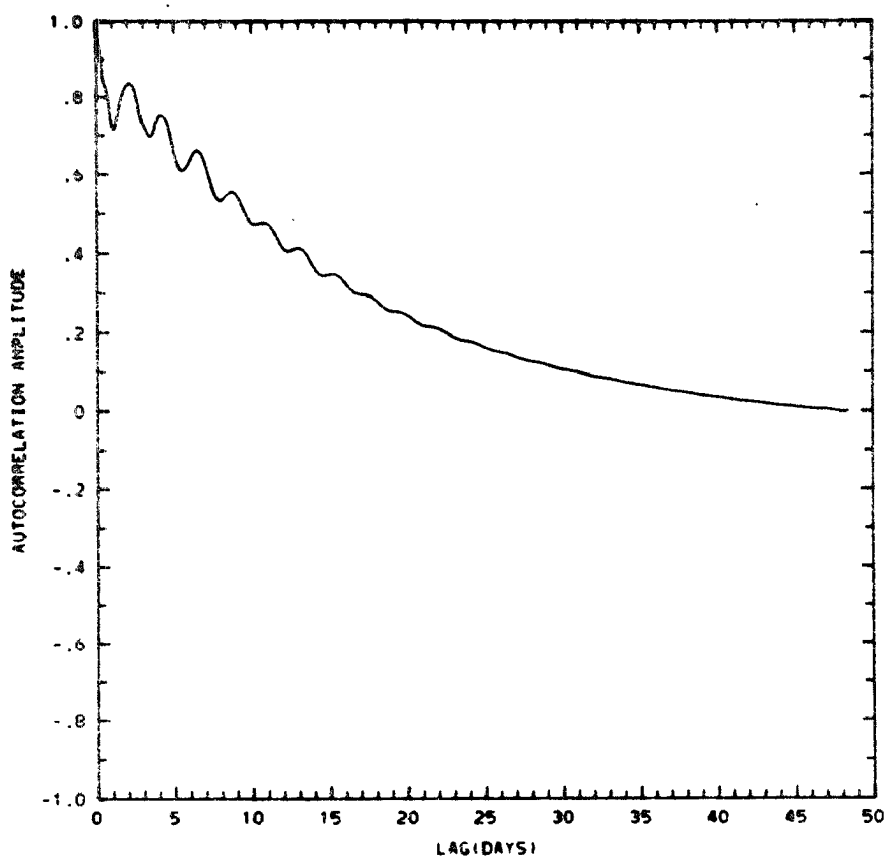

Fig. 3-2b. Autocorrelation estimate of θ_1 from run 1.

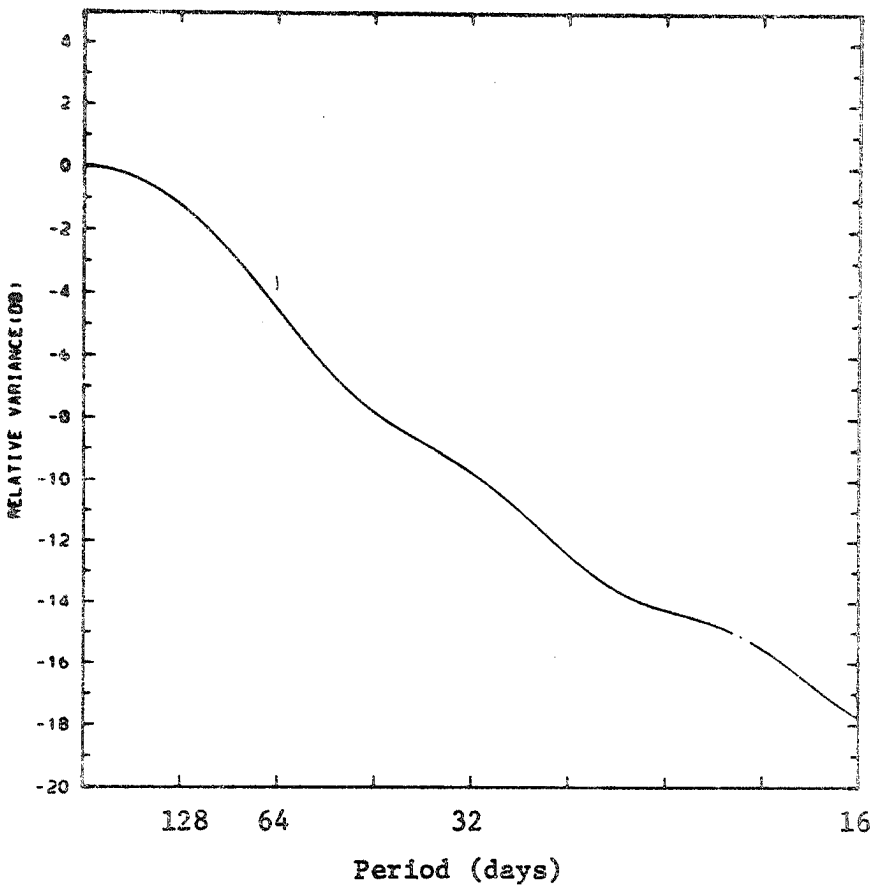

Fig. 3-2c. Variance response spectral estimate from run 1.

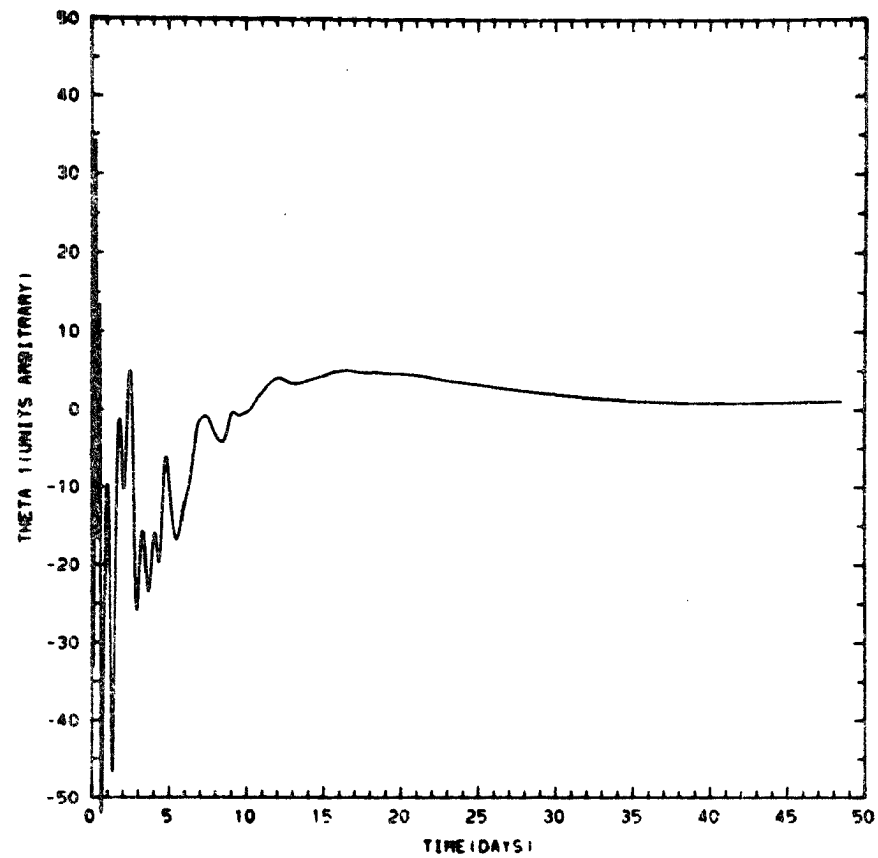

Fig. 3-3a. Time evolution of θ_1 from run 2. Baseline model with Hadley cell, $\tilde{M}_c$.

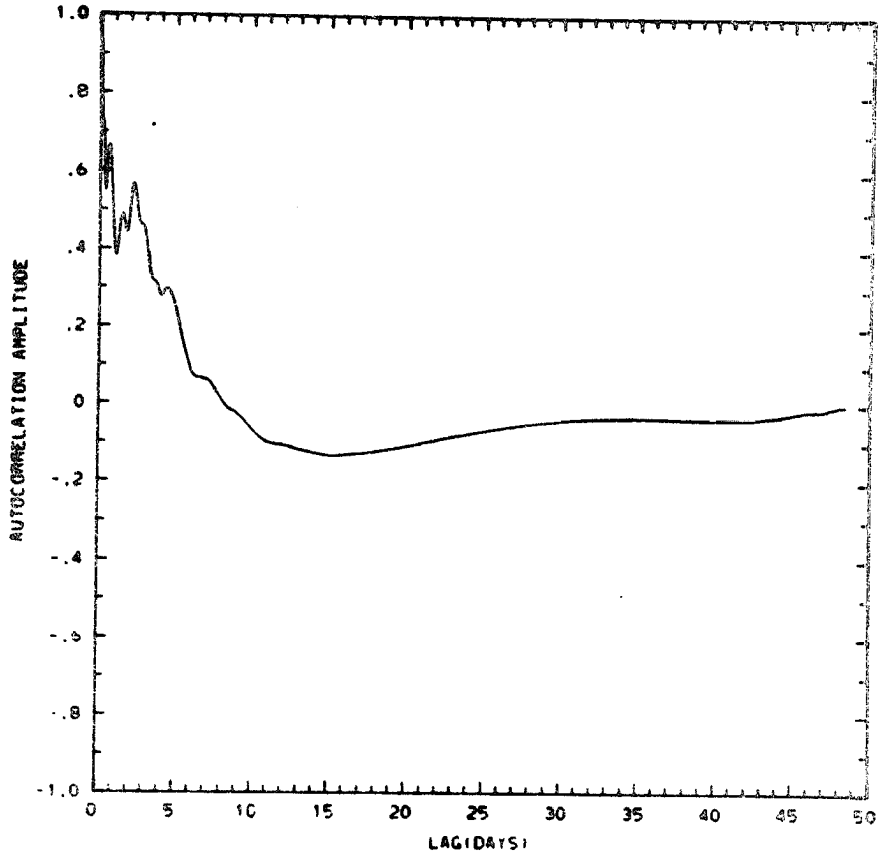

Fig. 3-3b. Autocorrelation estimate of θ_1 from run 2.

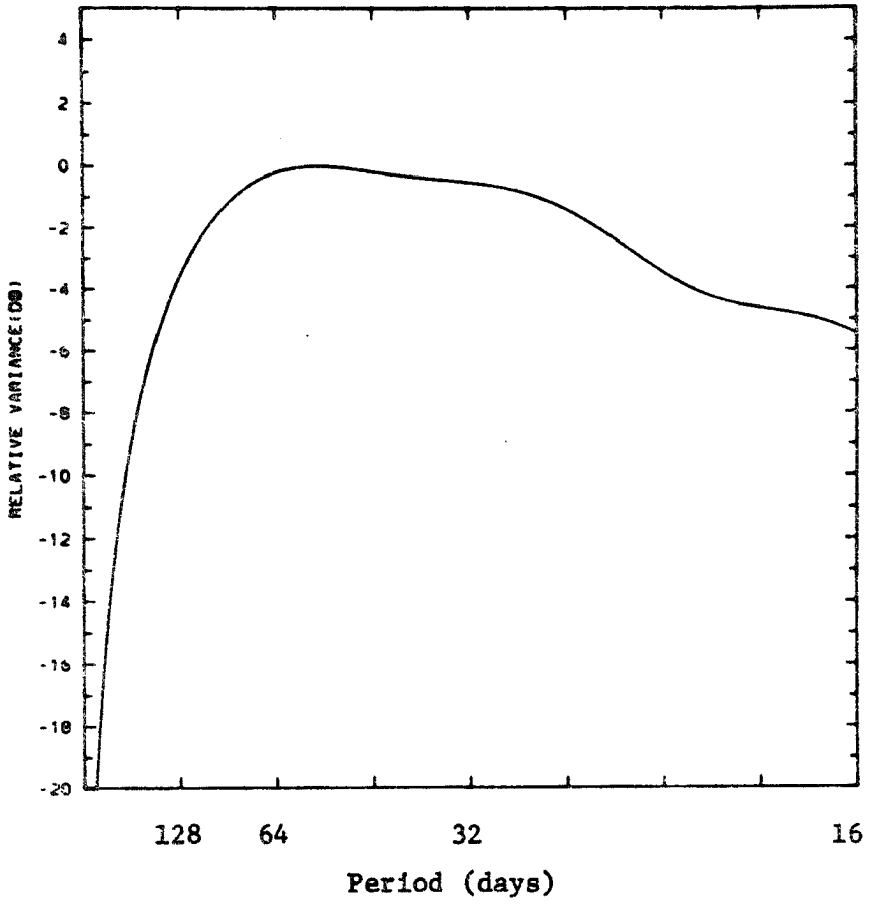

Fig. 3-3c. Variance response spectral estimate from run 2.

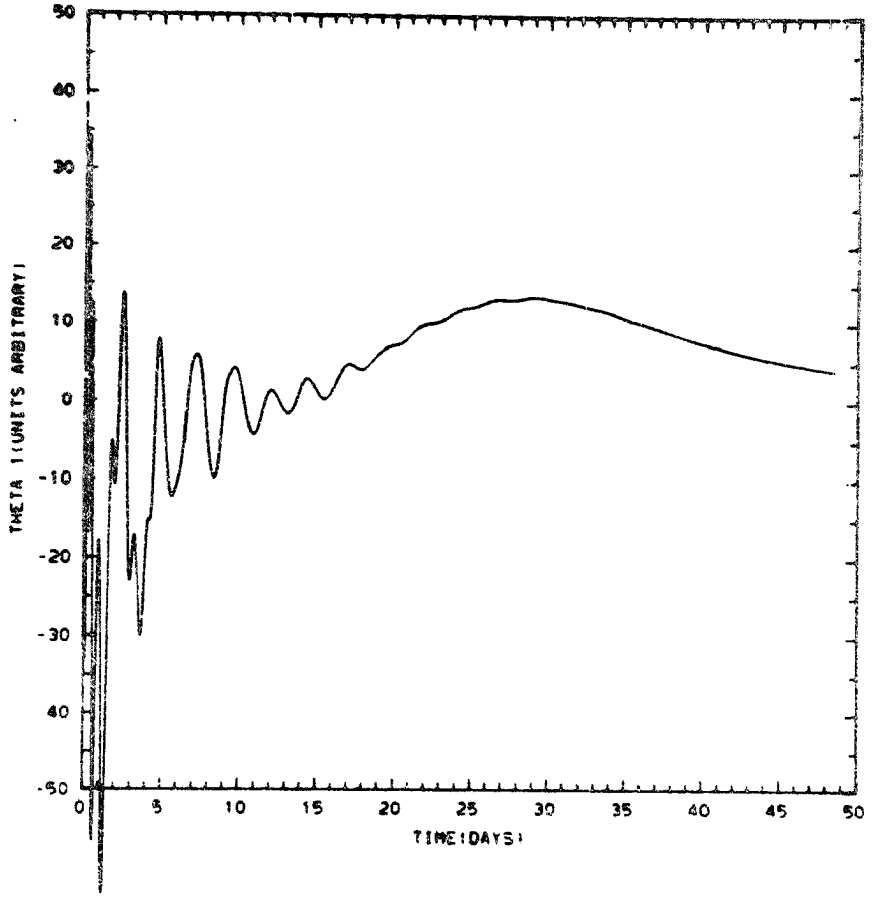

Fig. 3-4a. Time evolution of θ_1 from run 3. Hadley cell basic state, M_c=0.

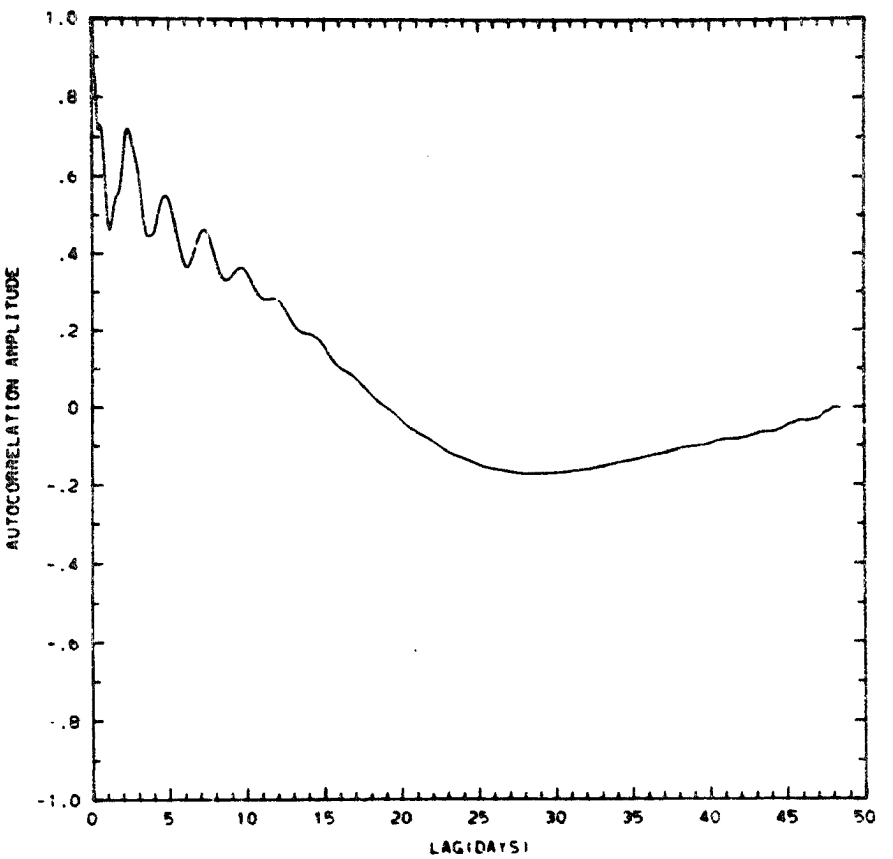

Fig. 3-4b. Autocorrelation estimate of θ_1 from run 3.

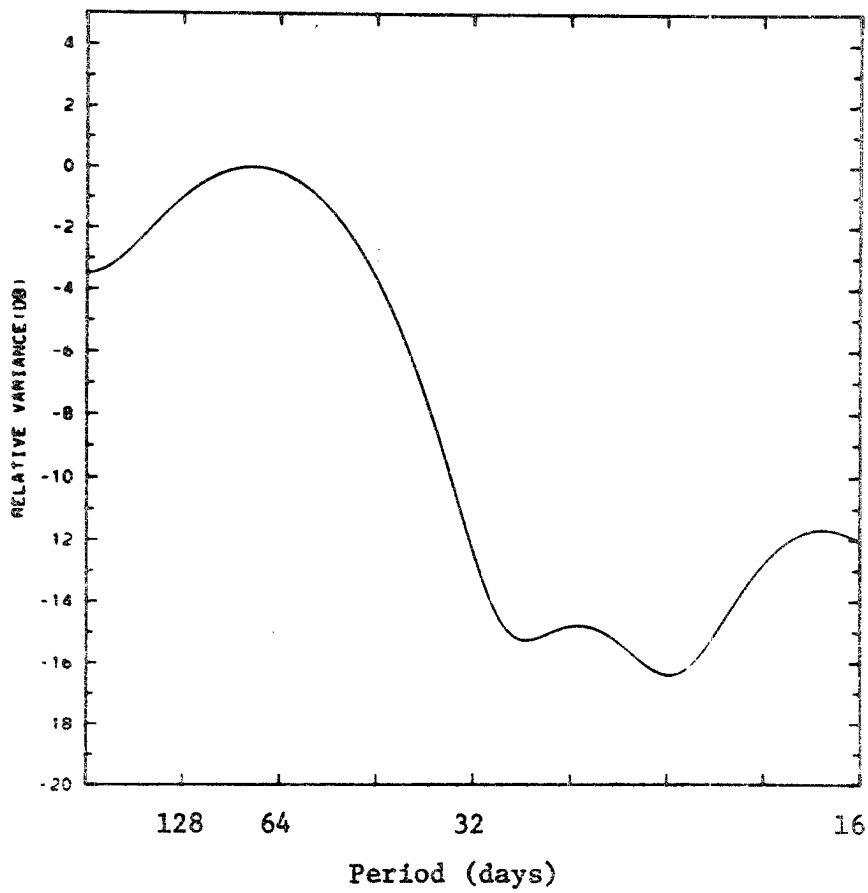

Fig. 3-4c. Variance response spectral estimate from run 3.

In Figs. 3-5 and 3-6 we present the results for a resting basic state (run 4) and a Hadley cell basic state (run 5) where the only damping which is included is the poleward boundary sponge and small (~1/50 days) Rayleigh friction and Newtonian cooling terms in the interior. The results of these runs generally agree with the previous runs showing slow exponential decay for the resting basic state case and low frequency oscillations for the Hadley cell basic state which now appear at periods of 40 days. In the absence of large values of dissipation the spectral peak at 40 days becomes sharper.

In order to get some idea of the spatial structure of the slow modes, plots of the u-component wind field for run 2 at T=20 days, and T=30 days and T=40 days are presented as Fig. 3-7. These figures show a poleward propagation of an upper tropospheric wind perturbation and equatorial propagation of a perturbation of the opposite sign at low levels. The vertical propagation in the wind appears to be generally downward, probably due to the fact that $\bar{w}-\bar{M}_c/\tilde{\rho}$ is negative over the entire domain. The runs also show the faster damping of the modes with small spatial scale.

In Fig. 3-8 we present the u-wind field of run 3 where $\bar{M}_c=0$ at 20, 30, 40, and 50 days into the run. These fields look like the baseline run with the exception of a tendency for upward vertical propagation in the equatorial region due to the lack of a cumulus mass transport correction to $\bar{w}$.

Next we would like to study the model structure more directly and introduce the effects of perturbation heating in the model. To do this we will reduce the model resolution to 10 meridional wavenumbers and 10 vertical levels so that a direct eigensolver can be used for $\underline{\underline{L}}$. In

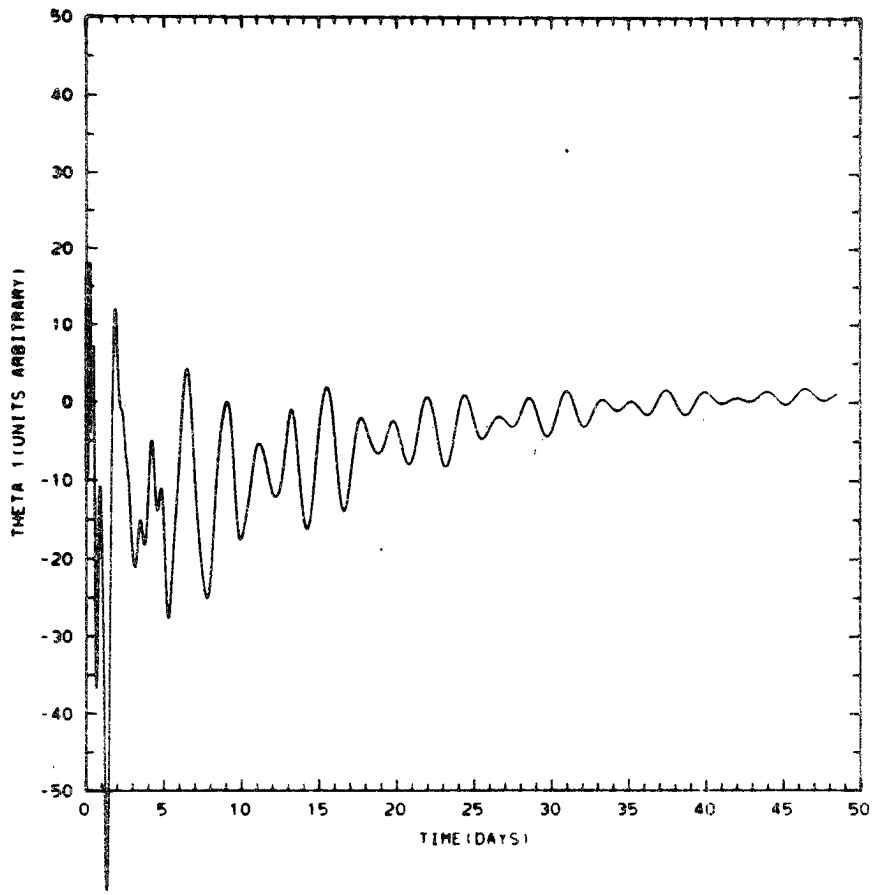

Fig. 3-5a. Time evolution of θ_1 from run 4. Rest basic state, minimum dissipation.

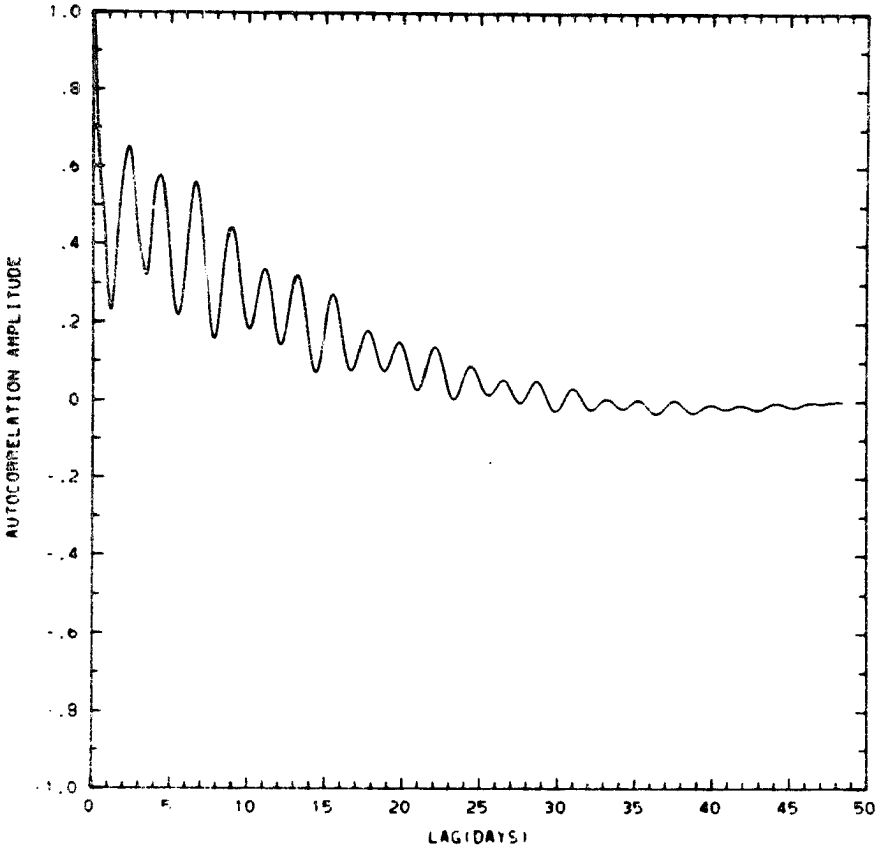

Fig. 3-5b. Autocorrelation estimate of θ_1 from run 4.

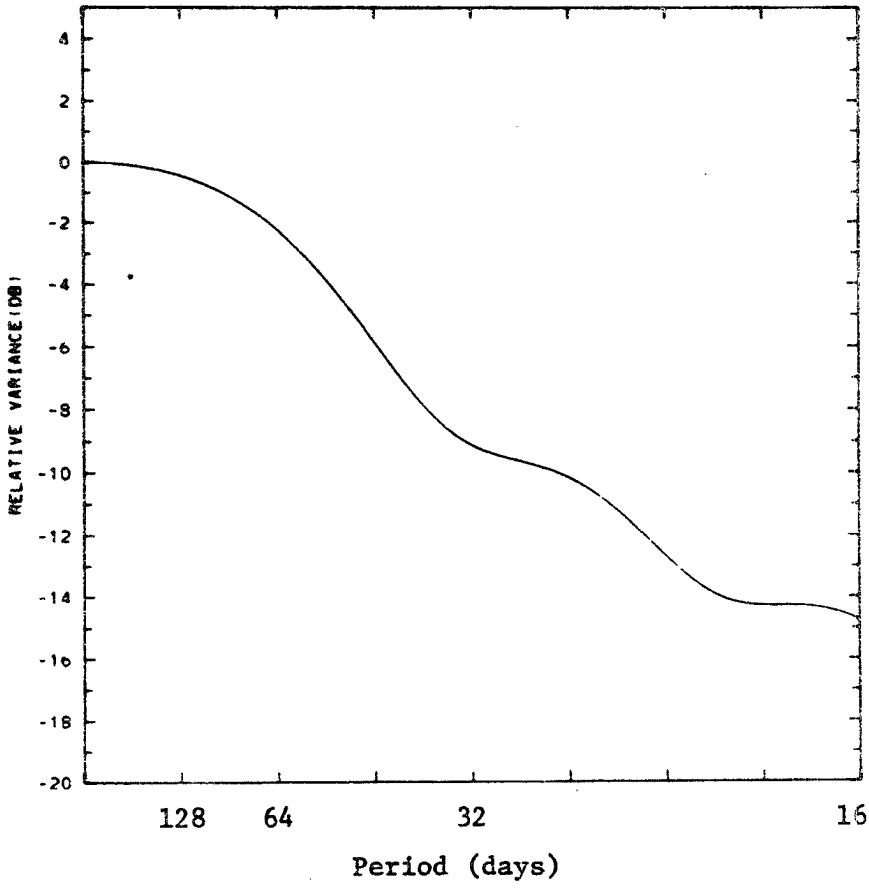

Fig. 3-5c. Variance response spectral estimate from run 4.

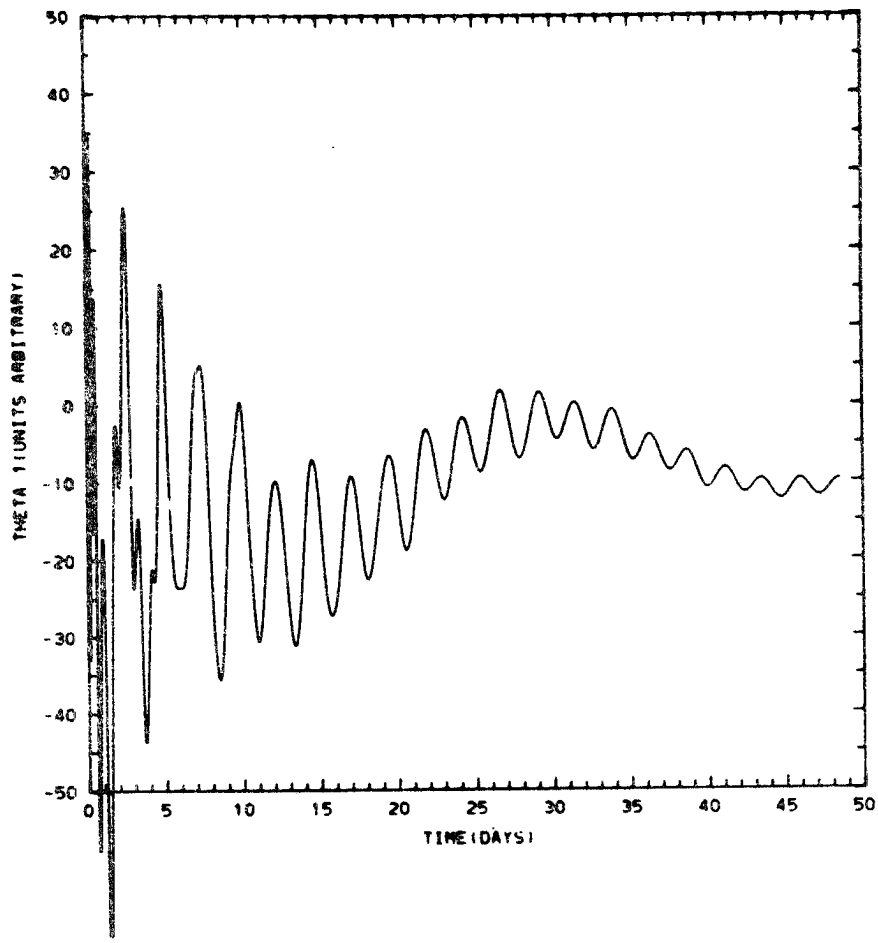

Fig. 3-6a. Time evolution of θ_1 from run 5. Hadley cell basic state, minimum dissipation.

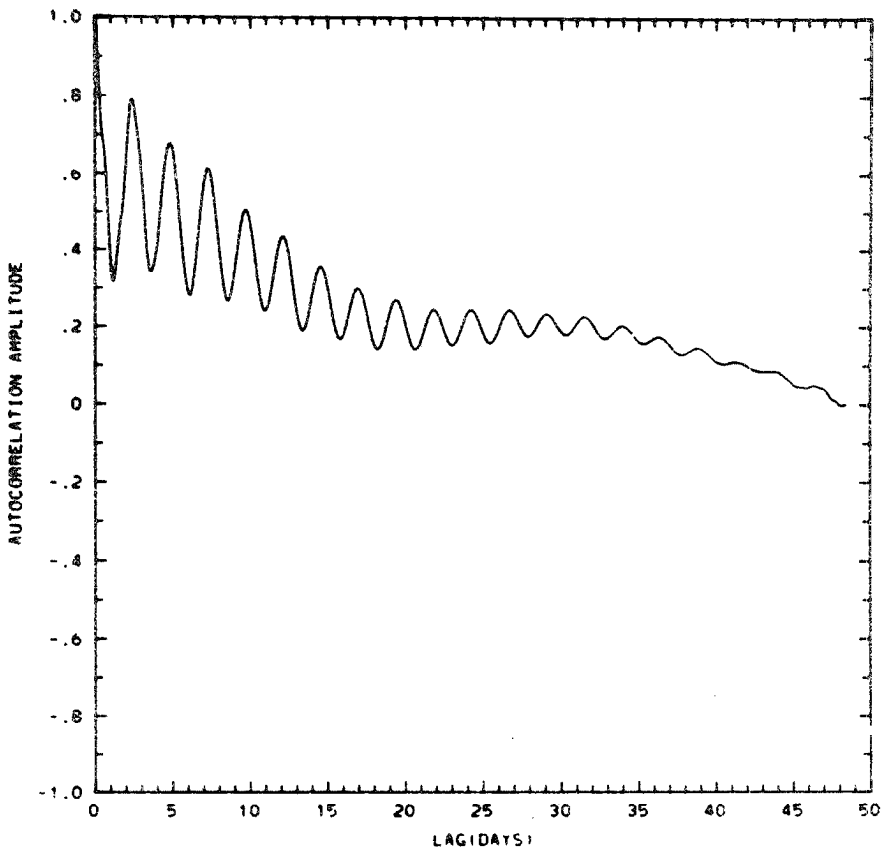

Fig. 3-6b. Autocorrelation estimate of θ_1 from run 5.

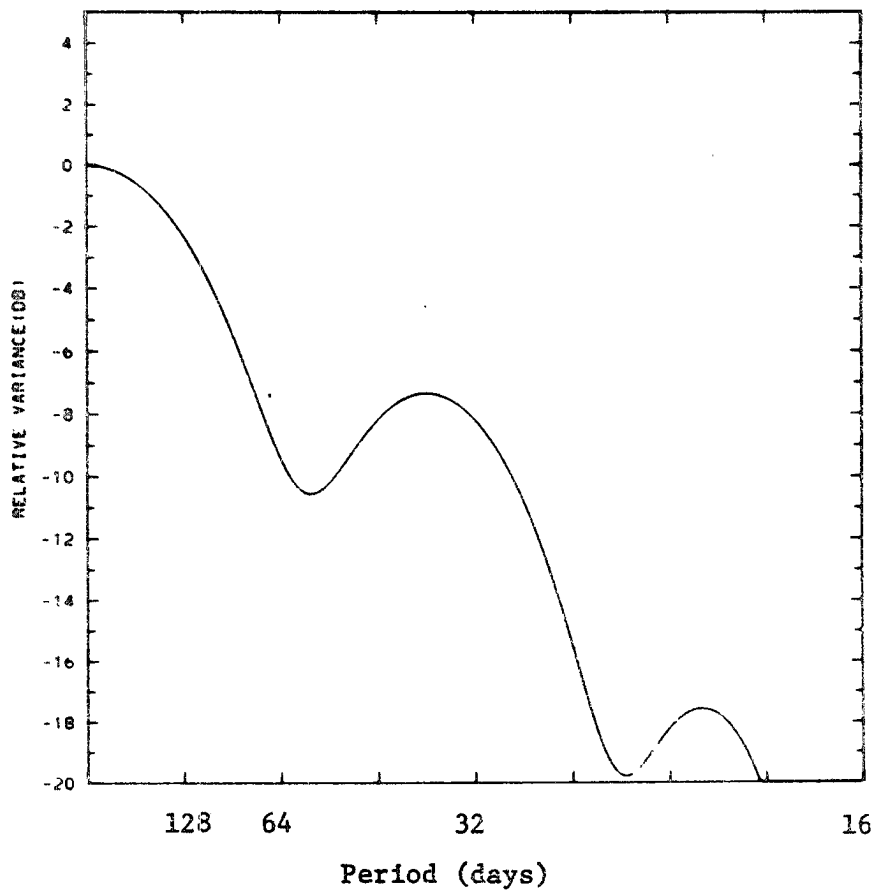

Fig. 3-6c. Variance response spectral estimate from run 5.

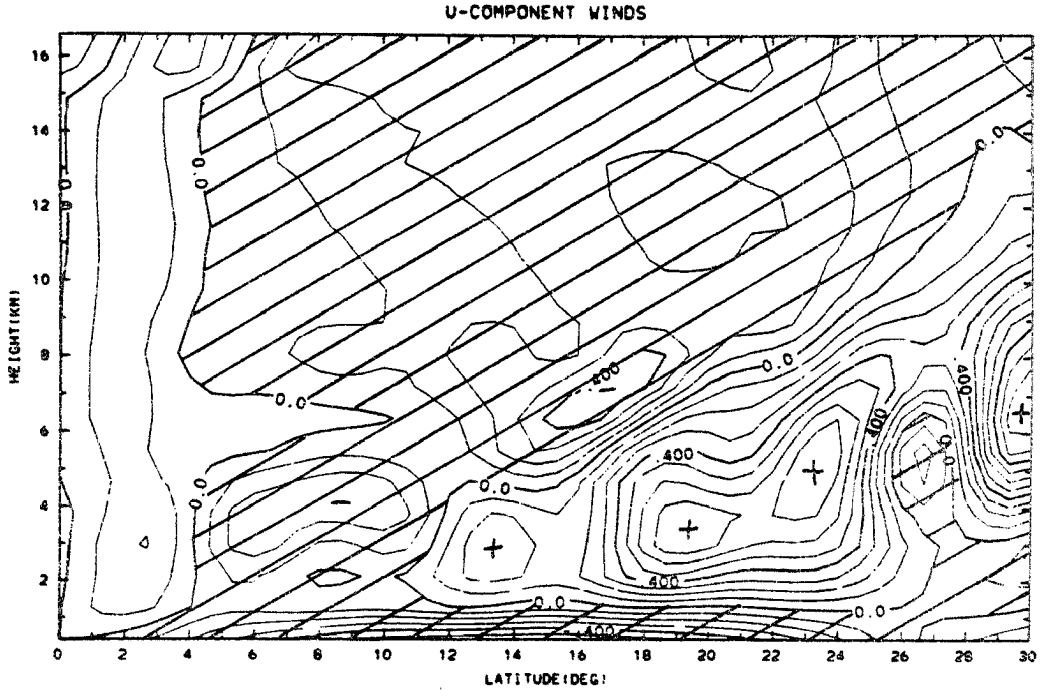

Fig. 3-7a. Run 2 (baseline model) u-winds at T=20 days. Maximum contour is 1.0.

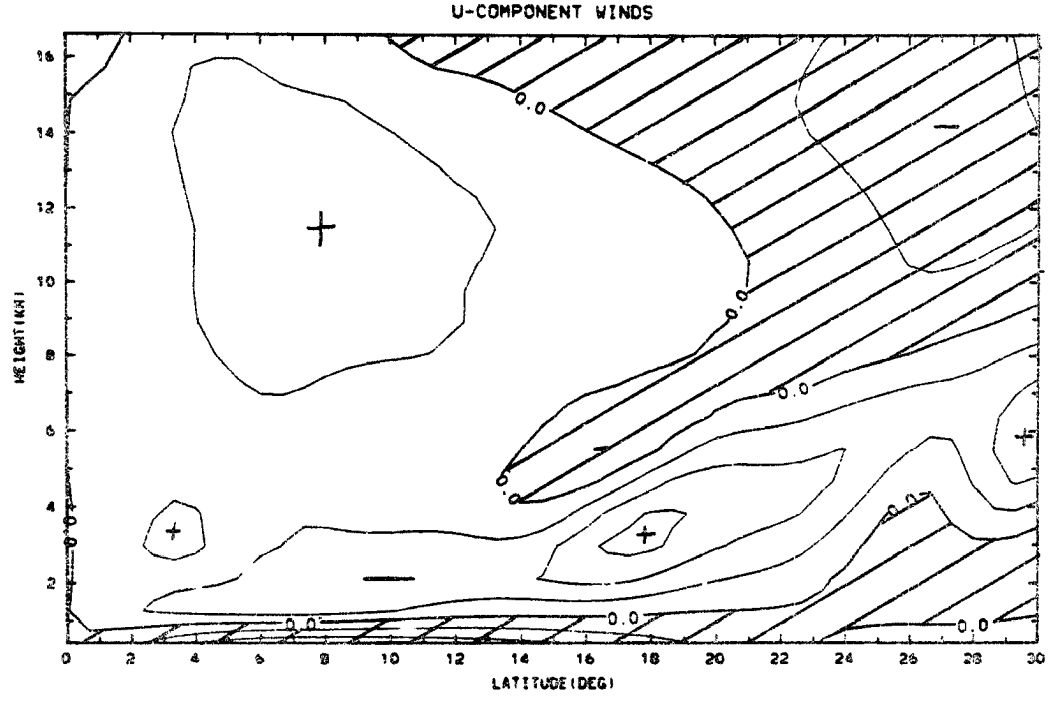

Fig. 3-7b. Run 2 (baseline model) u-winds at T=30 days.

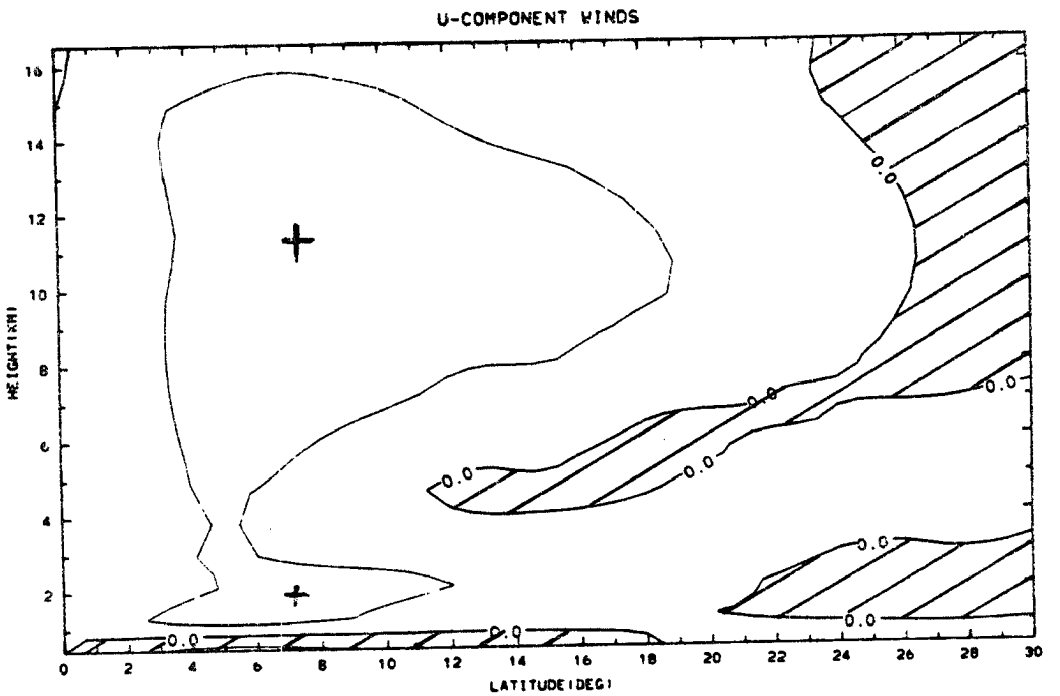

Fig. 3-7c. Run 2 (baseline model) u-winds at T=40 days.

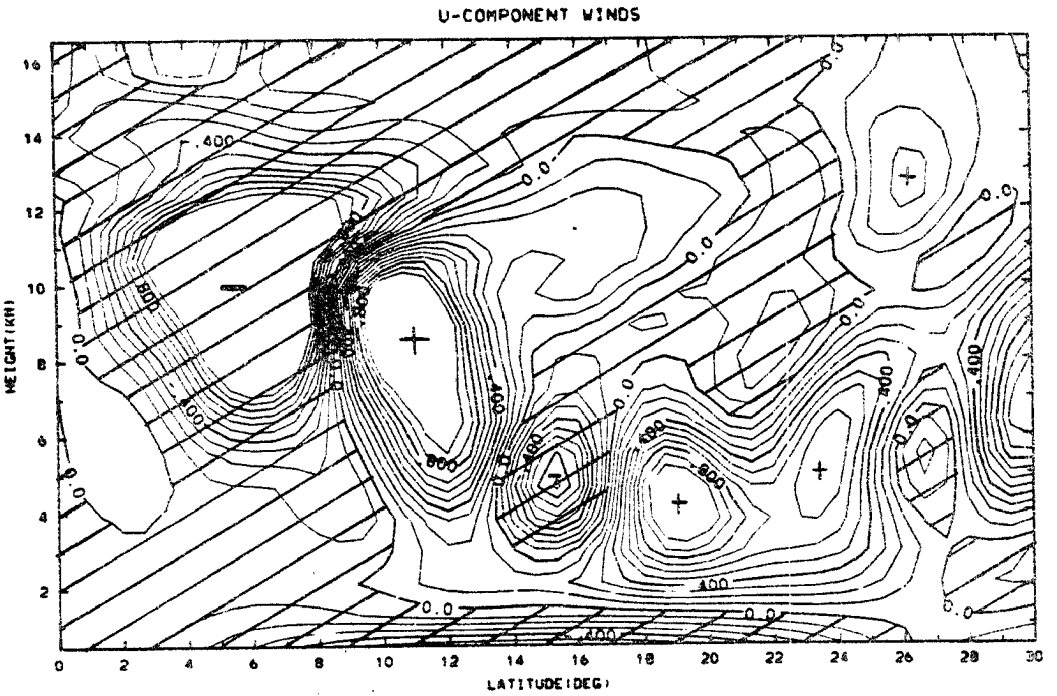

Fig. 3-8a. Run 3 u-wind field at T=20 days. Maximum contour is 1.0.

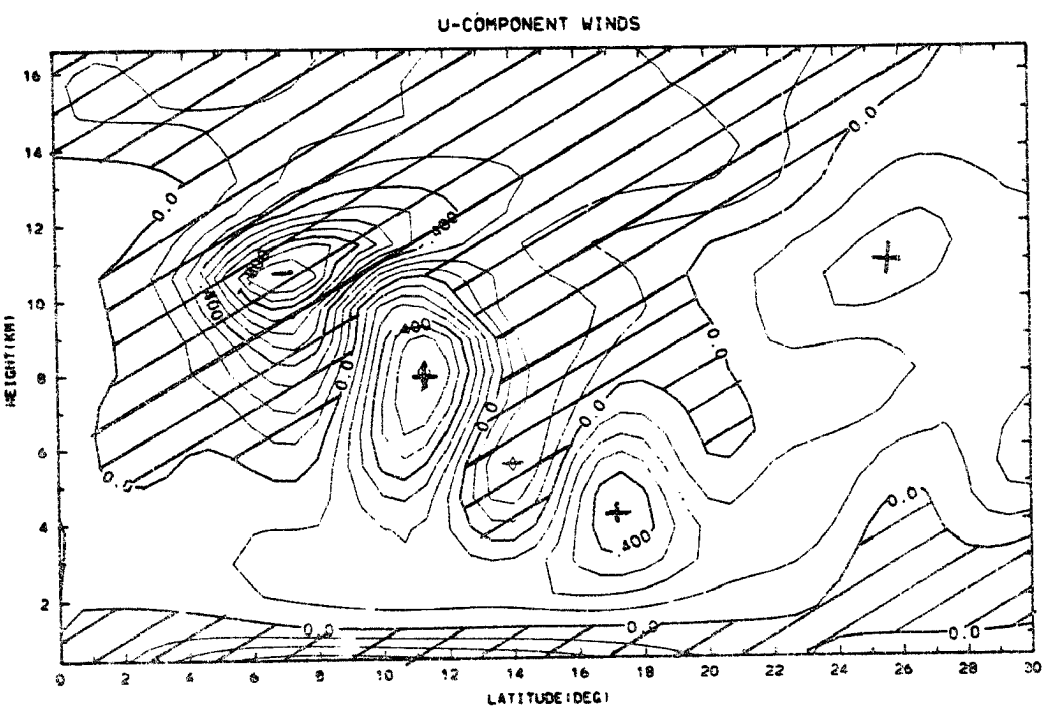

Fig. 3-8b. Run 3 u-wind field at T=30 days.

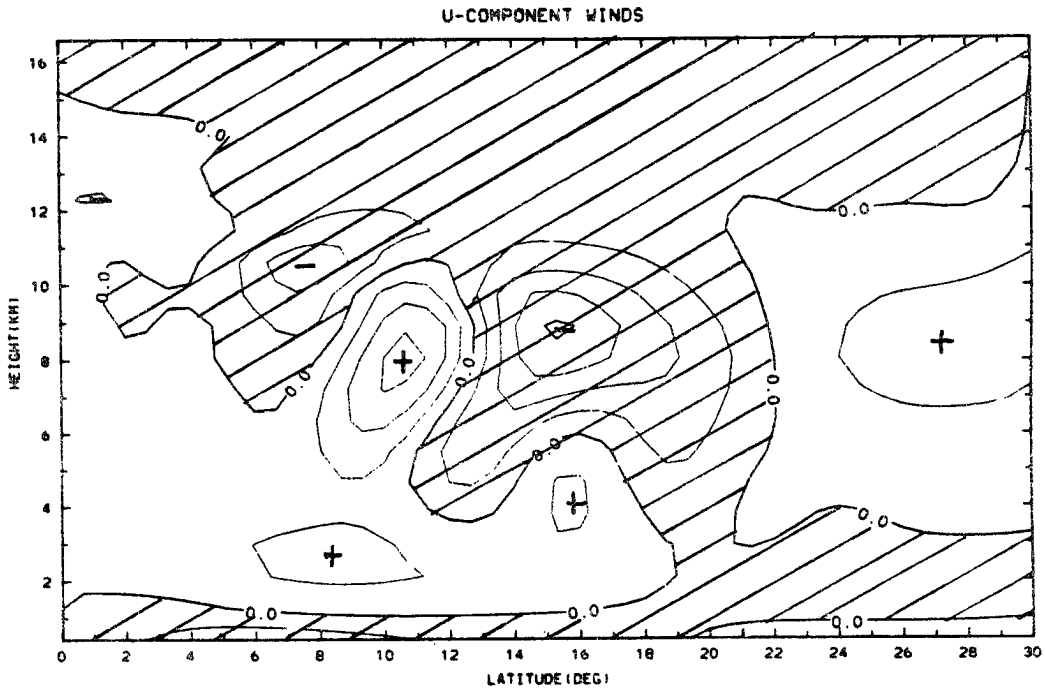

Fig. 3-8c. Run 3 u-wind field at T=40 days.

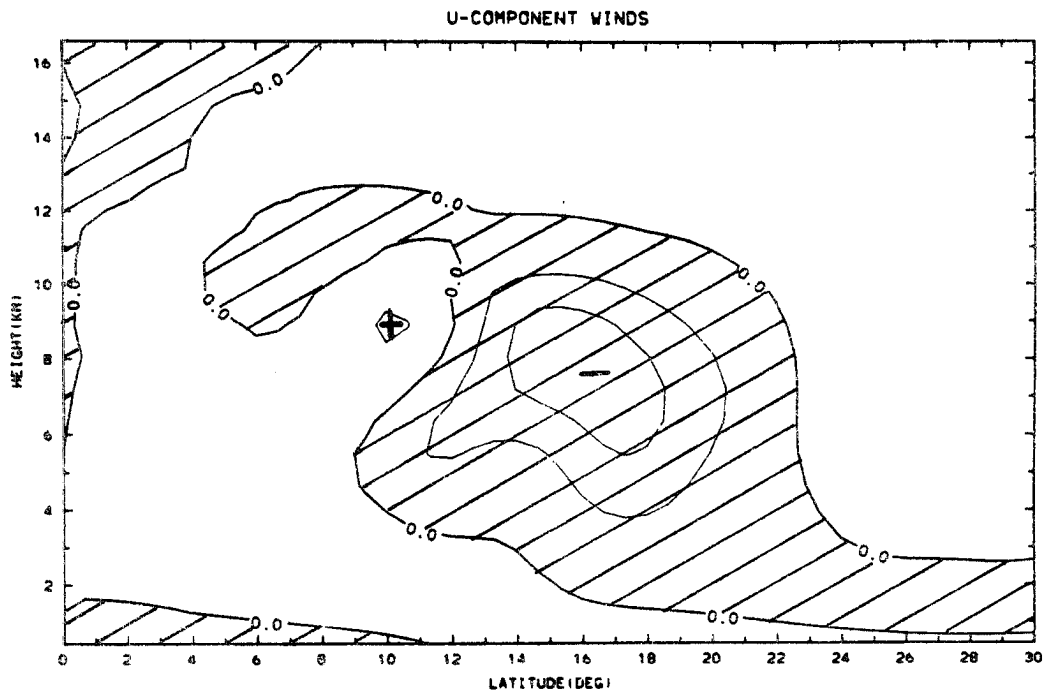

Fig. 3-8d. Run 3 u-wind field at T=50 days.

Fig. 3-9 we present the results of the non-linear basic state calculation for this truncation. Because of the equatorial symmetry of the basic state we can divide the eigenvalue problem into separate problems for the perturbation modes with equatorially even u-fields and odd u-fields. In this work we concentrate on the even modes because of the apparent nearly even equatorial symmetry of the observed oscillation (Anderson and Rosen, 1983) and the susceptibility of the odd modes to the fast growing inertial instabilities described by Dunkerton (1982) and Stevens (1983) due to their u-wind shear at the equator.

In Fig. 3-10 we plot a scatter diagram of the eigenvalues of the system for a resting basic state with $\bar{M}_c=M'_c=Q'=0$. Note the clean separation of the eigenvalues between exponentially decaying thermal wind modes and fast oscillating gravity modes. Next we include the effects of the Hadley cell basic state while still taking $\bar{M}_c=M'_c=Q'=0$. The results, plotted in Fig. 3-11, show that now there are a set of slow oscillatory modes in addition to the gravity modes. One of those modes with a period of ~52 days has a very slow decay time and is circled on the plot. The u-field structure of this mode is presented as Fig. 3-12 and is in good agreement with the prognostic runs clearly showing the poleward propagation in phase. The v-field is approximately two orders of magnitude smaller than the u-field and the θ-field is in thermal wind balance with the u-winds. In Fig. 3-13 we present the mode structure when $\bar{M}_c$ is set to baseline value and $M'_c=Q'=0$. For this case there are a set of modes with periods from ~30 to ~50 days which decay at approximately the same rate. This is in agreement with the broader frequency response seen in the prognostic runs. Finally, we add the representation for Q' and M'_c given in the Stevens-Lindzen

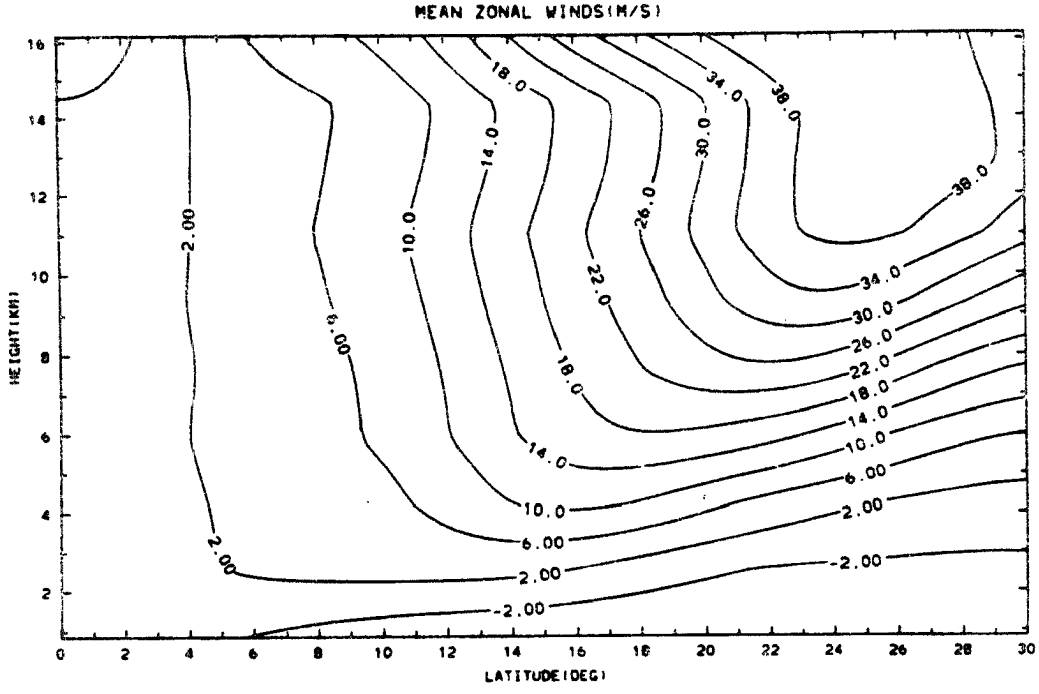

Fig. 3-9a. Basic state u=wind field for N_z=10, 10 meridional wavenumbers.

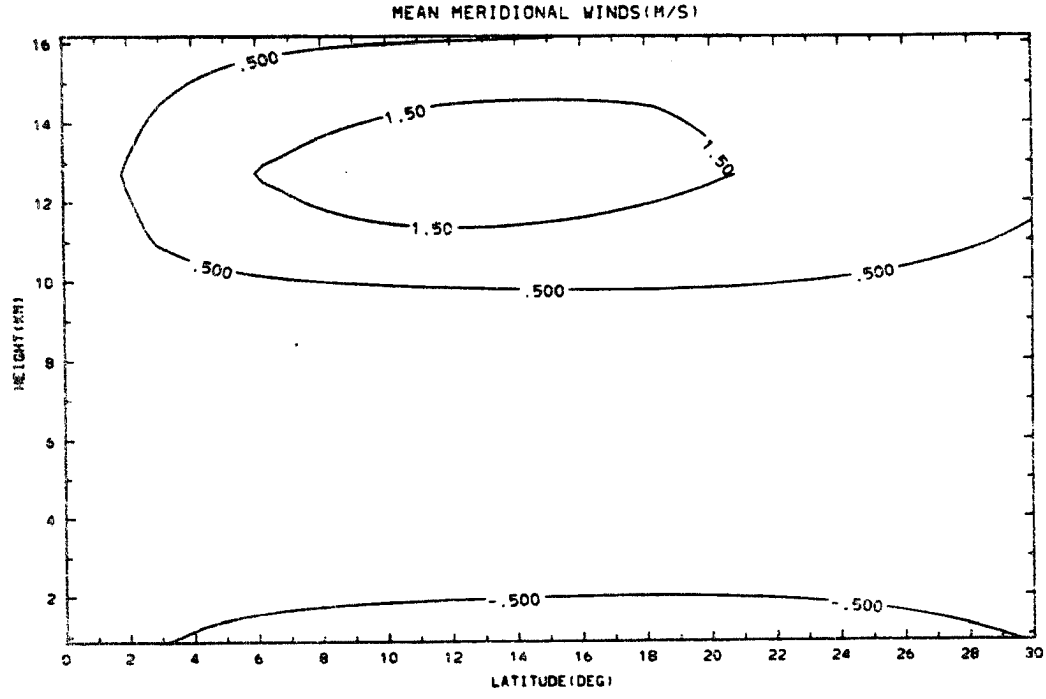

Fig. 3-9b. Basic state v-wind field for N_z=10, 10 meridional wavenumbers.

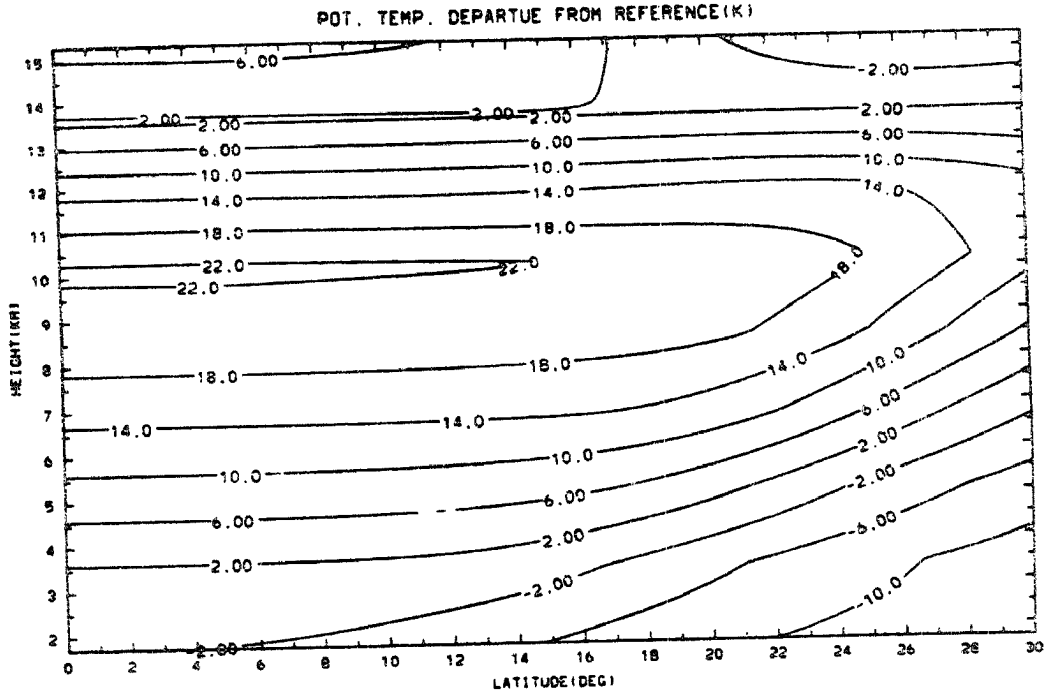

Fig. 3-9c. Basic state potential temperature field for N_z=10, 10 meridional wavenumbers.

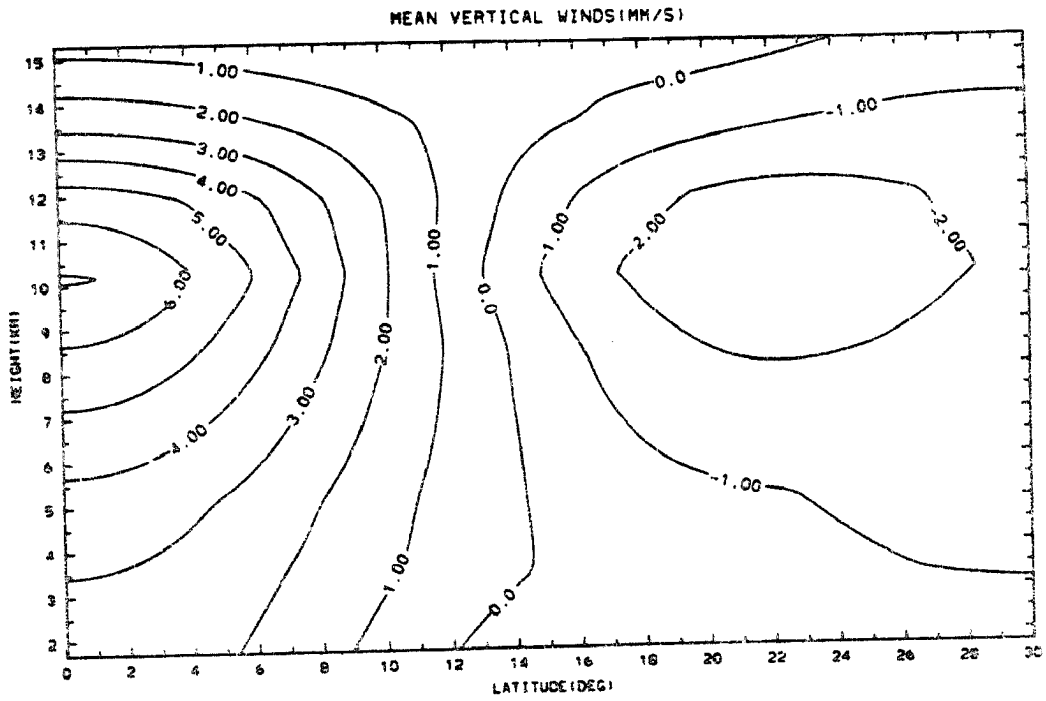

Fig. 3-9d. Basic state w-wind field for N_z=10, 10 meridional wavenumbers.

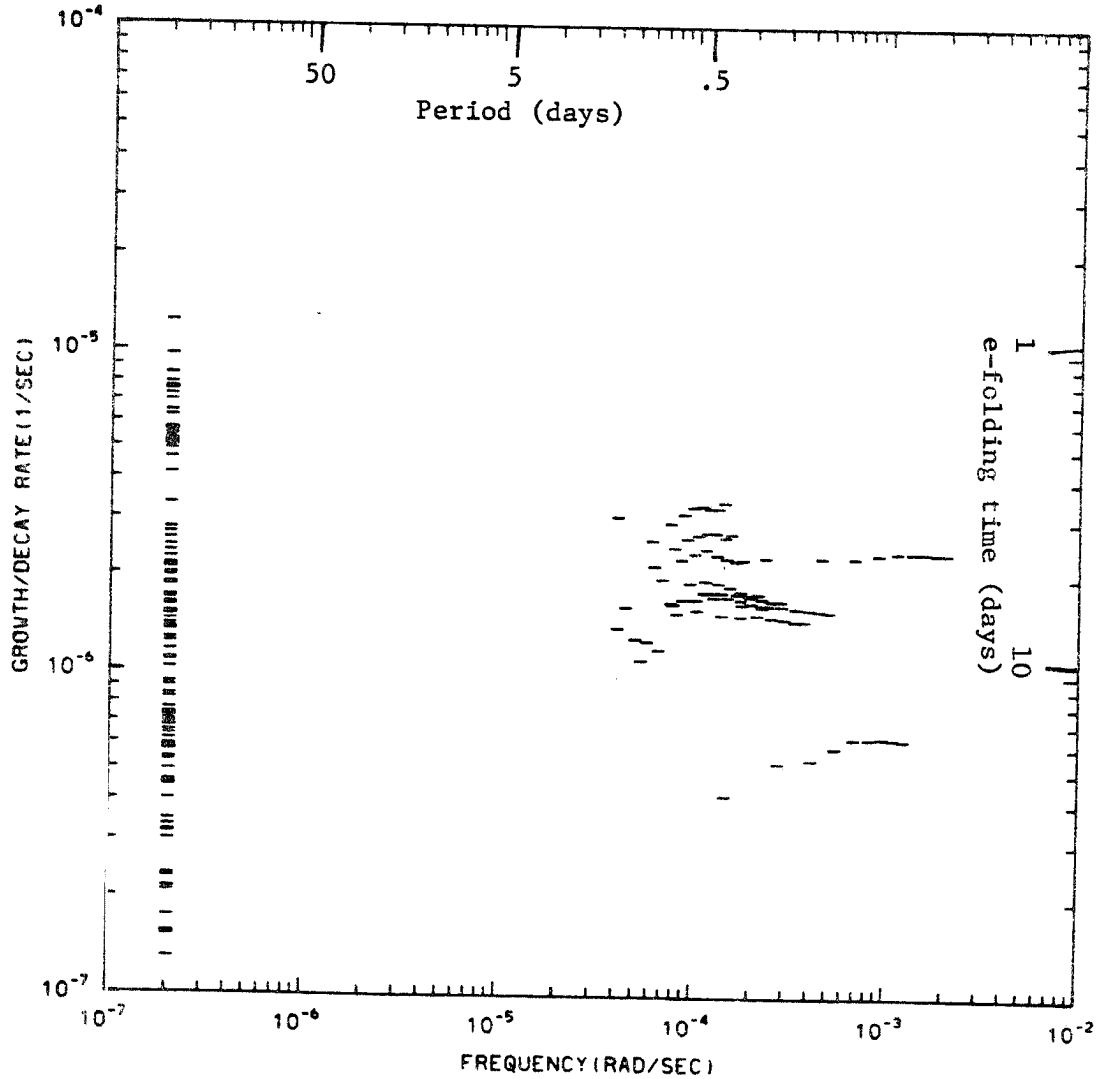

Fig. 3-10. Model normal mode complex frequencies for resting basic state. Modes with frequency <2. 10^{-7} rad/sec are plotted there. Damped modes are plotted as -, growing modes as +.

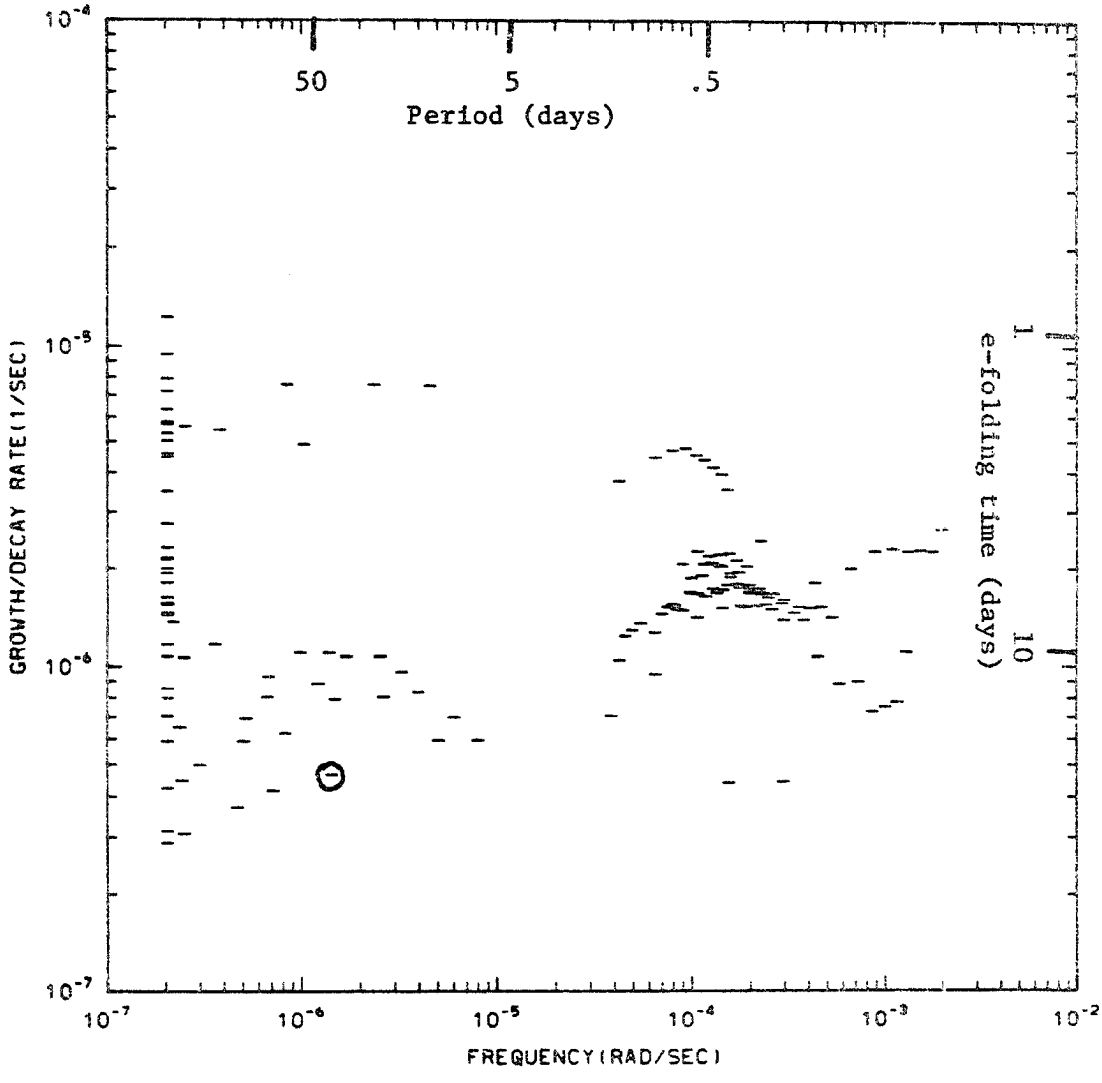

Fig. 3-11. Like Fig. 3-10 for parameters like run 3.

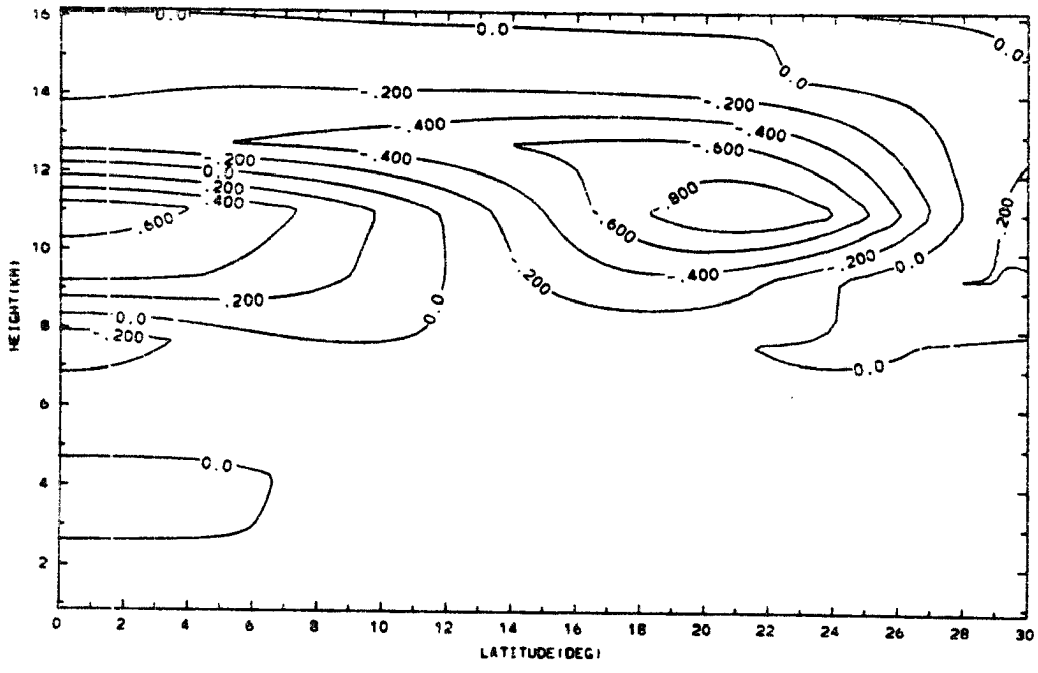

ωt=0°

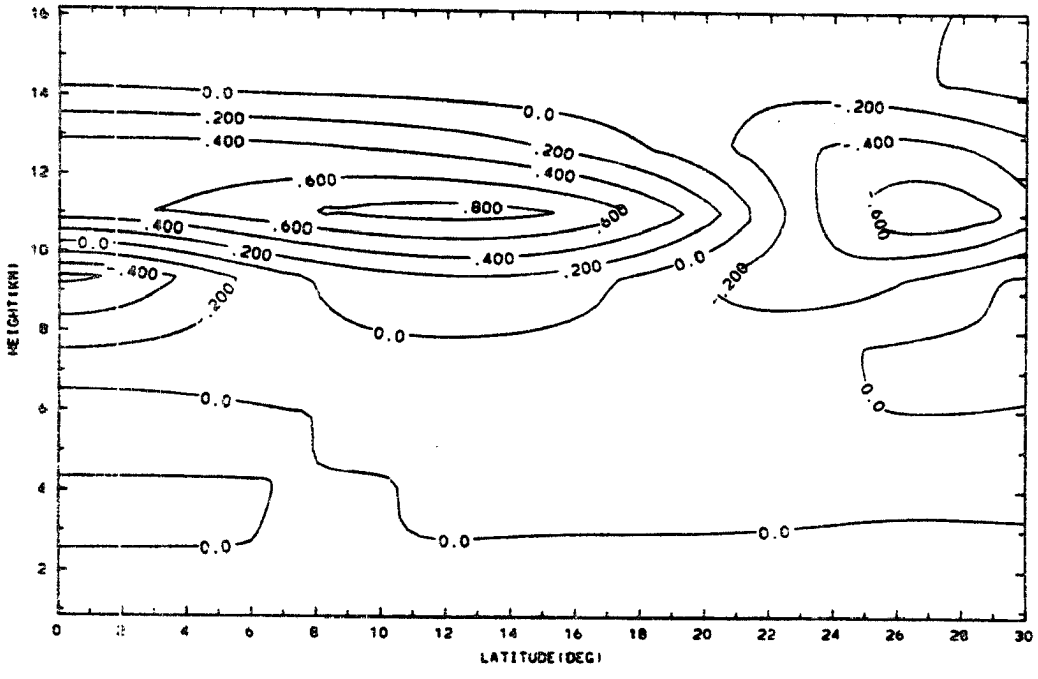

ωt=90°

Fig. 3-12. Spatial u-wind structure of mode which is circled on Fig. 3-11.

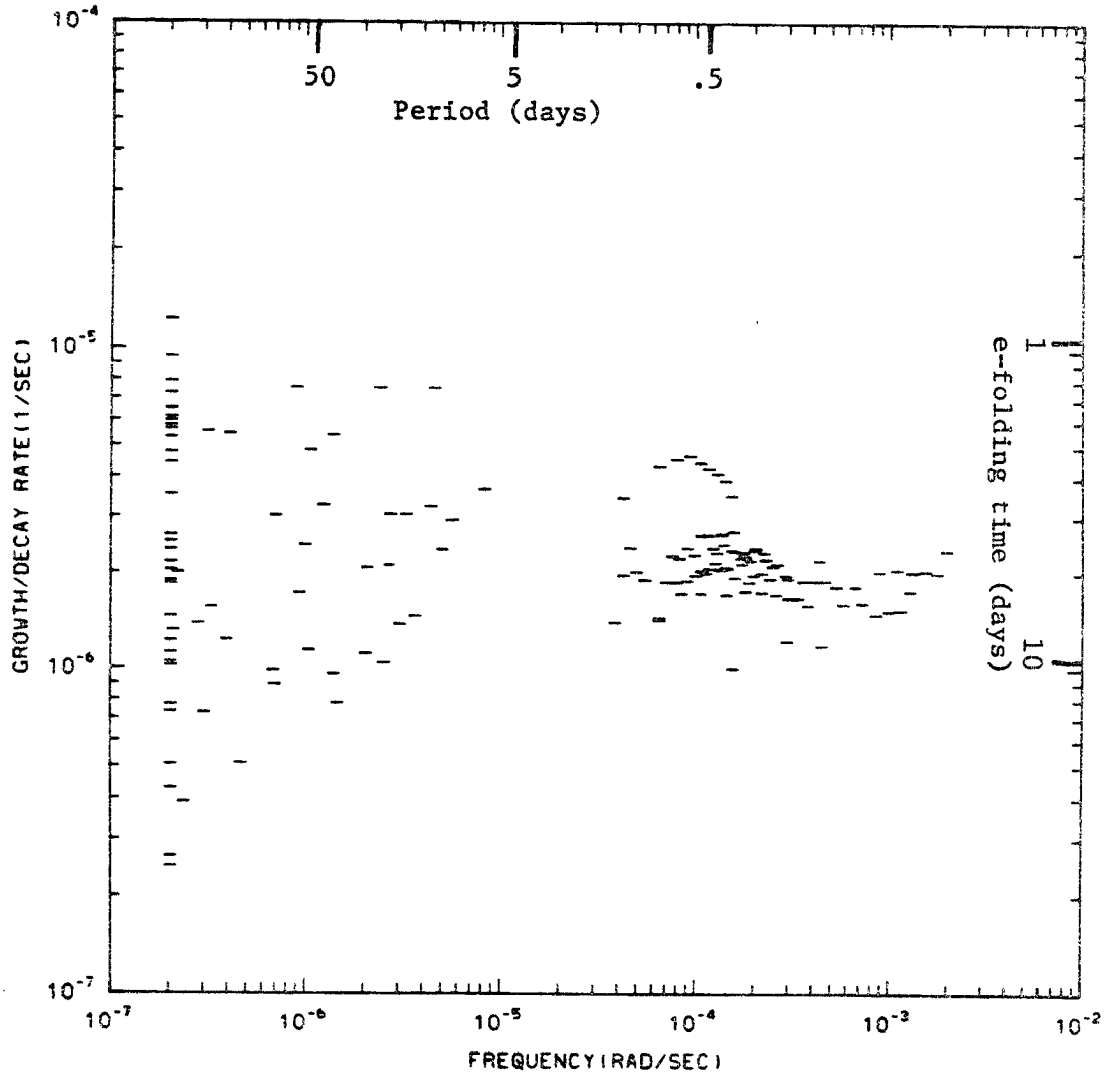

Fig. 3-13. Like Fig. 3-10 for baseline model.

parameterization scheme to produce the results which are shown in Fig. 3-14. In this set there are now some fast growing unstable modes which are marked with boxes. These modes are fast gravity waves which are destabilized by the convection. The slow modes on the other hand are essentially unchanged.

The inability of the current model to allow the slow modes to interact with the latent heating field is somewhat disappointing due to the strong evidence for such an association in the observed oscillation. This lack of response by the model slow modes is not too surprising since the Stevens-Lindzen scheme links latent heat release to boundary layer convergence and the model slow modes are essentially non-divergent. A more complete cumulus parameterization scheme would have to take into account the dependence of the convection on changes in the static stability and the effect of the zonal circulation on the tropical wave disturbances in which the clouds themselves are embedded.

In summary, the inclusion of a basic state Hadley circulation in the model creates a new class of slow oscillating modes which are capable of producing response peaks in the 40-50 day range from forcing which is random in time. The model however fails to couple the slow modes to cumulus heating when a simple moisture convergence cumulus parameterization is used.

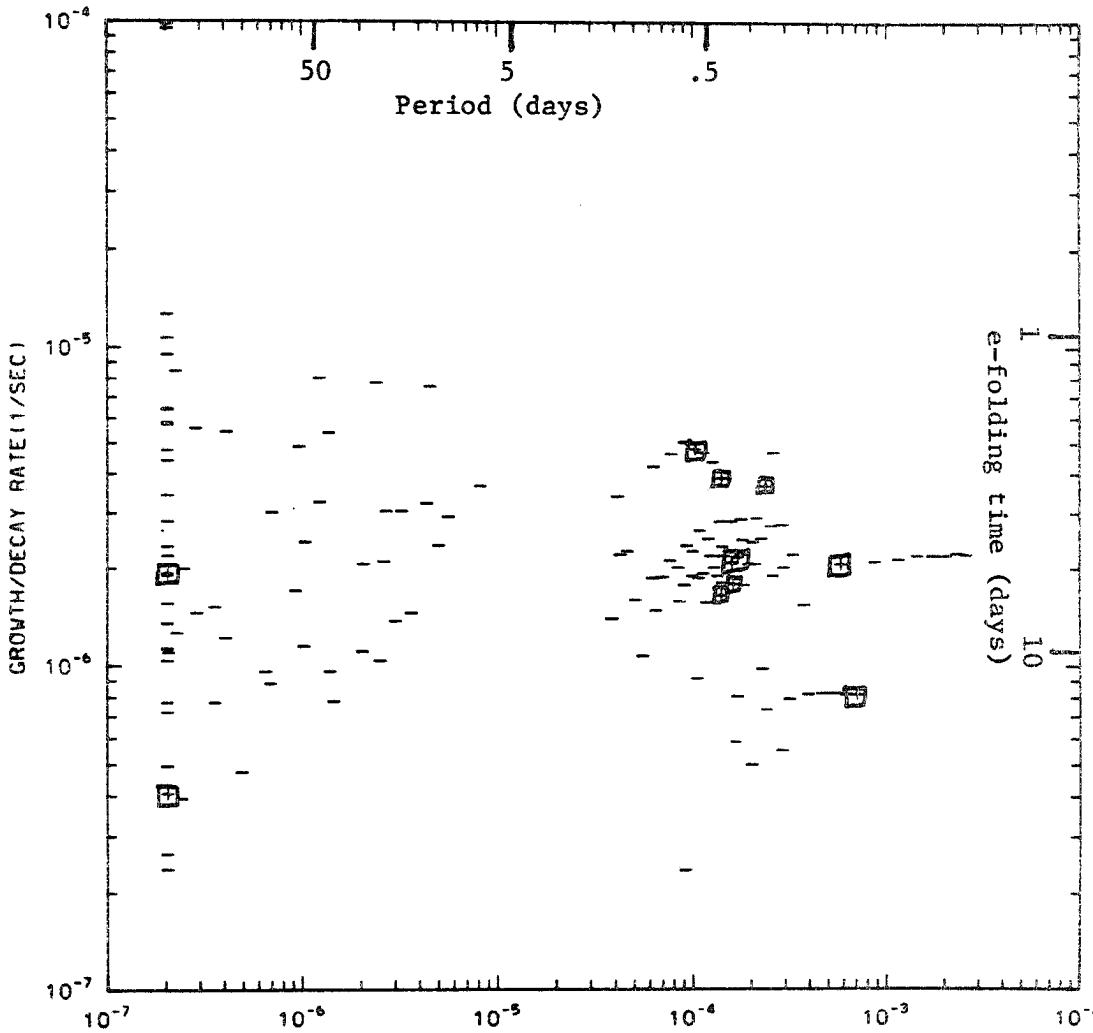

Fig. 3-14. Like Fig. 3-10 for baseline model with Stevens-Lindzen cumulus parameterization.

4. TROPICAL RESPONSE TO LOW FREQUENCY THERMAL FORCING

In the previous chapter we discussed the free wavenumber 0 modes of a tropical atmosphere. We found that when the effects of the basic state Hadley circulation were included the atmosphere tended to exhibit an amplified response in the 30-60 day period region due to the presence of model eigenmodes with those frequencies. On the other hand we were not able to couple the model slow modes to a feedback related cumulus heating using a simple moisture convergence model. Since there appears to be no question (Yasanari, 1980; Julian and Madden, 1981) that the observed oscillation is related to enhanced cloudiness and presumably latent heat release, we will now investigate the response of the tropical atmosphere to this thermal forcing.

The investigation of the forced response will be conducted in several steps. First we examine the shallow-water model results reported by Yamagata and Hayashi (1984), which is one of the simplest possible approaches to the problem. Next we will extend the Yamagata and Hayashi model to include the effects of a zonal mean flow which depends only on latitude, and finally we will investigate the zonally symmetric and non-symmetric responses when a full Hadley cell basic state is included.

The derivation of the model which Yamagata and Hayashi used follows closely the model developed by Gill (1980) to study the tropical response to steady state forcing. It is based on the separation of the

problem in the vertical and horizontal directions. The forcing is then projected onto one eigenmode of the resulting vertical structure problem and the evolution of the system can be studied by solving a set of shallow water like equations. The most general basic state for which this separation can be accomplished is given by $\bar{u}=\bar{u}(y)$, $\bar{v}=0$, $\bar{w}=0$, $\partial\bar{\theta}/\partial y = 0$ and yields the following system for the horizontal structure problem;

$$\frac{\partial u}{\partial t} + \bar{u}\frac{\partial u}{\partial x} - fv = -\frac{\partial \phi}{\partial x} - \alpha u \tag{4.1a}$$

$$\frac{\partial v}{\partial t} + \bar{u}\frac{\partial v}{\partial x} + fu = -\frac{\partial \phi}{\partial y} - \alpha v \tag{4.1b}$$

$$\frac{\partial \phi}{\partial t} + \bar{u}\frac{\partial \phi}{\partial x} = -gH\left(\frac{\partial u}{\partial x} + \frac{\partial v}{\partial y}\right) + Q - \alpha\phi. \tag{4.1c}$$

Here $u(x,y,t)$, $v(x,y,t)$ and $\phi(x,y,t)$ are the horizontal structure variables defined by $u(x,y,z,t) = u(x,y,t)\cdot\hat{u}(z)\ldots$, where $\hat{u}(z)$, $\hat{v}(z)$, and $\hat{\phi}(z)$ are the eigenvectors of the vertical structure problem. H is the equivalent depth which is determined from the eigenvalue of the mode which the forcing is taken to be projected onto, $Q(x,y,t)$ is the amplitude of the forcing and $\alpha(y)$ is a simple Rayleigh friction/ Newtonian cooling representation for the dissipation. With this choice of heating sign the wind field sign corresponds to the upper level winds for the original stratified fluid.

Yamagata and Hayashi also made an additional approximation to the above system known as the "long-wave" approximation which involves ignoring the terms involving v in (4.1b); however, as will be evident, this makes no noticeable difference in the solution. Since the system is constant coefficient in the x-direction, it is traditional to take a

discrete Fourier series representation in that direction yielding

$$\frac{\partial u^k}{\partial t} + \bar{u}\cdot ik u^k - f v^k = - ik\phi^k - \alpha u^k \tag{4.2a}$$

$$\frac{\partial v^k}{\partial t} + \bar{u}\cdot ik v^k + f u^k = - \frac{\partial \phi^k}{\partial y} - \alpha v^k \tag{4.2b}$$

$$\frac{\partial \phi^k}{\partial t} + \bar{u}\cdot ik\phi^k = - gH(iku^k + \frac{\partial v^k}{\partial y}) + Q^k - \alpha\phi^k, \tag{4.2c}$$

where $a(x,y,t) = \sum_k a^k(y,t) \exp(ikx)$.

Now if we use a suitable discretization in the y direction we can write the system in schematic form as

$$\frac{\partial \underline{S}^k}{\partial t} = \underline{\underline{A}}^k \underline{S}^k + \underline{Q}^k$$

where the matrix $\underline{\underline{A}}^k$ represents the time derivative operator, which can be found in the same way as the system derived in Chapter 2. If we take the system to be stable (real part of all eigenvalues of $\underline{\underline{A}} < 0$) and the forcing $\underline{Q}^k \alpha \exp(i\omega t)$ then we can represent the forced system by the matrix problem

$$i\omega \underline{R}^k = \underline{\underline{A}}^k \underline{R}^k + \underline{Q}^k$$

or $$(i\omega \underline{\underline{I}} - \underline{\underline{A}}^k)\, \underline{R}^k = \underline{Q}^k, \tag{4.3}$$

where $\underline{R}^k$ is the system response vector for zonal wavenumber k. The complete response is then determined by solving (4.3) to get $\underline{R}(x,y)$ for each zonal wavenumber component of the forcing and summing the results.

Yamagata and Hayashi used the parameters previously determined by Gill, which are listed below, and simply made the forcing oscillatory.

$$Q = \begin{cases} \exp(i\omega t)\cdot\exp\left[-\left(\frac{y}{L_y}\right)^2\right] \cdot \cos(k_x x) & k_x x < \pi \\ 0 & k_x x > \pi \end{cases}$$

$L_y = 2.34\cdot10^6$ m

$k_x = \pi/(9.4\cdot10^6$ m)

$\alpha = 1/(2.2$ days)

$\bar{u} = 0$

$\omega = 2\pi/(45$ days)

A plot of the heating field is given in Fig. 4-1. It should be noted that the y-extent of the heating is rather large and the damping time is very fast, even by tropical standards; these points will be addressed later.

The result of solving (4.3) using the Yamagata and Hayashi parameters on a domain extending from 60°S to 60°N with 20 meridional wavenumbers zonal wavenumbers ranging from -10 to 10 are shown in Fig. 4-2 and are essentially identical to those derived by Yamagata and Hayashi. Notice that for each variable the response at $\omega t=0$ is large compared to the propagating response depicted by $\omega t=90°$. This result is due to the damping time being significantly shorter than the oscillatory time scale ($\alpha >> \omega$). In fact the results are nearly identical to those obtained by Gill for $\omega=0$.

The next case we will consider is for a case where $L_y=1.125\cdot10^6$ m which appears to be more in keeping with the observed convection and the same dissipation used in our previous zonally symmetric calculations except that a minimum dissipative rate of 1/(12 days) is taken

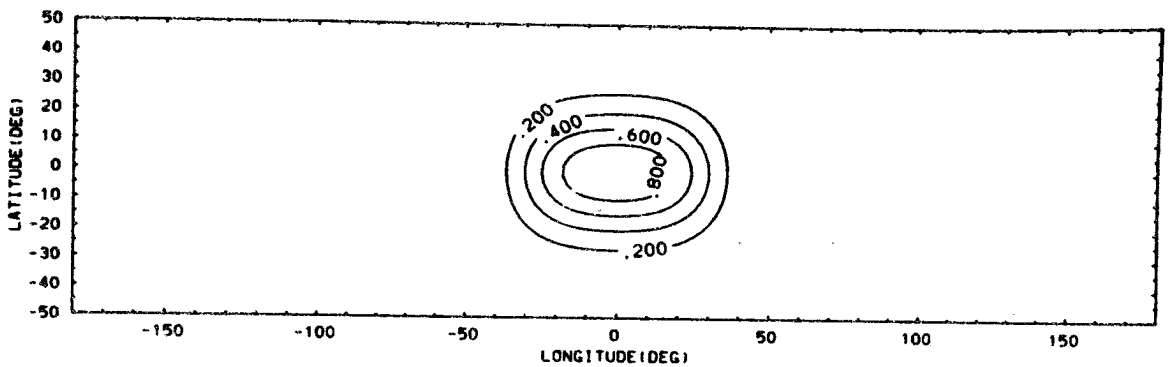

Fig. 4-1. Heating (mass source) field for Yamagata and Hayashi formulation.

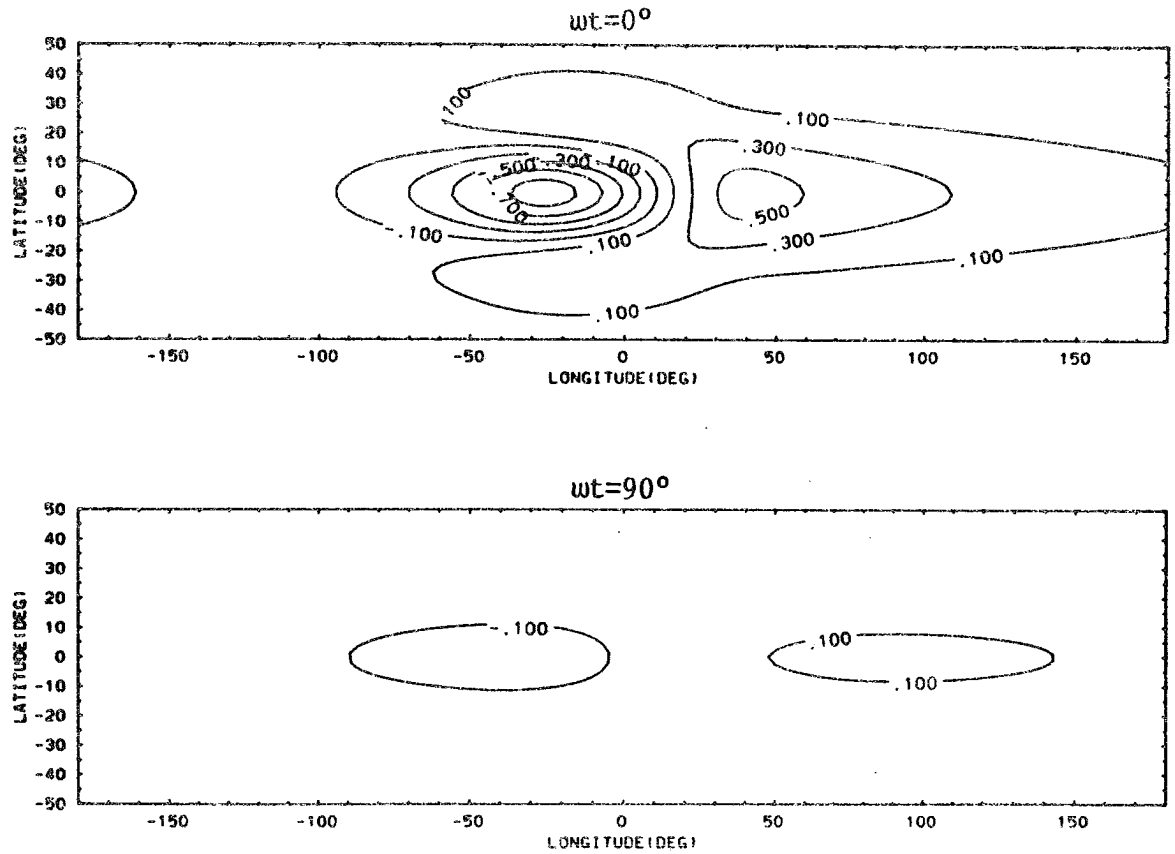

Fig. 4-2a. u-wind response for Yamagata and Hayashi problem formulation.

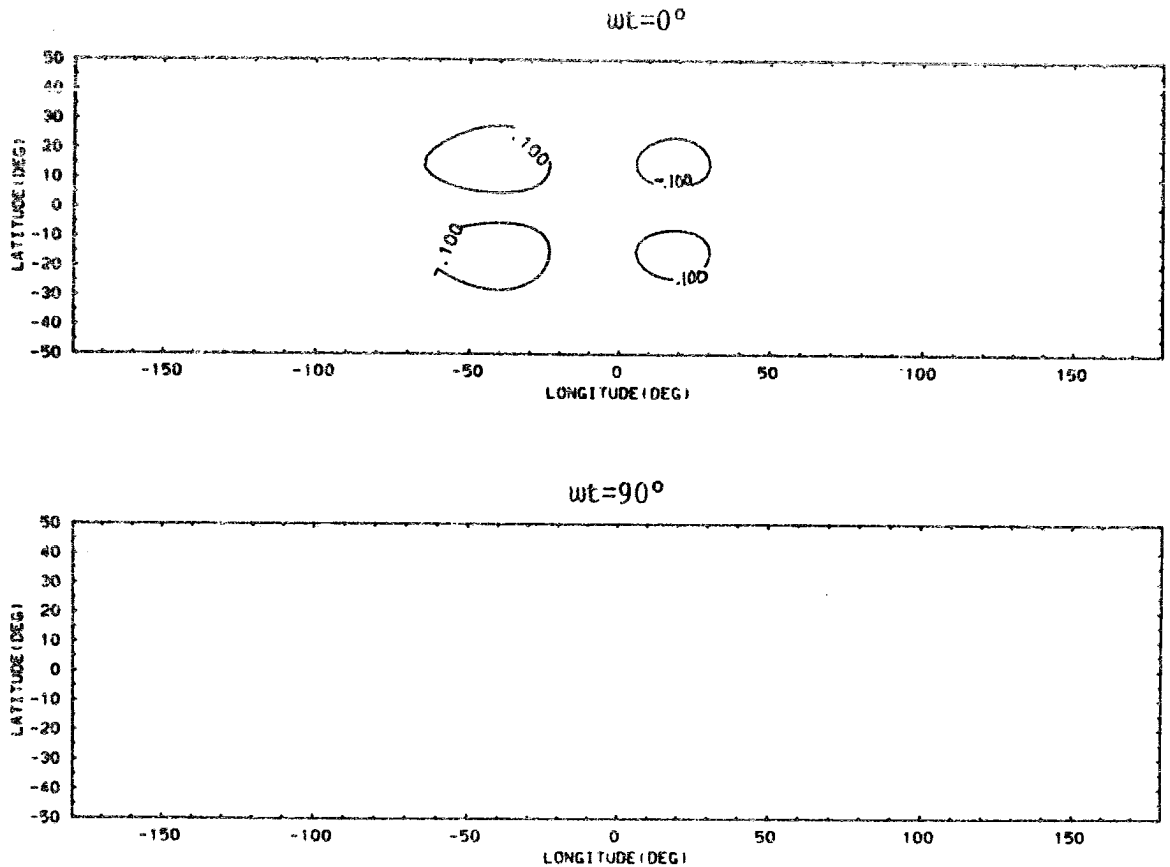

Fig. 4-2b. v-wind response for Yamagata and Hayashi problem formulation.

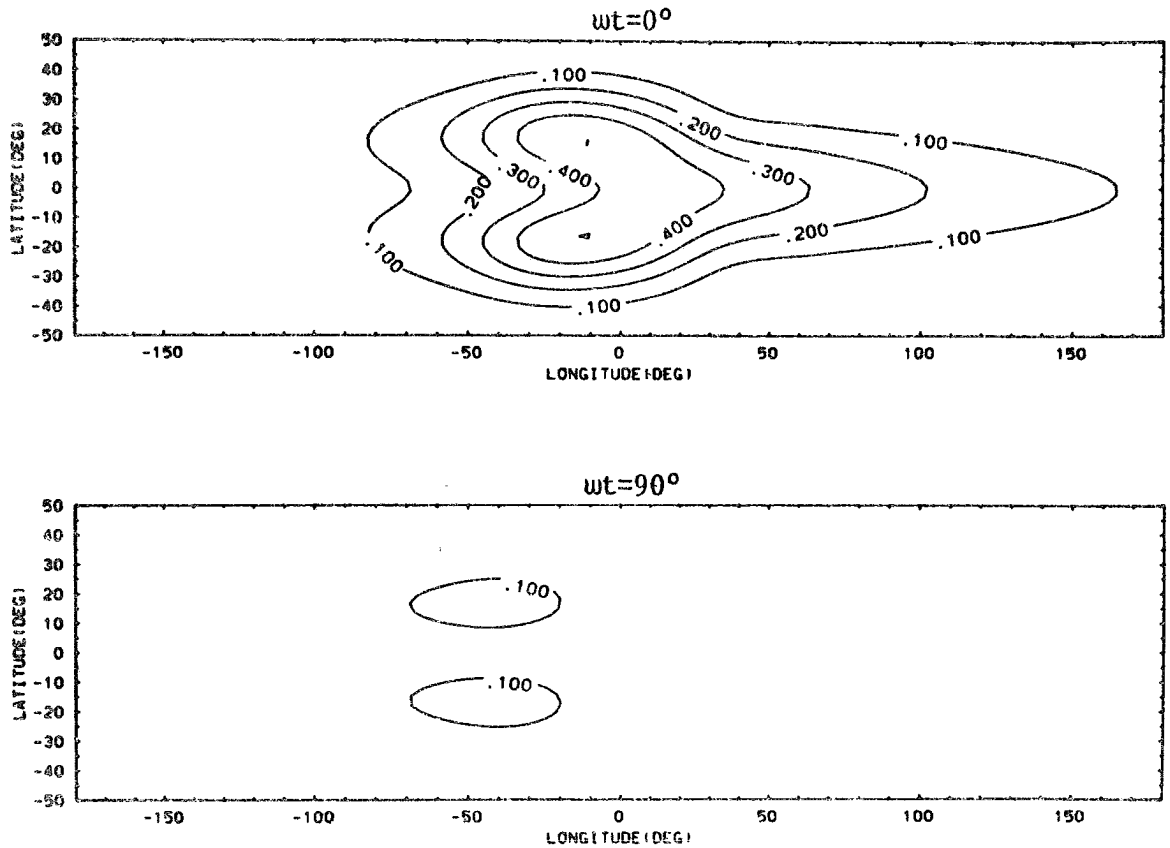

Fig. 4-2c. Geopotential response for Yamagata and Hayashi problem formulation.

due to our inability to include cumulus momentum mixing effects. The results of this calculation are shown in Fig. 4-3. Here we see a similar response field at $\omega t=0$; however, we now see a considerable amplitude westward-propagating Rossby wave displayed in the u-field and some evidence for slight poleward propagation, particularly in the region east of the heating. For this case the maximum response is on the equator at $\omega t=0$ and has a mainly wavenumber 1 character. The response at $\omega t=90$ has a much more zonally symmetric character, particularly in the subtropics (20° lat).

For the next case we will take the $\bar{u}$ field as the u-component wind field from our non-linear calculation at the 400 mb level. The choice of an "advective" wind level to be used with models of this type is a difficult one but 400 mb appears to be a reasonable choice (McWilliams, 1980).

The results of this calculation are shown in Fig. 4-4 and depict a much less smooth structure in the y-direction. These sharp variations are due to critical latitude for the model Rossby waves (latitudes where $c-\bar{u}=0$). Another effect of the basic state is to increase the amplitude of the meridional winds and the zonal winds in the area around 25° latitude.

Having studied the behavior of a system where $\bar{v}=0$ and $\bar{w}=0$, we are now interested in the effects of including a Hadley cell in the basic state. Based upon the results of the previous section one would expect the forcing to mainly project on the slow oscillating modes of the model and give rise to a response with features similar to the slow free modes.

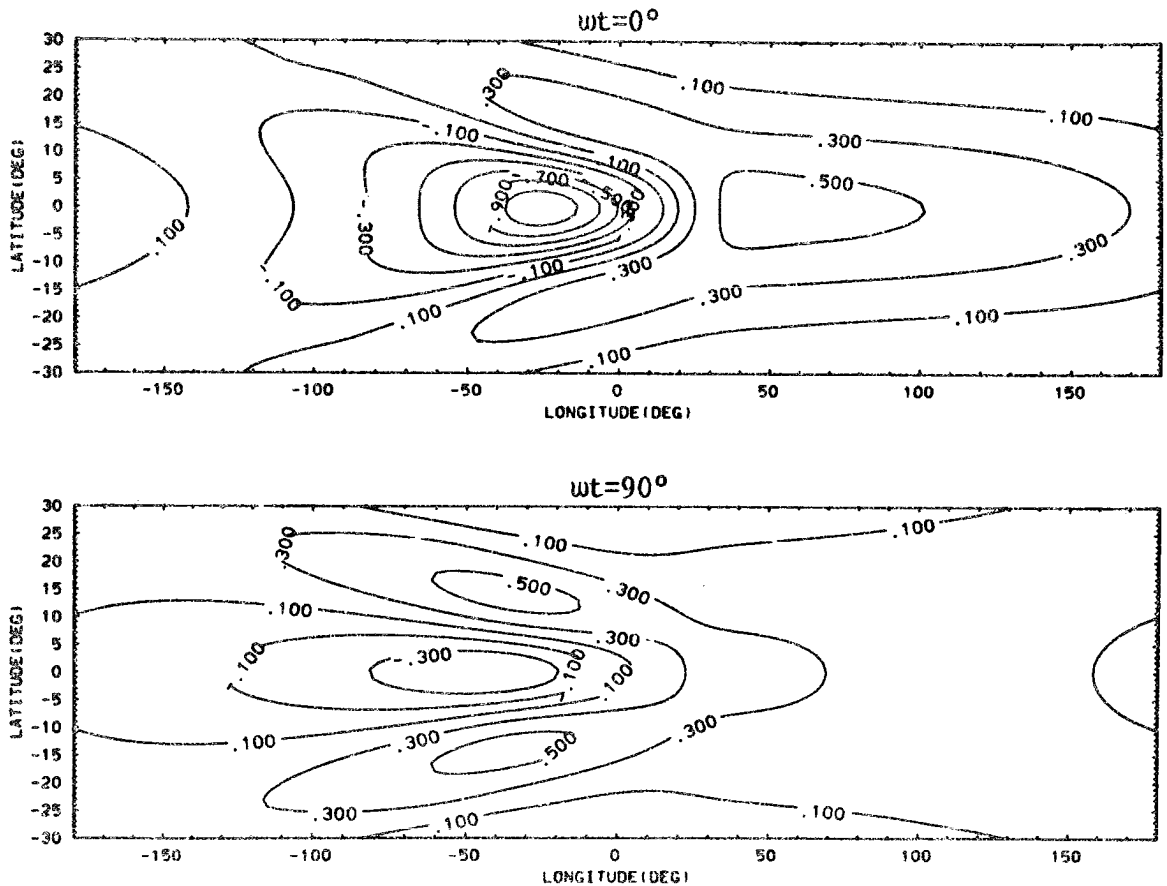

Fig. 4-3a. u-wind response for $\bar{u}$=0 but baseline-like dissipation.

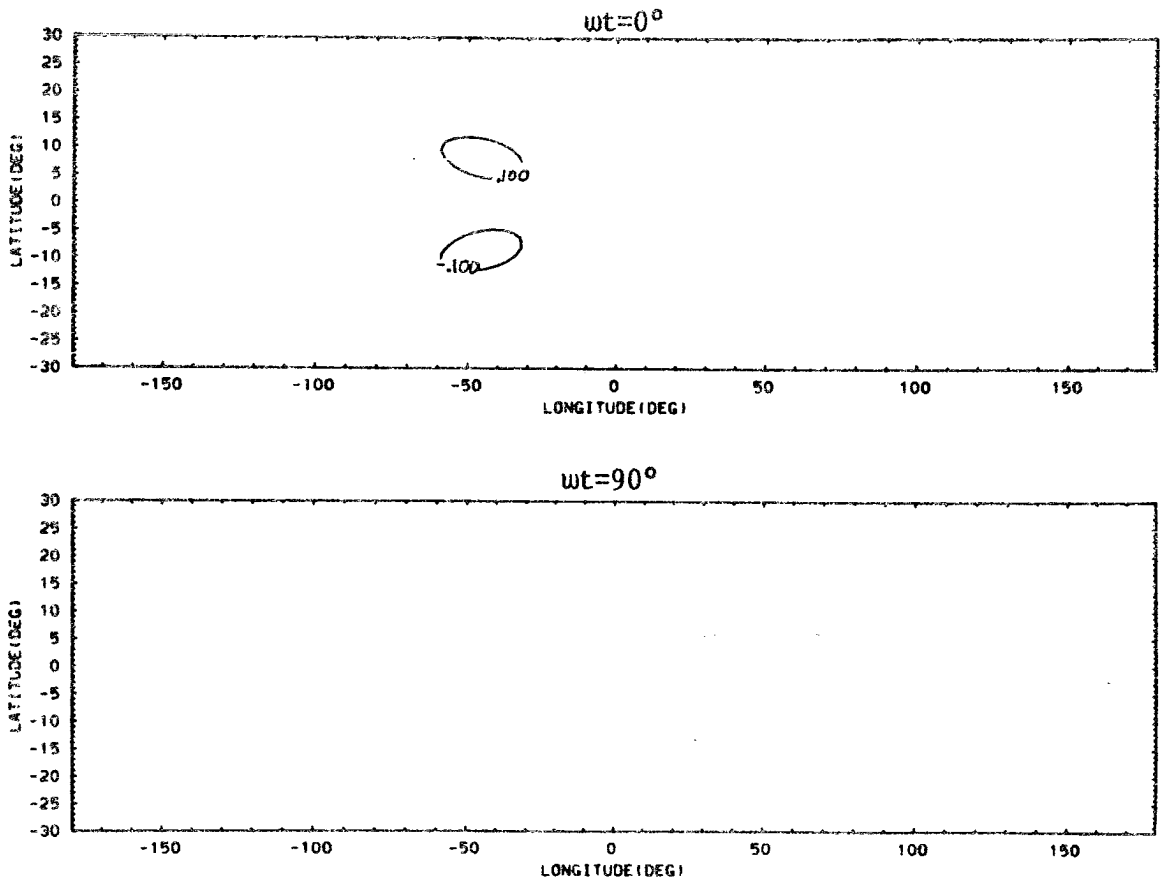

Fig. 4-3b. v-wind response for $\bar{u}$=0 but baseline-like dissipation.

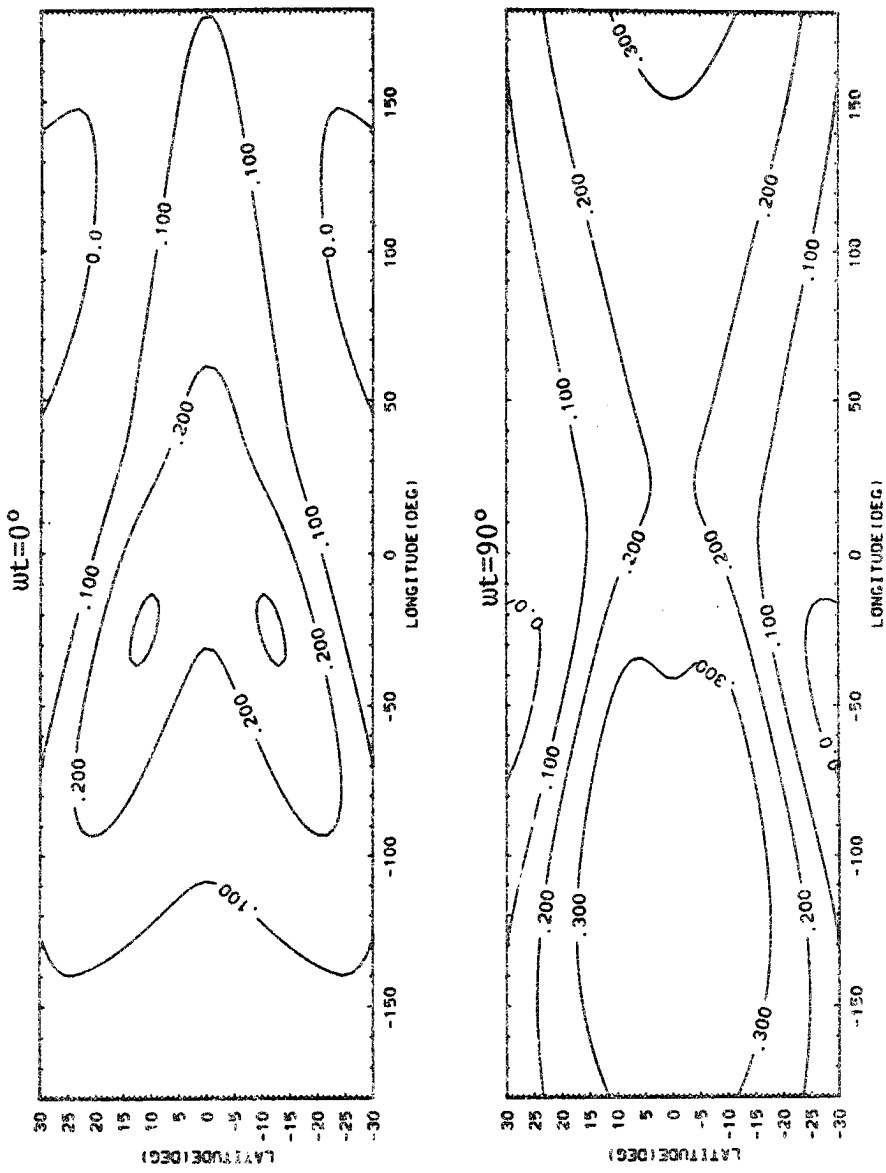

Fig. 4-3c. Geopotential response for $\bar{u}$=0 but baseline-like dissipation.

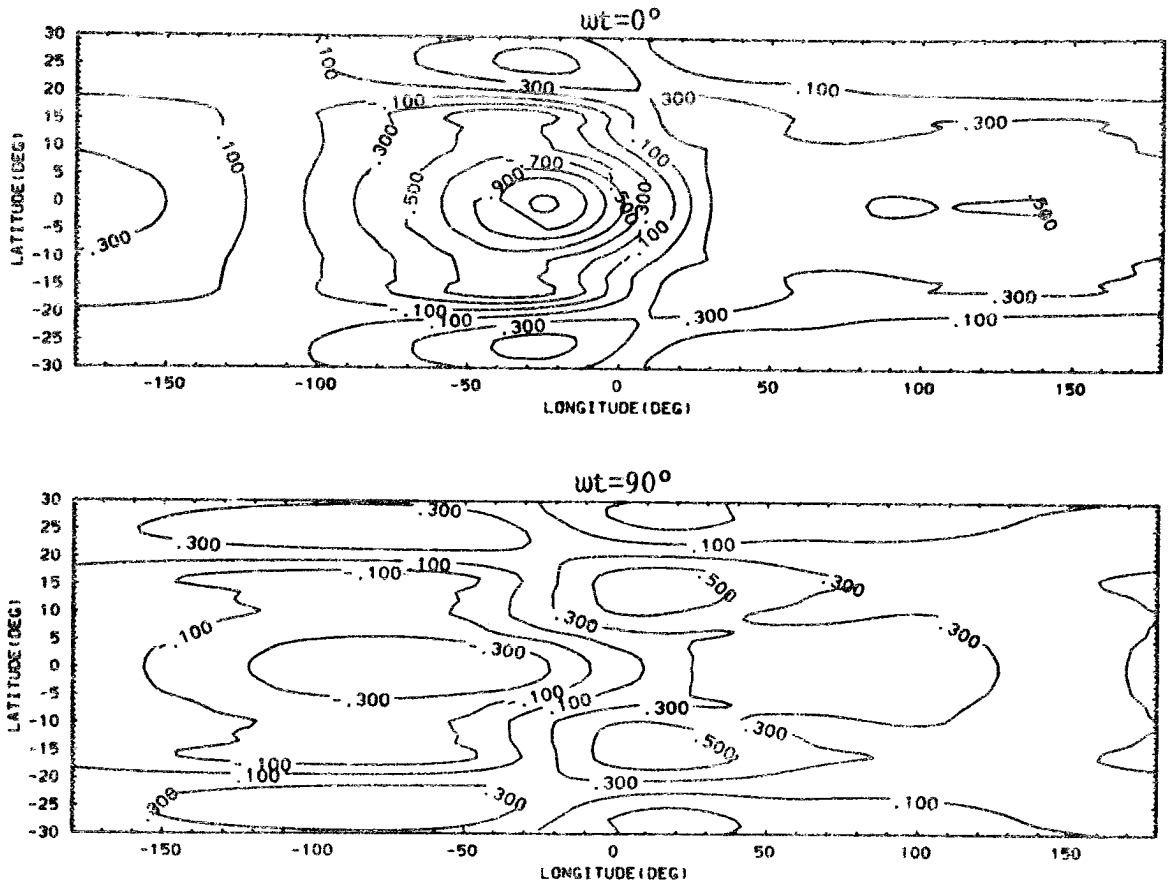

Fig. 4-4a. u-wind response for $\bar{u}=\bar{u}(y)$ and baseline-like dissipation.

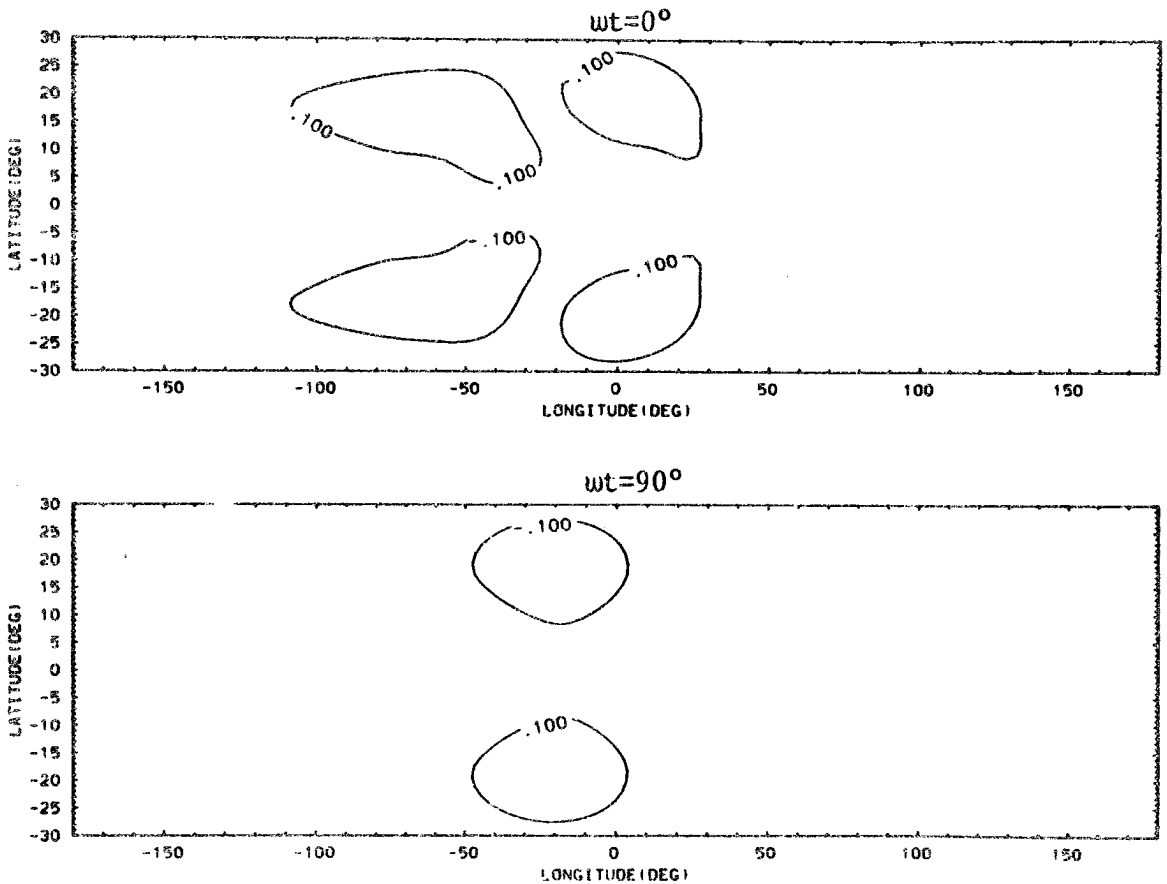

Fig. 4-4b. v-wind response for $\bar{u}=\bar{u}(y)$ and baseline-like dissipation.

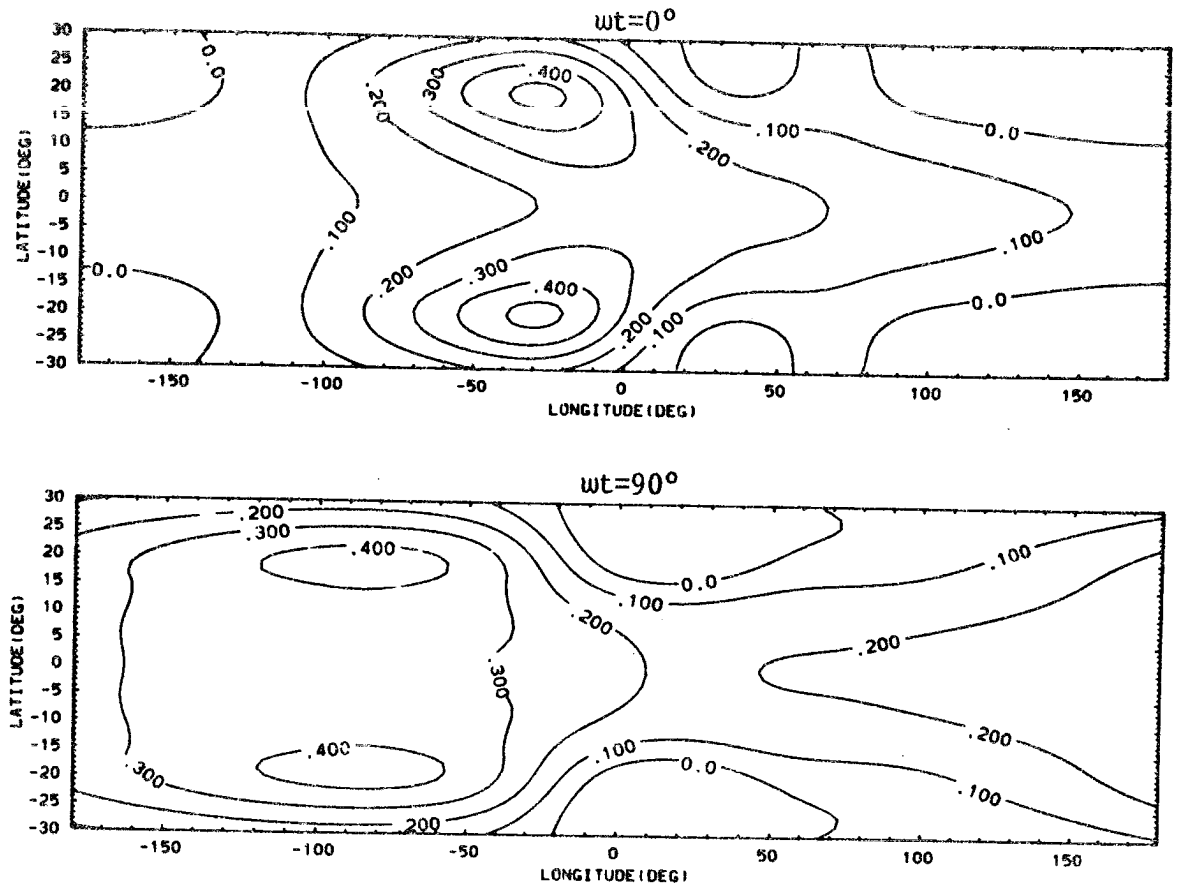

Fig. 4-4c. Geopotential response for $\bar{u}=\bar{u}(y)$ and baseline-like dissipation.

For this case we generate the solution by prognostically integrating the model which was used in the previous chapter with an oscillatory forcing until the model reaches a steady oscillatory response. All of the calculations reported here were done with the baseline model which includes a full cumulus momentum transport parameterization. The horizontal structure of the heating is taken to be the same as in the two previous calculations and the vertical structure is taken to be a gaussian centered at 400 mb with a 1/e distance of 5.1 km (6 grid points) full width.

We will first consider the zonally symmetric response. The results of this calculation are presented in Figs. 4-5 through 4-8. In 4-5a we present the u-wind response when $\omega t = -90°$. At this time the heating amplitude is zero and increasing in magnitude. The figures show an easterly maximum centered in the upper troposphere at about 22° latitude and a westerly maximum in the middle troposphere at 10° latitude. The potential temperature field is in near thermal wind balance with the u-wind and the v-wind field is small except in the region of the heating. In the next figure at $\omega t = -45°$ we see the westerly winds strengthening while the easterly flow weakens. At this point easterly winds appear on the surface between 10° and 20° latitude. At $\omega t=0$, which is the time of maximum heating, the westerly maximum is now propagating poleward and at this point the westerlies extend over the whole domain upper troposphere and the easterly maximum is now near the surface and moving equatorward. There is also a region of easterlies remaining in the equatorial stratosphere. An interesting point here is that at this time when the heating is at a maximum, the potential temperature field shows a clear minimum in the equatorial upper troposphere with a maximum in the lower troposphere, indicating a reduction

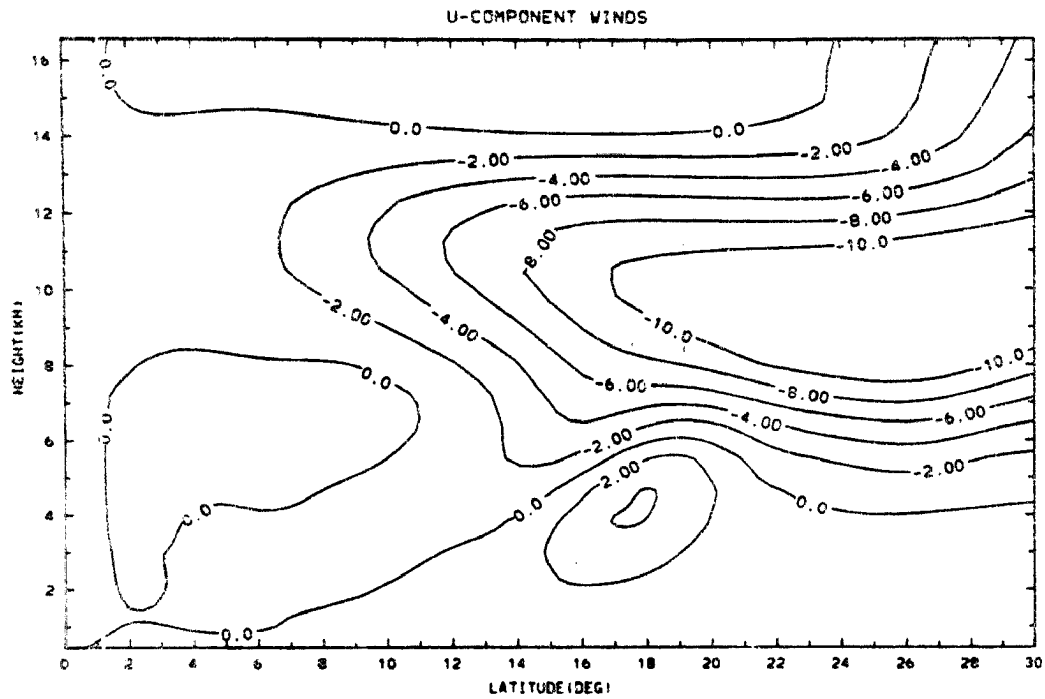

Fig. 4-5a. Forced zonally symmetric u-winds at ωt=-90.

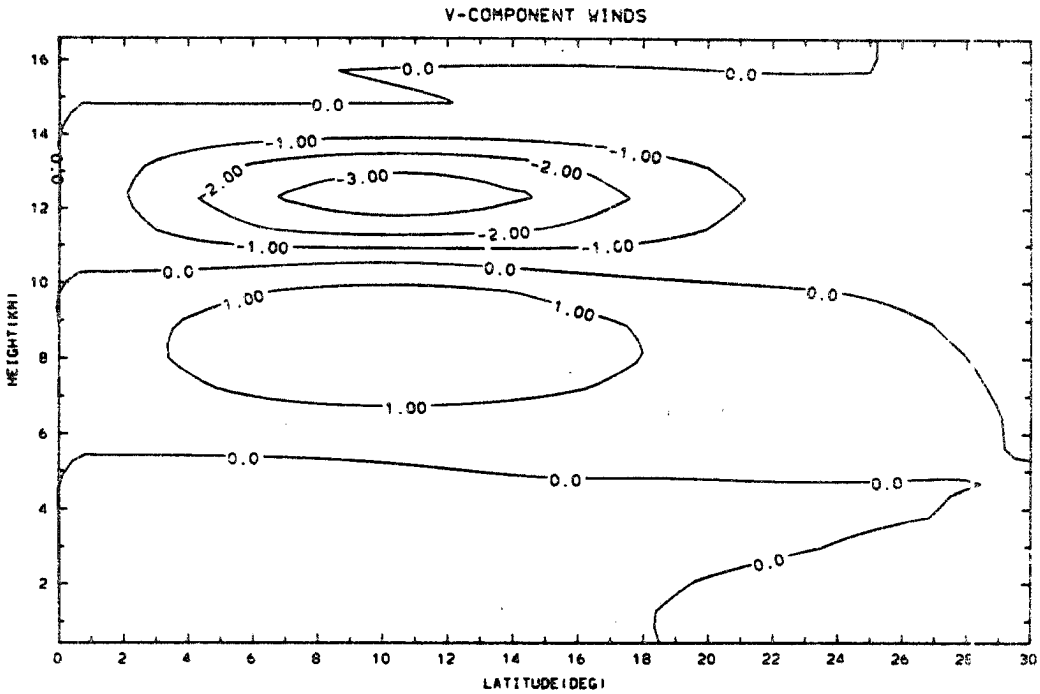

Fig. 4-5b. Forced zonally symmetric v-winds at ωt=-90.

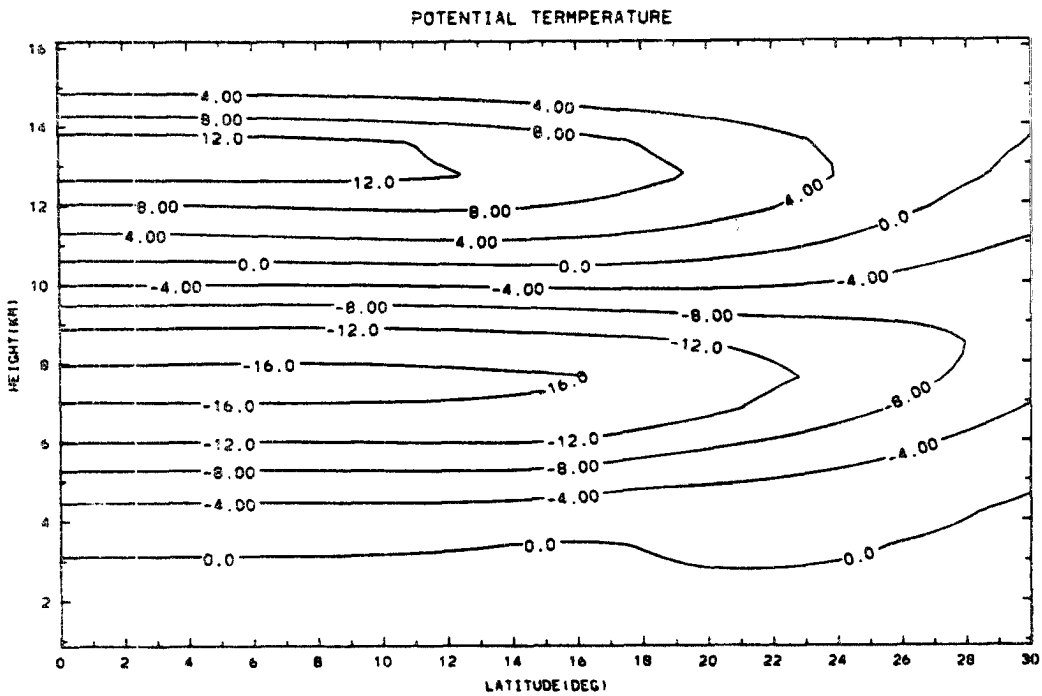

Fig. 4-5c. Forced zonally symmetric geopotential at ωt=-90.

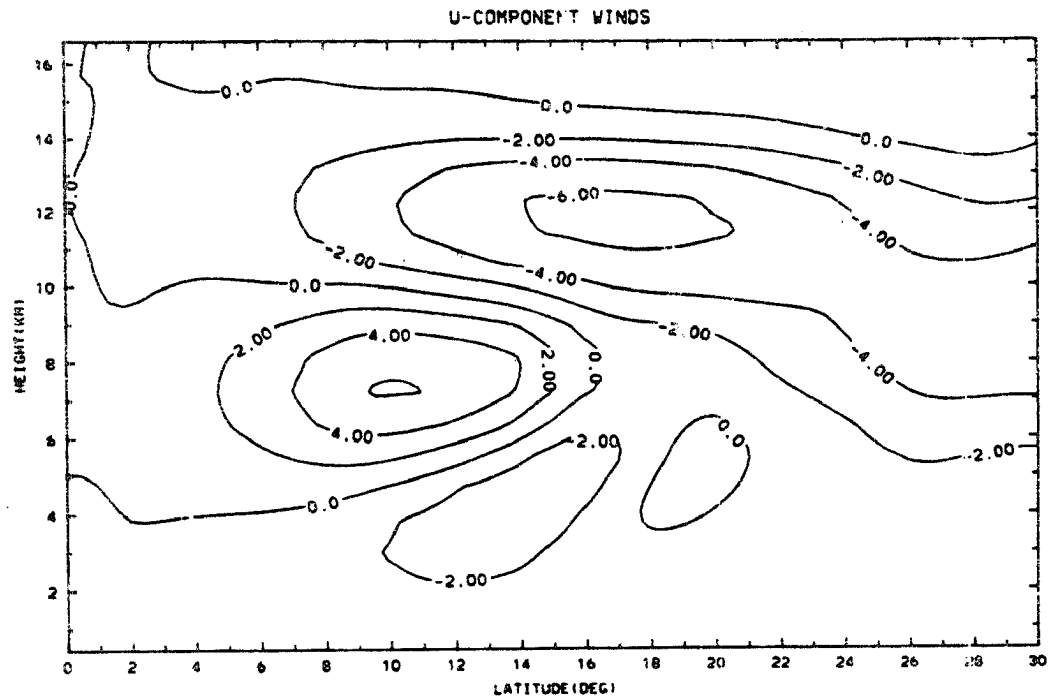

Fig. 4-6a. Like Fig. 4-5a but wt=-45.

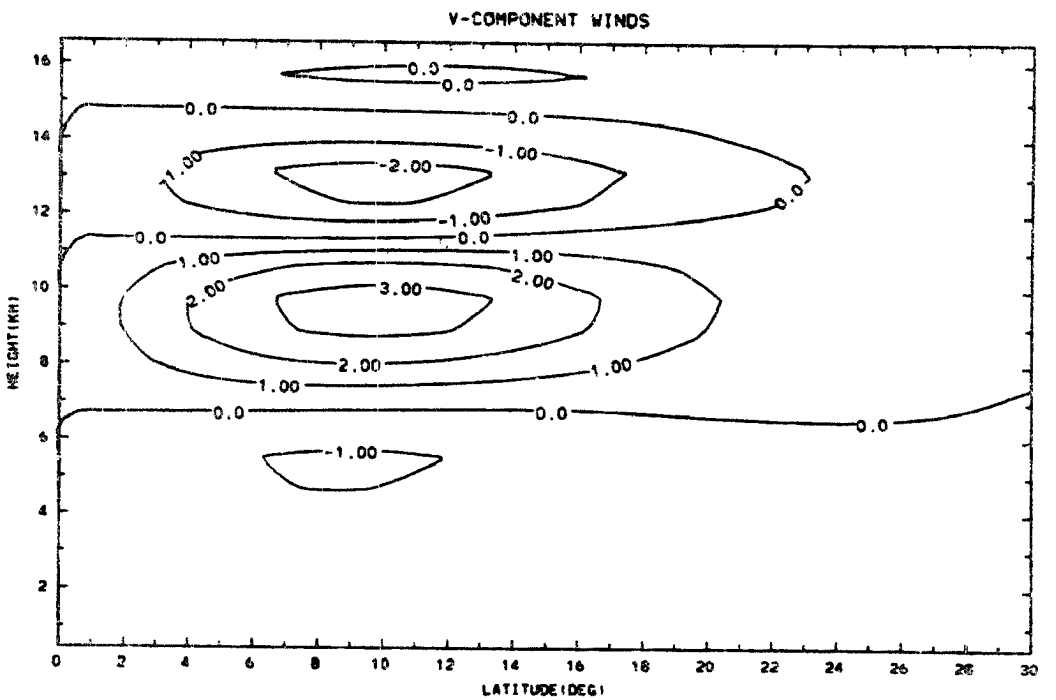

Fig. 4-6b. Like Fig. 4-5b but wt=-45.

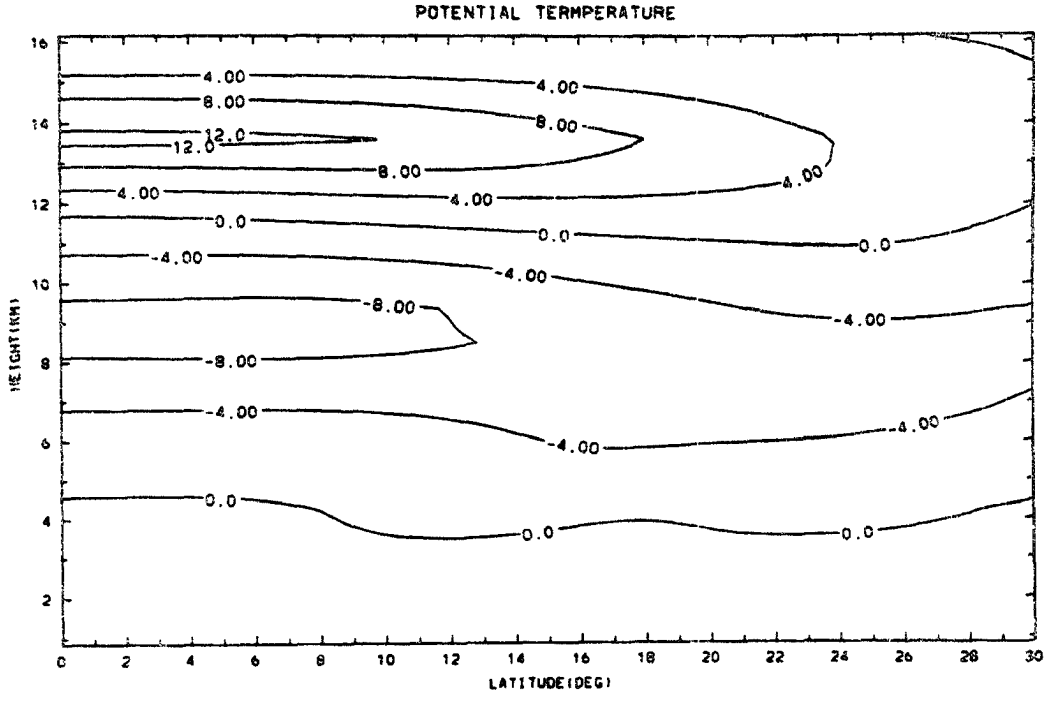

Fig. 4-6c. Like Fig. 4-5c but ωt=-45.

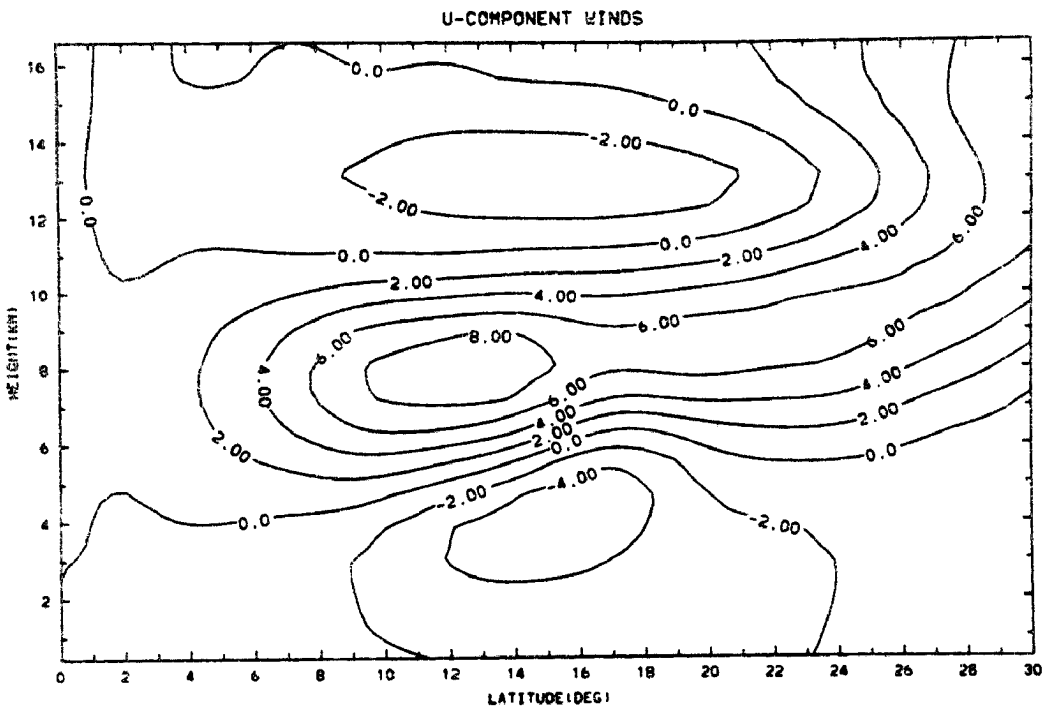

Fig. 4-7a. Like Fig. 4-5a but wt=0.

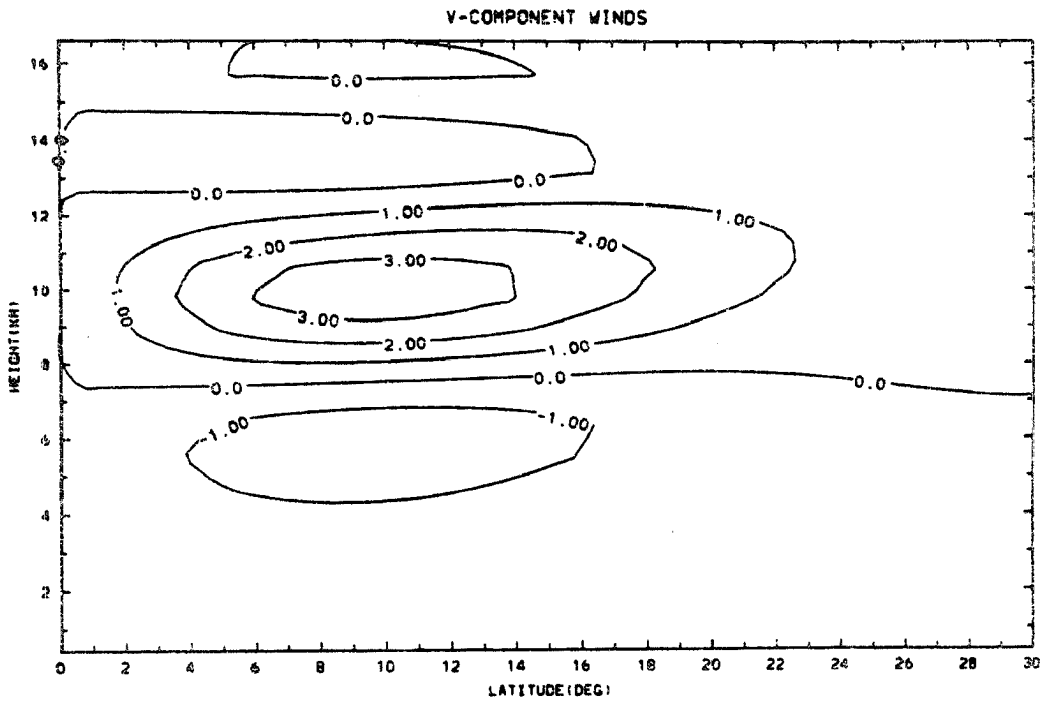

Fig. 4-7b. Like Fig. 4-5b but ωt=0.

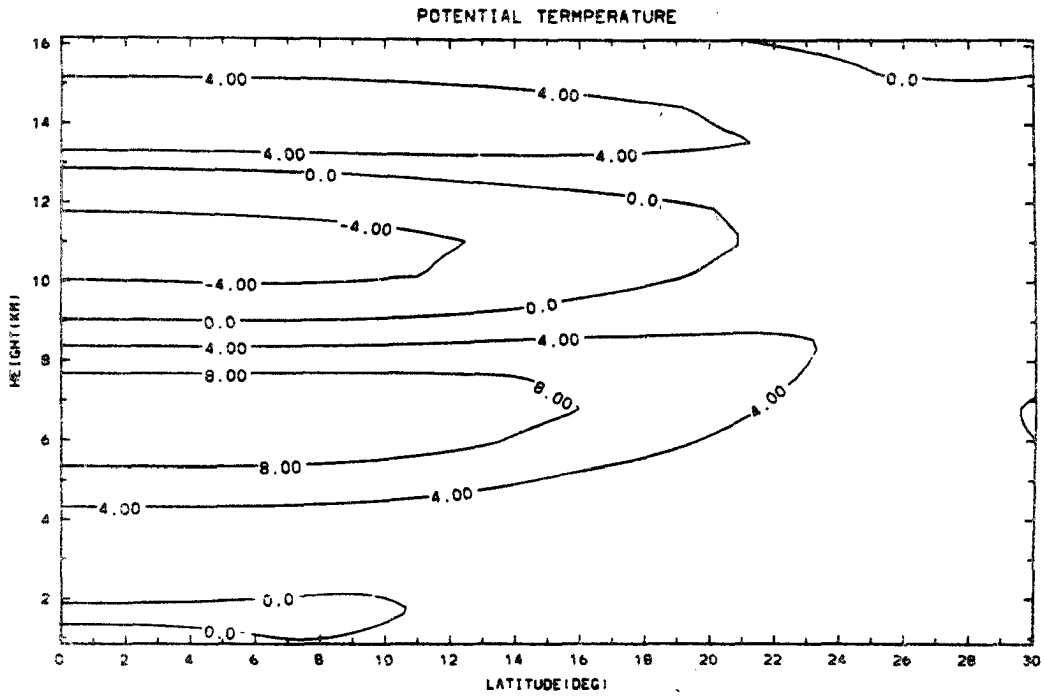

Fig. 4-7c. Like Fig. 4-5c but $\omega t=0$.

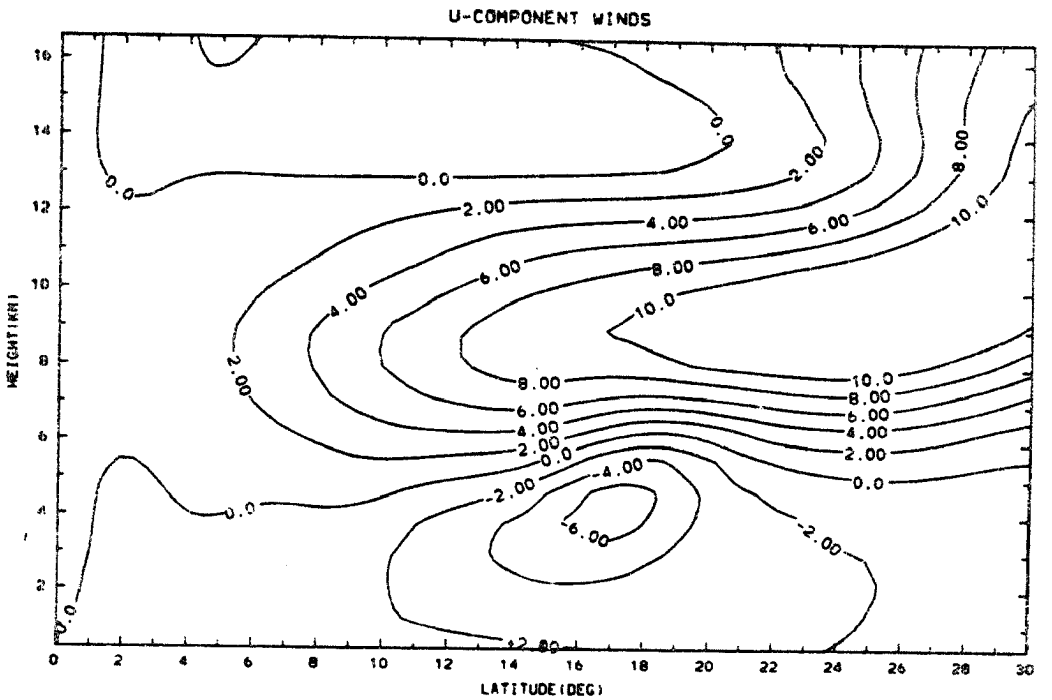

Fig. 4-8a. Like Fig. 4-5a but wt=45°.

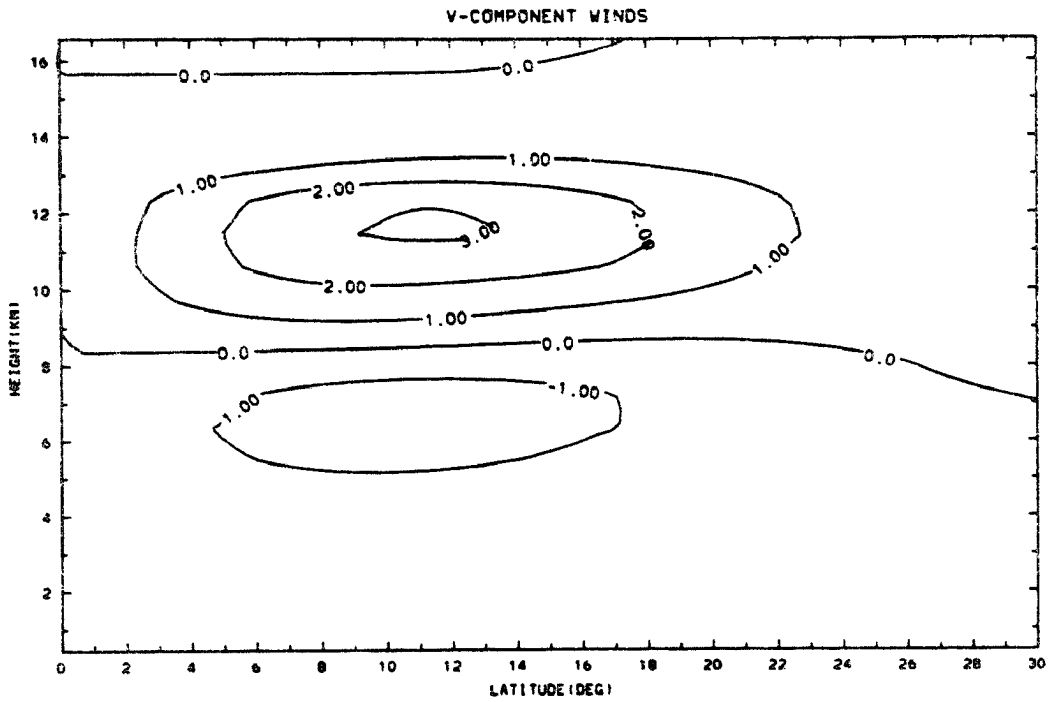

Fig. 4-8b. Like Fig. 4-5b but $\omega t=45°$.

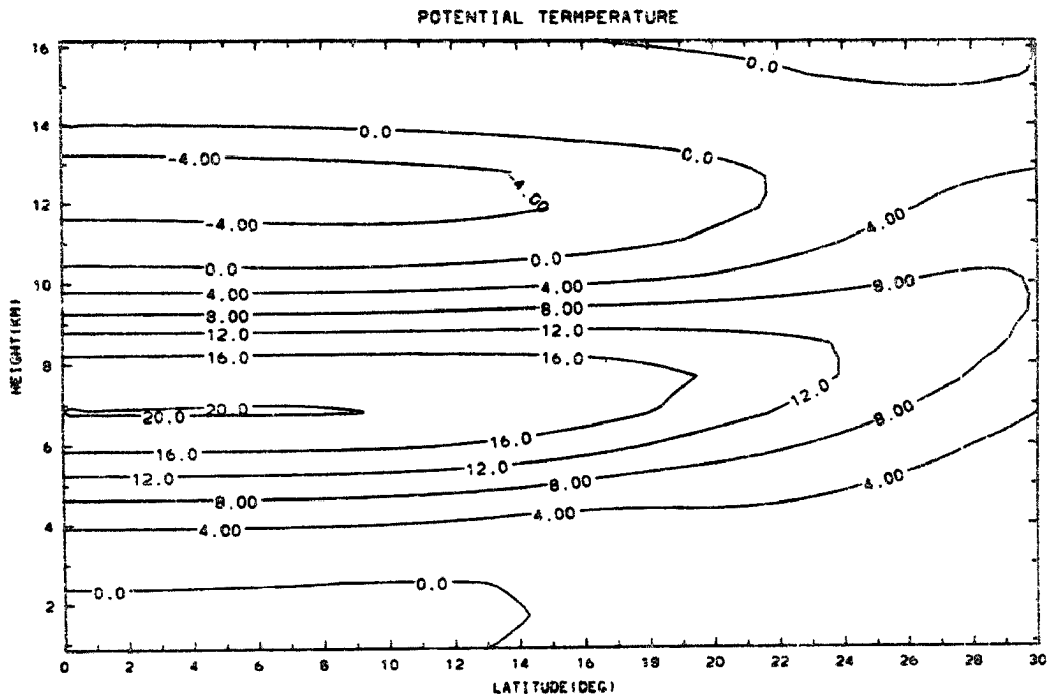

Fig. 4-8c. Like Fig. 4-5c but ωt=45°.

in the middle tropospheric static stability and suggesting a possible mechanism for interaction between the clouds and the large scale motion. At $\omega t = +45°$ the westerly maximum continues to propagate poleward as the surface easterlies extend upward. The motion then continues with the fields at $\omega t = +90°$ being opposite in sign to our starting point.

We will now extend the Hadley cell basic state calculations to include the non-zonally symmetric response. This is done by constructing a version of the linear perturbation model for a single non-zero wavenumber. The response for each wavenumber is then multiplied by the projection of the forcing on that wavenumber and finally the response fields are combined to produce a three dimensional description of the forced motions. The results presented here are generated using only the zonal wavenumber 0, 1, and 2 components which were found to be the largest responses for the shallow water models.

In Fig. 4-9a we present the u-component wind field response for the full model with the Hadley cell basic state plotted at a height corresponding to ~250 mb which is representative of the model upper troposphere. The model response at 830 mb is shown in Fig. 4-9b. The model response has a number of similarities with the shallow water calculations which can be seen by comparing the general structure of the response with Fig. 4-3. There are also a number of important differences in the upper tropospheric response the first of which is a reduction in the size of the equatorial wavenumber 1 response and an increase in the amplitude of the subtropical wavenumber 0 response. The reduction in the equatorial motions is probably due to the inclusion of the cumulus "friction" terms which are maximum in that region.

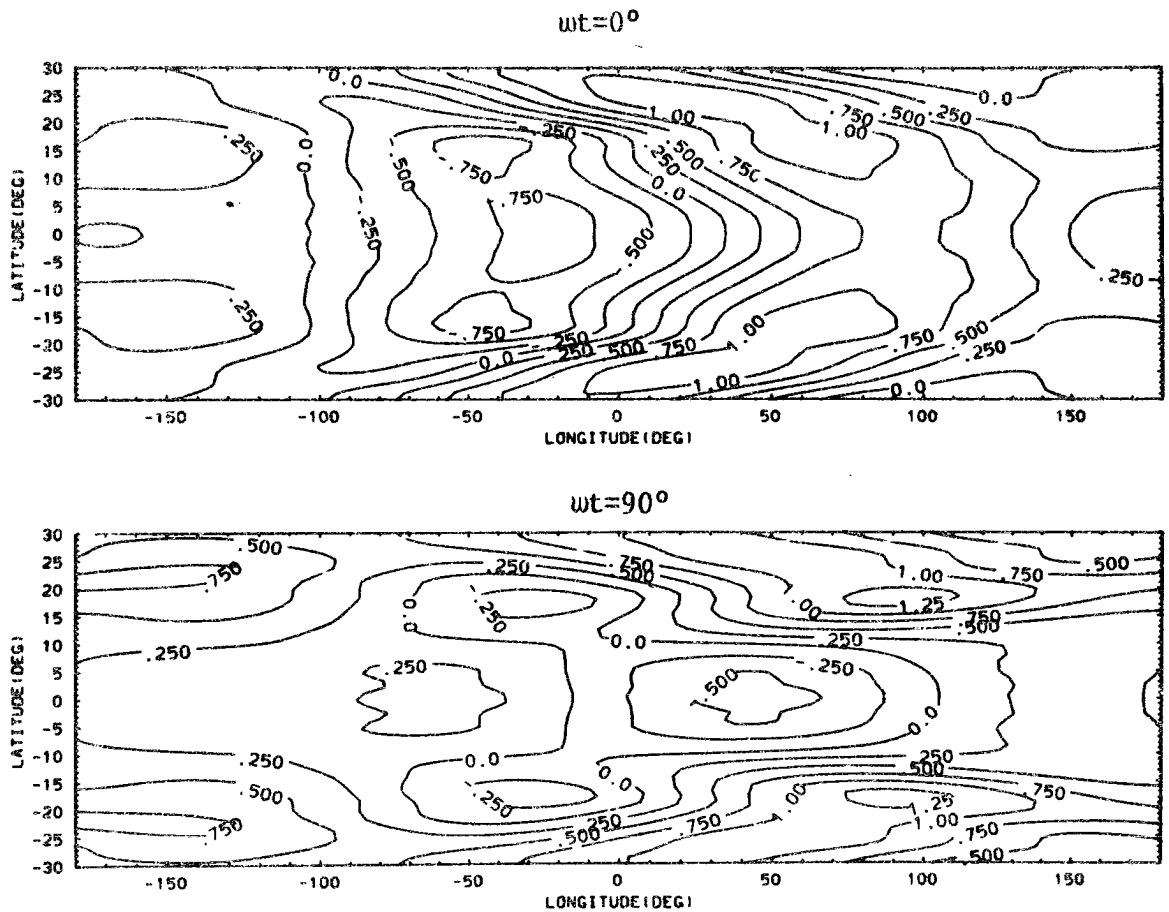

Fig. 4-9a. u-wind field response at ~250 mb for full baseline model.

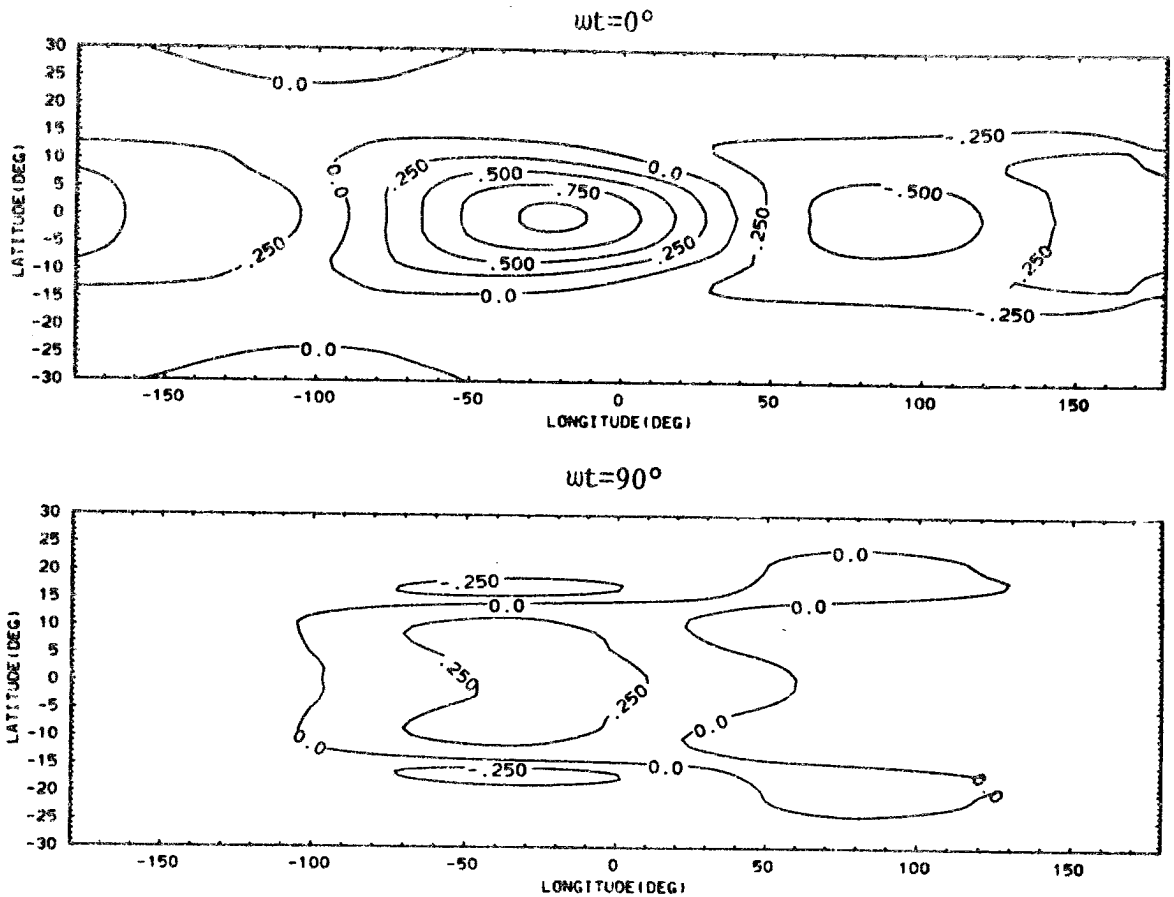

Fig. 4-9b. u-wind field response at ~830 mb for full baseline model.

In addition to the amplitude changes the Hadley cell basic state model exhibits a clear tendency for the subtropical maximum to more poleward and eastward in the region east of the heating. The lower tropospheric response remains primarily a wavenumber 1 meridional overturning.

In conclusion all of the models tend to produce the same general type of response with an equatorial "Walker" type circulation which exhibits a sharp u-wind phase transition in the region of the heating and a more zonally symmetric u-wind response in the subtropics. When the Hadley cell basic state is included the upper tropospheric subtropical response is enhanced with respect to the equatorial one and the subtropical motions exhibit poleward and eastward phase propagation.

5. TEMPORAL VARIATIONS IN THE OBSERVED OSCILLATION

A major question concerning the observed oscillation is the cause of the 40-50 day period. Chang (1977) proposed a mechanism where the time scale arises from stochastic excitation of a zonal wavenumber 1 equatorial Kelvin wave. Chang showed that for a particular choice of dissipation parameters this mechanism could provide a possible explanation for the oscillation as a Doppler shifted traveling wave. More recently Webster (1983) has constructed a model where monsoon variations on this time scale result from surface hydrological effects. In this work we propose a possible explanation which derives its time scale from the advective time scale associated with a "Hadley cell" type background circulation.

The effort presented here is an attempt to learn how the amplitude and frequency of the observed oscillation vary with time for the purpose of investigating possible causes of the motion. In particular we are interested in whether there is any detectable seasonal variation of either the oscillation amplitude or frequency.

If the time scale for the oscillation results from a Doppler shifted wave mechanism as proposed by Chang, one would expect to see a seasonal change in the oscillation frequency corresponding to the annual and semi-annual changes in the zonal winds responsible for the Doppler shifting. The magnitude of this effect is examined at the end of this Chapter. The expected frequency variations for the mechanism proposed by Webster and the one described in this thesis are not clear.

It is hoped that an understanding of the seasonal variations in amplitude will offer some insight into the relationship between the observed oscillation and the monsoon circulations. In particular we would like to know if the monsoon causes an amplification of the oscillation or if changes in the monsoon circulation on this time scale which were reported by Krishnamurti and Subrahmanyan (1982) are (primarily) a response to the planetary scale motion.

For the purpose of this study we have selected two data sets. The first is the atmospheric relative angular momentum series described by Anderson and Rosen (1983). This series represents the planetary scale, zonally averaged component of the oscillation and is perhaps the atmospheric parameter for which the oscillation signal is most dominant. One disadvantage of this time series is that the data are only easily available for the period 1977-1980 and thus it is difficult to make a sensitive determination of the seasonal dependences.

The second data set which we have chosen is the 850 mb to 200 mb shear of the zonal wind at Truk (7°28'N, 151°5'E). This time series also has a strong signal in the 40-50 day range, and data are available for a rather long time period with few missing days. The analysis presented here makes use of data for the 25 years from 1953-1977.

The goal of this work is to determine the temporal variation of the parameters of the observed oscillation. To accomplish this task, representive time series are first constructed and then band-pass filtered to isolate the "40-50 day" signal. This filtered series is then examined over relatively small blocks of 100 days duration to determine the parameters for that interval. This analysis is done for the 100 day block centered on each day of the series to construct a

time series of the amplitude and frequency. For Truk, where a long data record is available, a seasonal climatology of the oscillation parameters and the standard deviation of the departure from this climatology are also calculated.

The first step in the analysis is to roughly characterize the time series by removing a mean seasonal signal and then calculating an estimate of the signal autocorrelation function.

The autocorrelation estimate, $a(\tau)$, is constructed directly from the time series using the relationship

$$a(\tau) = \frac{1}{\Sigma u^2(t)} \sum_{t=0}^{N-T} u(t) \cdot u(t-\tau).$$

Here T is the truncation length of the autocorrelation estimate which we take as 256 days and N is the total number of daily observations. Since the series is real we can take $a(-\tau)=a(\tau)$. Once the autocorrelation function is known, an estimate of the power (variance) spectral density, $\hat{p}(w)$, is constructed using the classical Blackman-Tukey (1959) technique with the optimal window function $w(\tau)$ proposed by Papoulis (1973),

$$\hat{p}(\omega) = \sum_{\tau=-T}^{T} w(\tau)\, a(\tau)\, \cos(\omega t)$$

where $$w(\tau) = \frac{1}{\pi} \frac{\sin(\pi\tau)}{T} + (1-\frac{\tau}{T})\cos(\pi\tau)$$

For the frequency-amplitude analysis a signal representing the oscillation is generated by using a finite impulse response filter whose impulse reponse, $h(\tau)$, is given in Fig. 5-1. The filtered

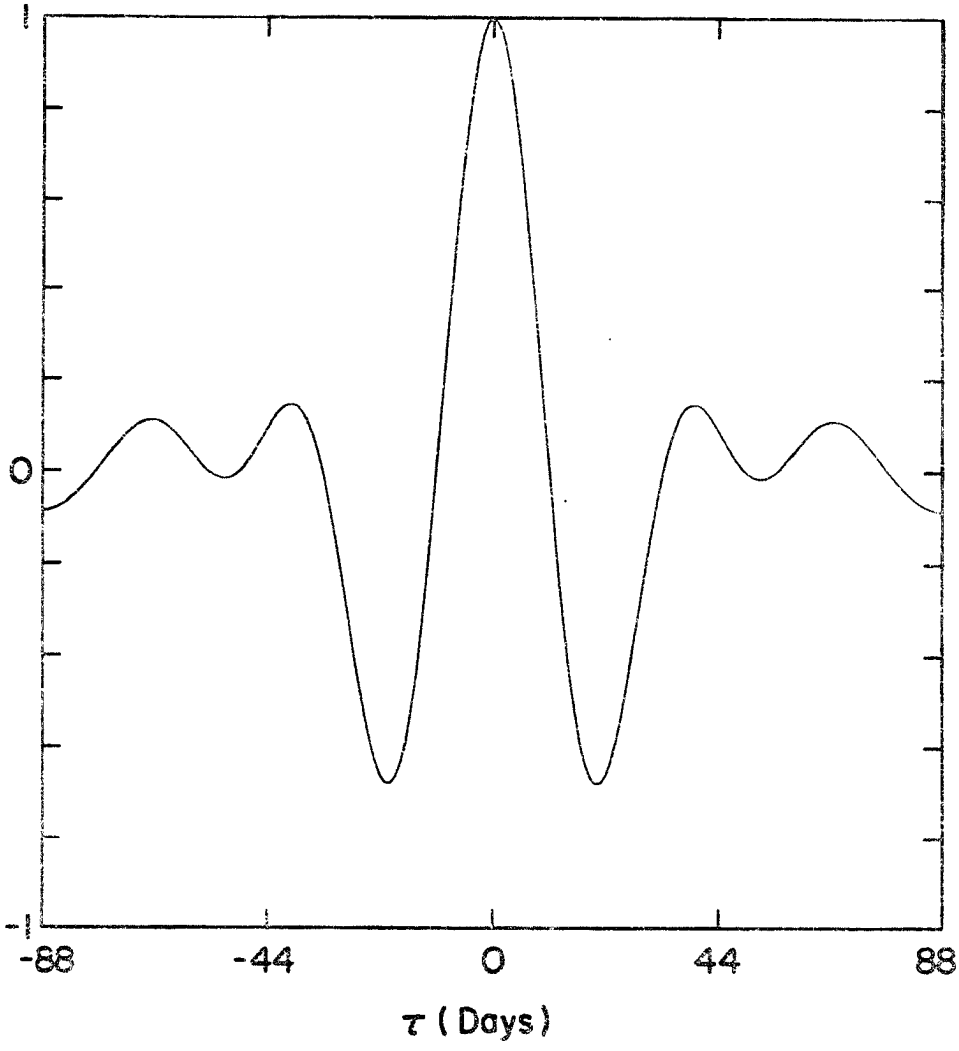

Fig. 5-1. Impulse response of finite impulse response filter.

series, $u_f(t)$, is constructed from the original series u(t) by computing the convolution sum of $h(\tau)$ with u(t)

$$u_f(t) = \sum_{\tau=-M}^{M} h(\tau)u(t+\tau)$$

Here M is 88 days and $h(\tau)=0$ for $\tau>88$. This filter is designed to pass the frequency band from frequencies corresponding to 32 day periods to those corresponding to 64 day periods and has a frequency response given in Fig. 5-2. The filter was designed using the frequency sampling technique described by Oppenheim and Schafer (1975). Details of the filter design are given in Appendix II. A useful property of this filter is the large rejection of the annual and semi-annual components which makes it unnecessary to remove the seasonal signal before filtering. This eliminates the possibility of contaminating the signal with a fluctuation contained in the climatology.

Once the filtered series has been constructed we must then derive a technique for determining the oscillation parameters. The technique which we have chosen is to fit an autoregressive model to a segment of the data series and derive an estimate of the frequency from the fit parameters. A second order autoregressive model is fit to the data with the prediction equations applied in both the forward and backward directions

$$\hat{u}_f(t) = \alpha u(t-\Delta t)+\beta u(t-2\Delta t)$$
$$\hat{u}_b(t) = \alpha u(t+\Delta t)+\beta u(t+2\Delta t)$$

where α and β are chosen to minimize the error function

$$E^2 = \sum_t [(u-\hat{u}_f)^2 + (u-\hat{u}_b)^2]$$

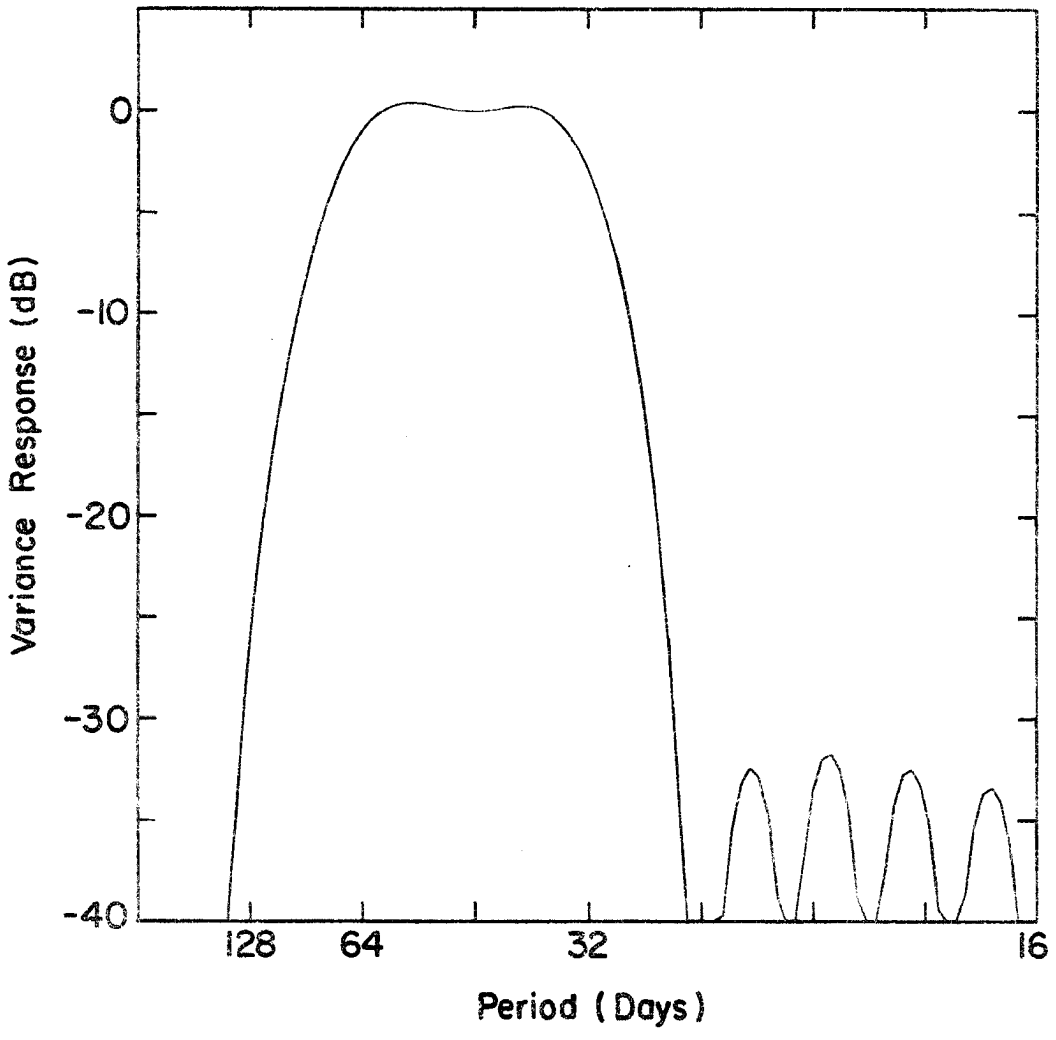

Fig. 5-2. Frequency response of finite impulse response filter.

when summed over the chosen segment. For this analysis Δt has been chosen to be 10 days and the sums are calculated on 100 day segments with 1 day sampling intervals. As noted by Kay and Marple (1981) this model corresponds to a process which has spectrum peaks (system function poles) whose frequencies are estimated by finding the roots of the polynomial

$$f(z) = z^2-\alpha z-\beta$$

to get $(z-p_1)(z-p_2) = 0$.

The frequencies of the poles are then found from

$$\omega_1 = \frac{\arg[p_1]}{\Delta t}, \quad \omega_2 = \frac{\arg[p_2]}{\Delta t} \quad .$$

Since the data and thus α and β are real, it follows that $p_1=p_2^*$ and $\omega_1=-\omega_2$, so that we can define a single frequency $\omega= \omega_1 = \omega_2$. Once the frequency ω is known, the amplitude is found from the linear least square problem

$$\hat{u}(t) = a \sin(\omega t) + b \cos(\omega t),$$

where a and b are found by minimizing

$$E^2 = \sum_t (u(t)-\hat{u}(t))^2,$$

and the amplitude A is given by

$$A = (a^2 + b^2)^{\frac{1}{2}}.$$

This process is then continued by moving the segment one day forward and performing the same steps to generate the time series $\omega(t)$ and $A(t)$.

It is an unfortunate consequence of the non-linear nature of the frequency analysis that there are no statistical bounds for the error of the frequency estimates, although for the case of a pure sinusoid the above technique is exact. Also a subjective analysis based on the time between amplitude peaks showed good agreement with the above technique for sample data segments.

The first series analyzed is total relative angular momentum of the atmosphere. This parameter, which we will call M, is computed using the NMC twice daily operational analysis data for levels from 1000 mb to 100 mb assuming a surface pressure of 1000 mb

$$M = \frac{2\pi a^3}{g} \int_{1000\ mb}^{100\ mb} \int_{\pi/2}^{-\pi/2} [u]\cos^2\phi \, d\phi dp,$$

where a is the radius of the earth, g is acceleration due to gravity, [u] is the zonally averaged eastward component of the wind, ϕ is the latitude, and p is pressure. A complete description of the calculation of the series and a discussion of possible error is given in Rosen and Salstein (1983). Anderson and Rosen (1983) provide a description of the spatial structure of the zonally-symmetric 40-50 day oscillation. A plot of the daily departure from the seasonal mean is given in Fig. 5-3 for the years 1977-1980. This figure shows the prominent nature of the 40-50 day oscillation in this atmospheric variable.

In Figs. 5-4 and 5-5 we present estimates of the autocorrelation function and power spectral density for the M series. The power spectrum clearly shows a significant broad-band peak in the frequency range corresponding to 40-50 day periods. This peak falls entirely into the pass-band of the filter described above.

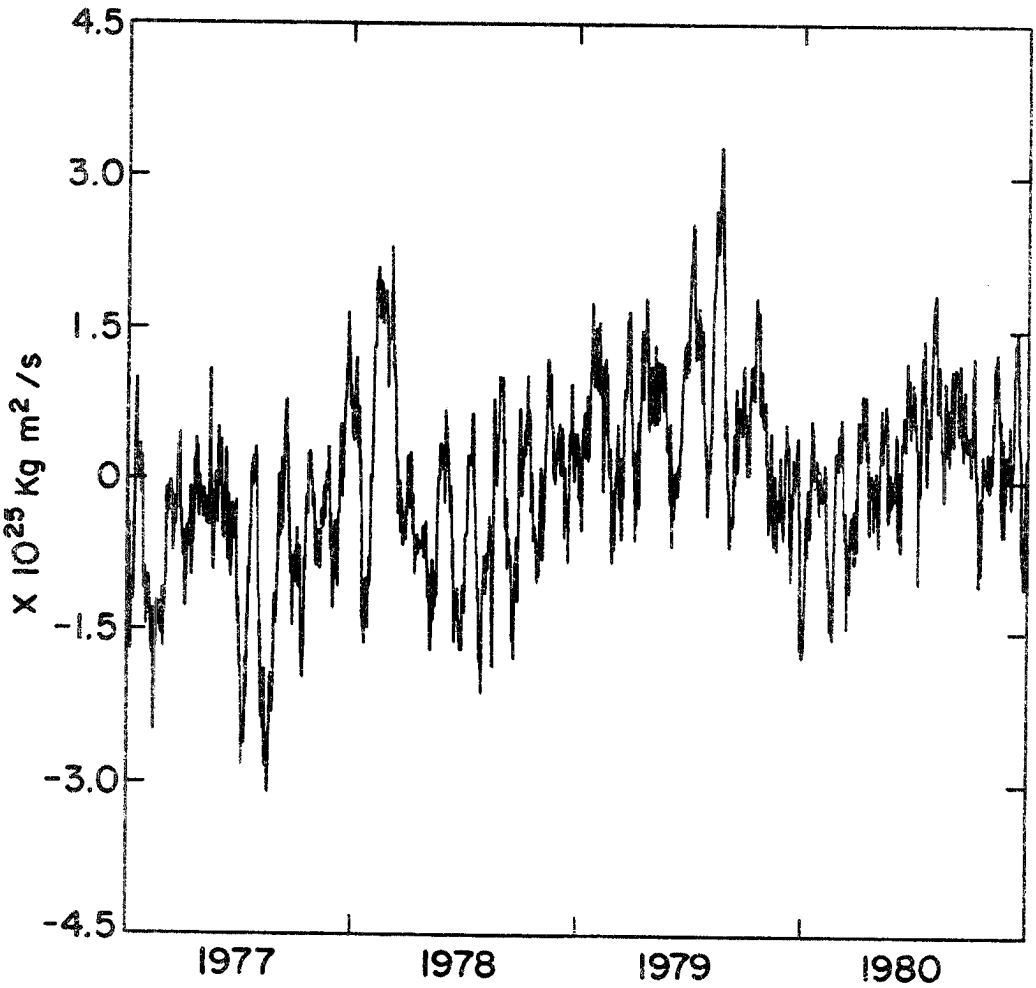

Fig. 5-3. Global M series with seasonal signal removed.

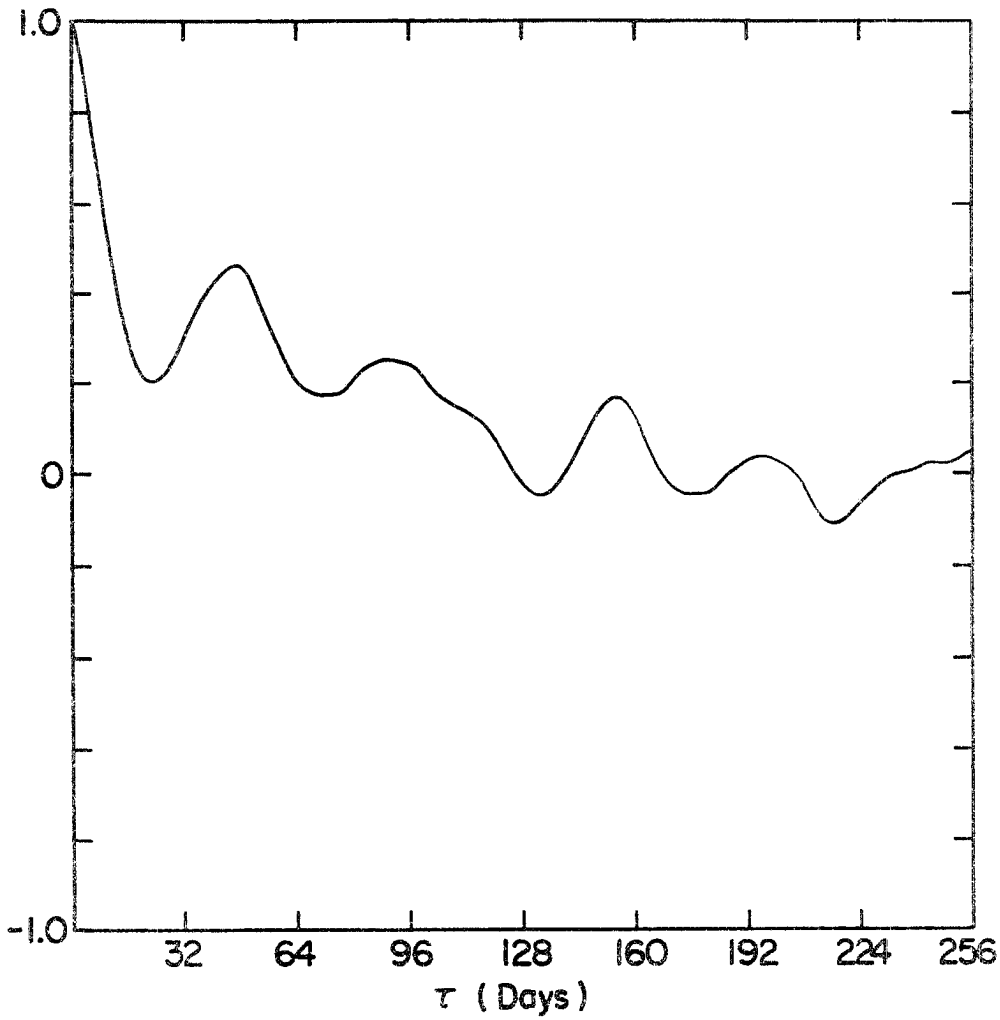

Fig. 5-4. Autocorrelation function of the series depicted in Fig. 5-3.

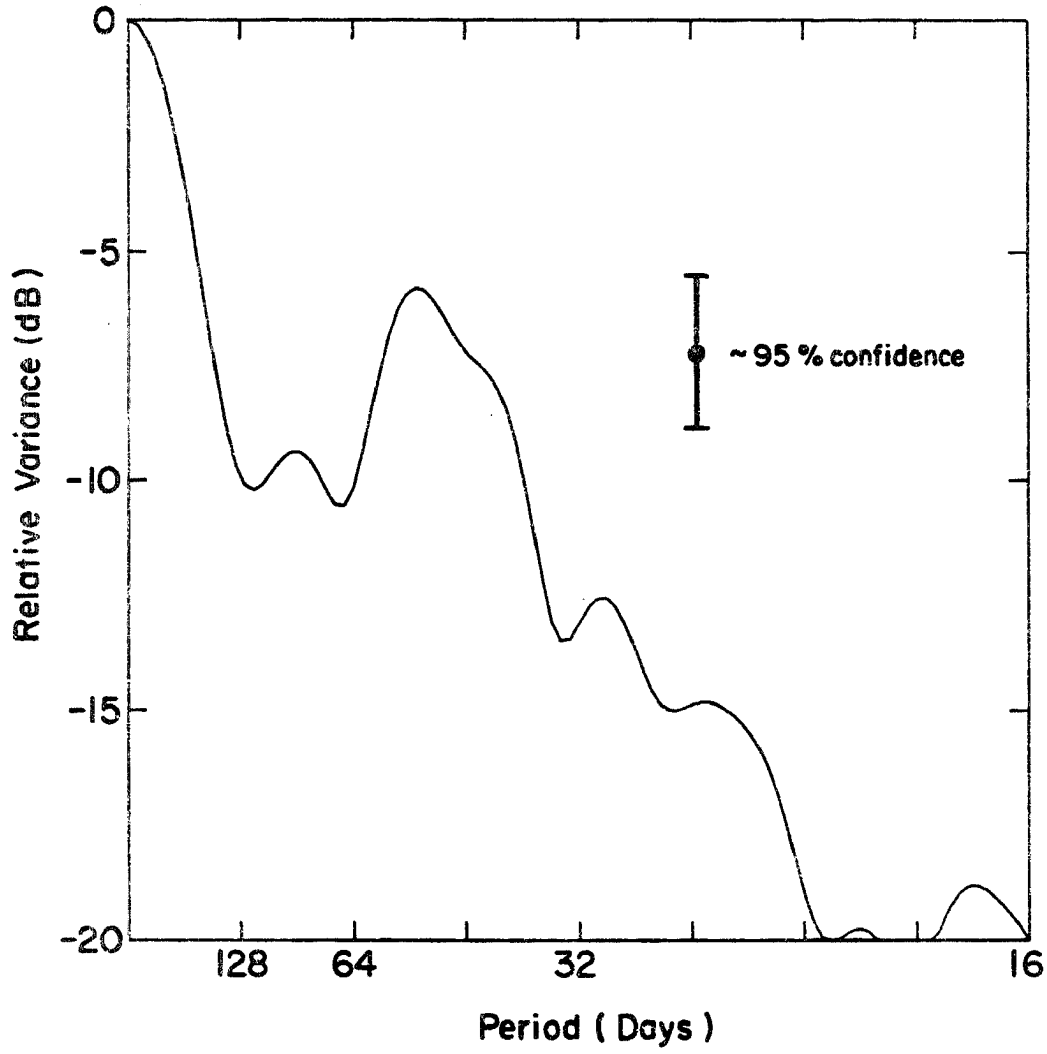

Fig. 5-5. Variance spectra estimate of the series depicted in Fig. 5-3.

The next step in the analysis is to produce a filtered version of the original M series. This filtered series is reproduced in Fig. 5-6 and seems to provide a good representation of the oscillation present in Fig. 5-3 with the high and low frequency variations removed. The seasonal signal present in the original series has also been removed by the filter.

The filtered signal is then processed to provide a time series representing the oscillation amplitude and frequency. These results, which are given in Fig. 5-7, show good agreement with hand estimates of the oscillation parameters and indicate that both the amplitude and frequency display definite variations on 6 month to 2 year time scales; however, there is no evidence of a clear seasonal cycle. It is also interesting to note that although the mean period is about 45 days, periods near 55 or 40 days are not uncommon. No values are plotted for the last 94 days of 1980 because the extra days are needed for the computation of the band-pass filter output and the last half of the final parameter estimation segment. The estimates for early 1977 include data for late 1976.

For a more sensitive determination of possible seasonal variations it is necessary to find an atmospheric parameter with a longer available record than the global M series. The series which we have chosen is based on Truk upper air data which was available to us for the period from mid-1952 to mid-1978. This allows the computation of oscillation parameters for the 25 year period 1953-1977. Since the upper and lower tropospheric zonal winds at Truk tend to be out of phase at these time scales, we have chosen the 850 mb to 200 mb zonal wind shear as our time series.

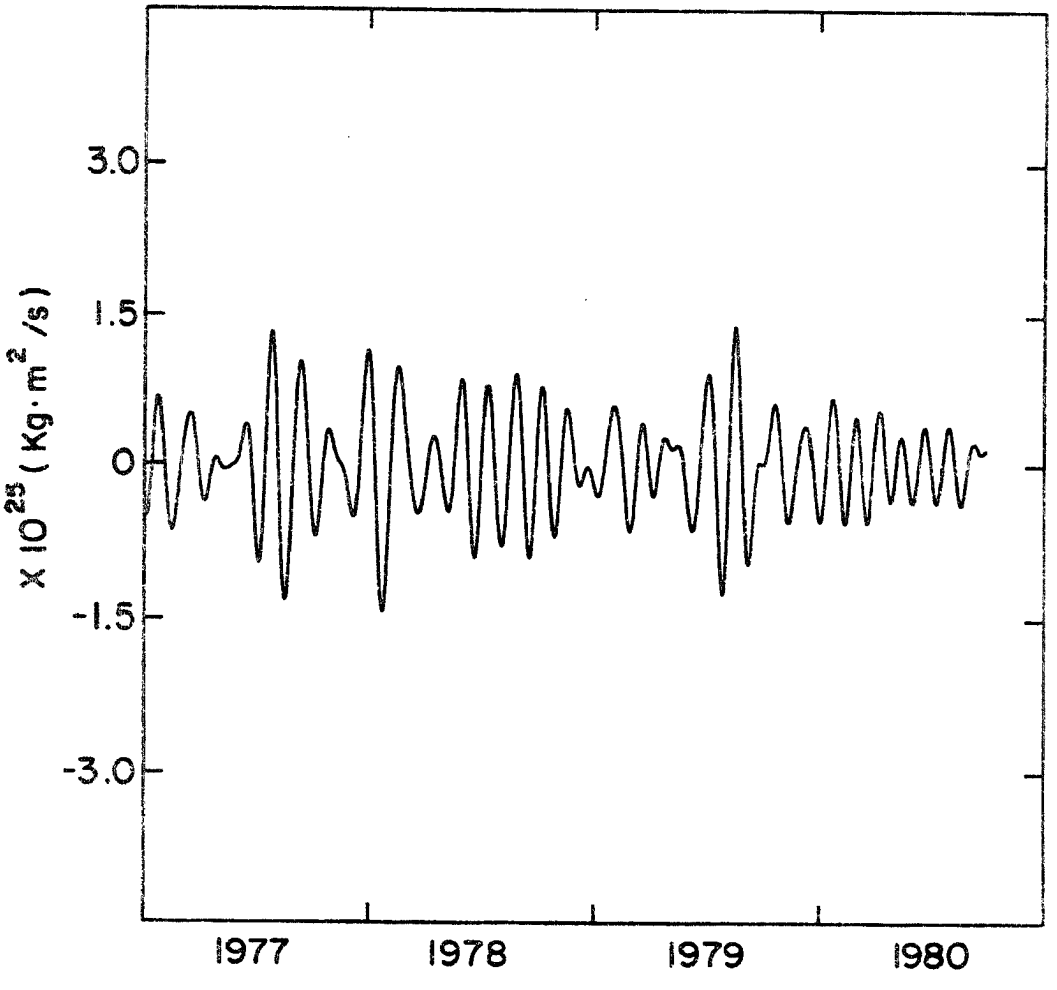

Fig. 5-6. Band-pass filtered global M series.

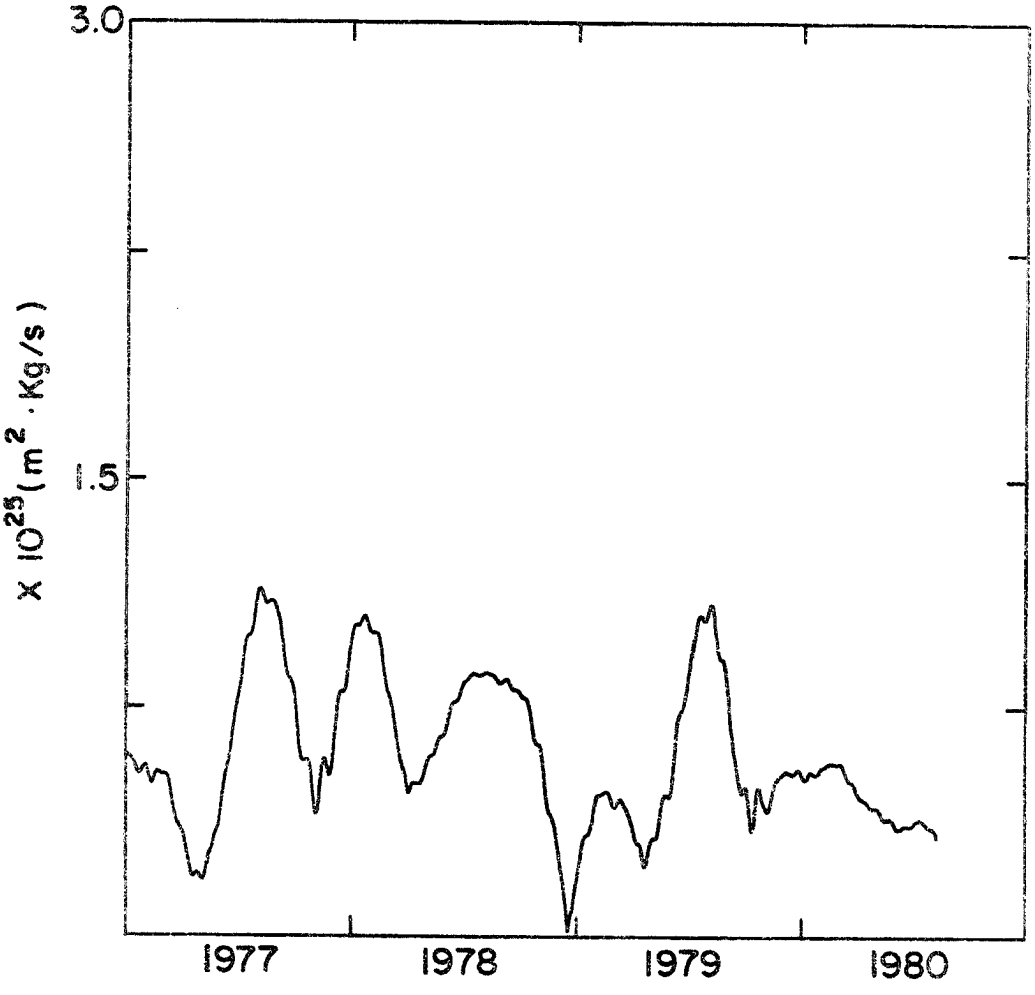

Fig. 5-7a. Amplitude estimate of band-pass M series.

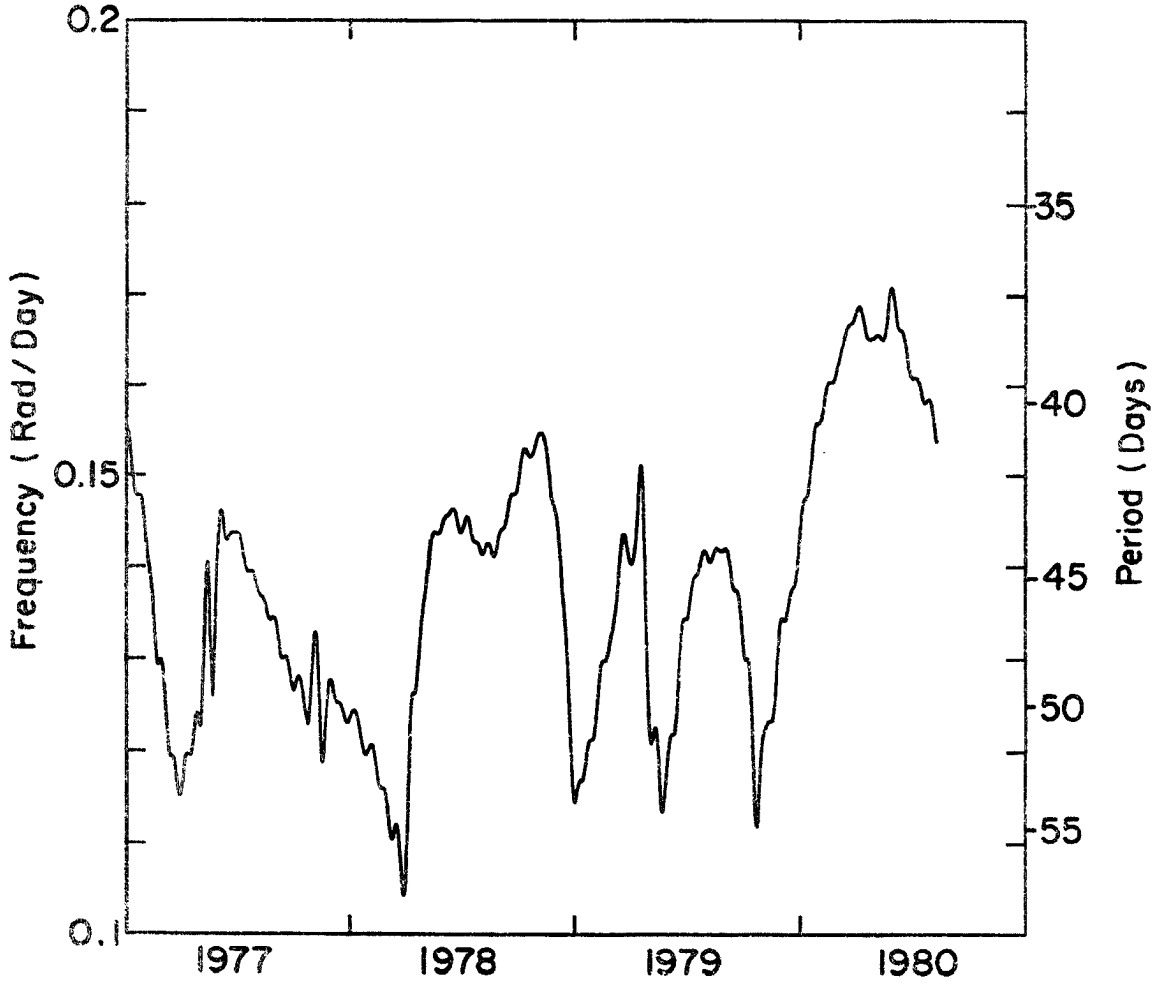

Fig. 5-7b. Frequency estimate of band-pass M series.

The Truk series with the seasonal cycle removed and the autocorrelation and spectral estimates for that series are given in Figs. 5-8, 5-9 and 5-10. Although the 40-50 day signal explains less of the variance at Truk than it does for the M series, the spectral peak is just as statistically significant due to the longer data record.

Figs. 5-11 and 5-12 present the filtered time series, the amplitude estimate and the frequency estimate for a 4 year sample of the Truk data. These figures display the tendency of the oscillation to change frequency very rapidly from a period near 32 days during the 1970-1971 northern hemisphere winter to a period near 55 days at the end of 1971.

The time series of the oscillation amplitude and frequency for the entire 25 year period are given in Fig. 5-13. Although the oscillation parameters show large low frequency variations, these variations do not appear to be associated with other low-frequency atmospheric signals. A possible association is that the oscillation amplitude is above its mean value during the 1956-1957, 1972-1973, and 1976-1977 El Nino/ southern oscillation warm events; however, the large amplitudes appear to last 2 to 3 years, which is generally longer than the duration of the Pacific warm event.

The final step in the analysis was the construction of a mean seasonal cycle for the Truk oscillation parameters. This climatology is presented in Fig. 5-14. In each of the plots the center line represents the mean value of the parameter on that date for the 25 year period. The upper and lower lines represent the mean value plus and minus one standard derivation of the parameter from the mean value for that data. The figures also include a 95% confidence bound on the value of the mean assuming a normal error distribution.

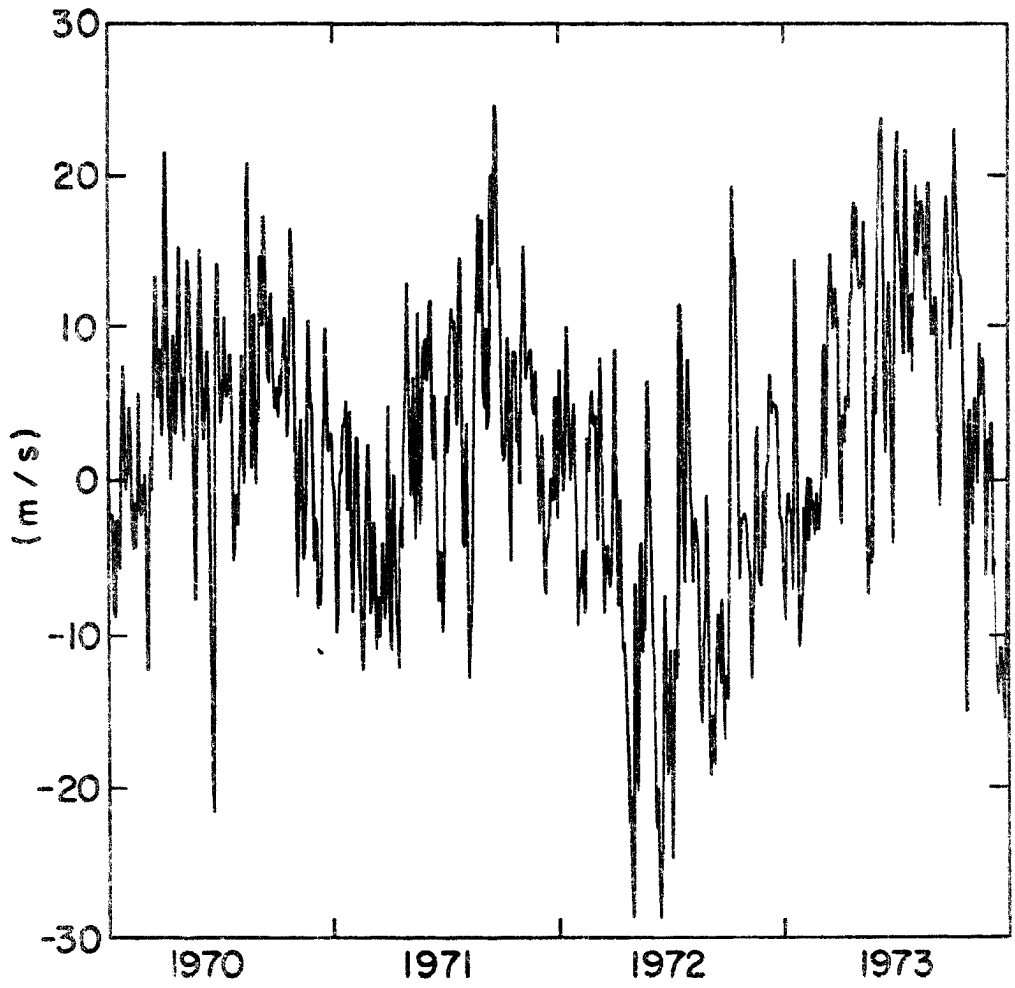

Fig. 5-8. Truk series with seasonal signal removed for sample period 1970-1973.

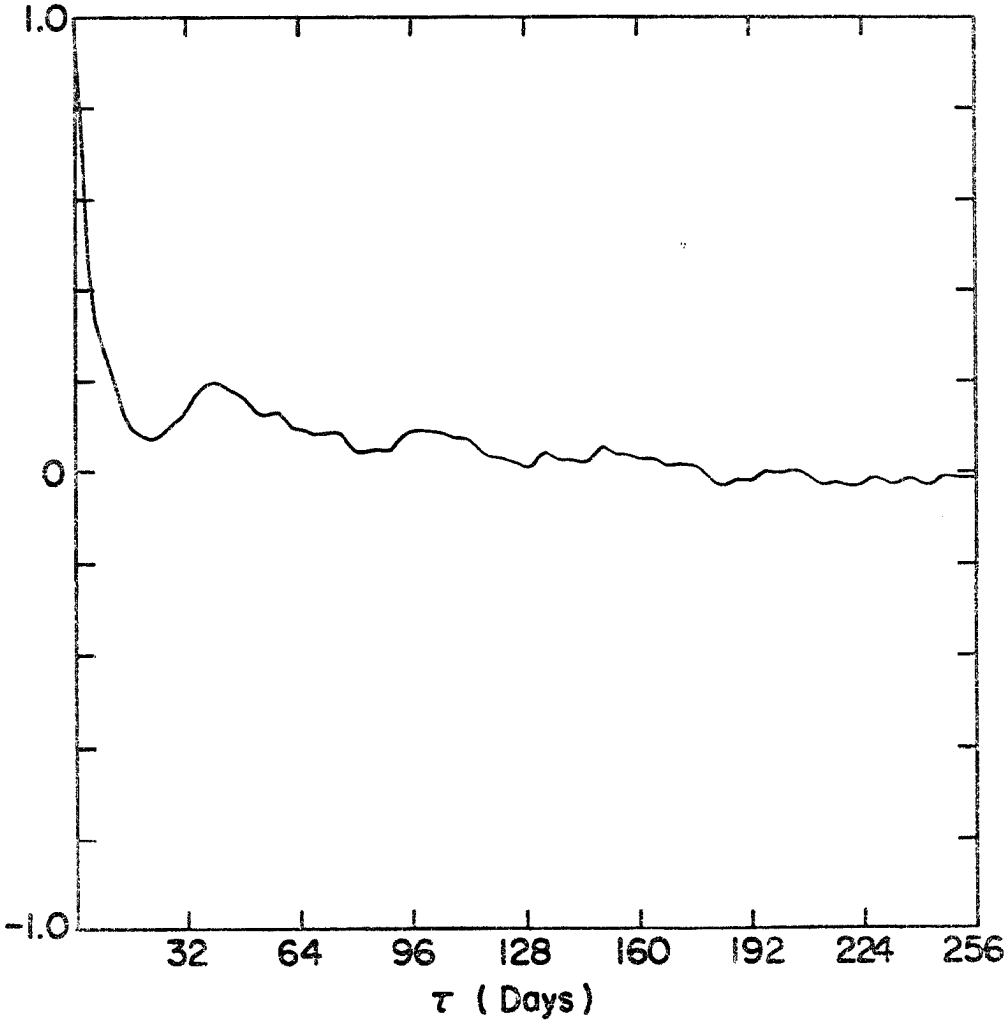

Fig. 5-9. Autocorrelation of Truk 200-850 mb u-wind shear for 1953-1977 with seasonal signal removed.

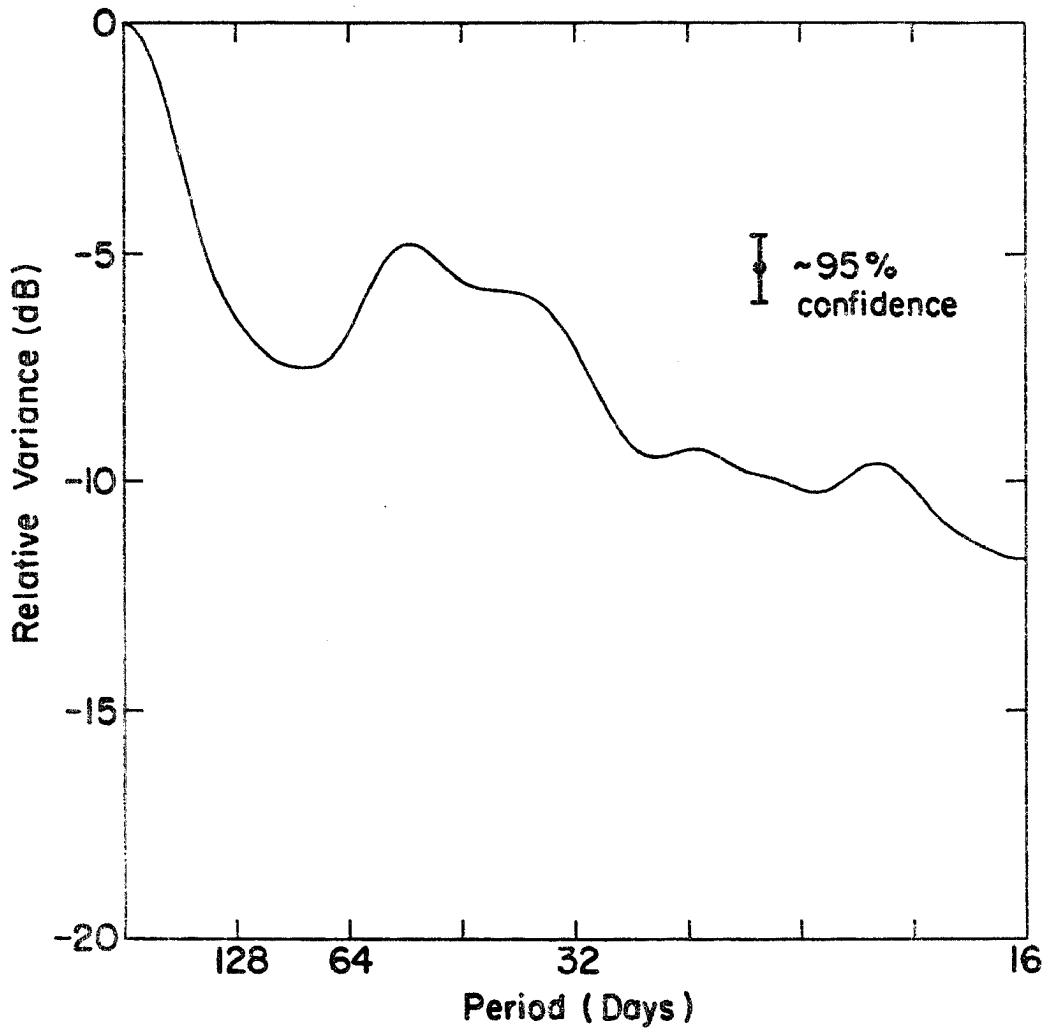

Fig. 5-10. Variance spectra estimate for Truk series corresponding to Fig. 5-9.

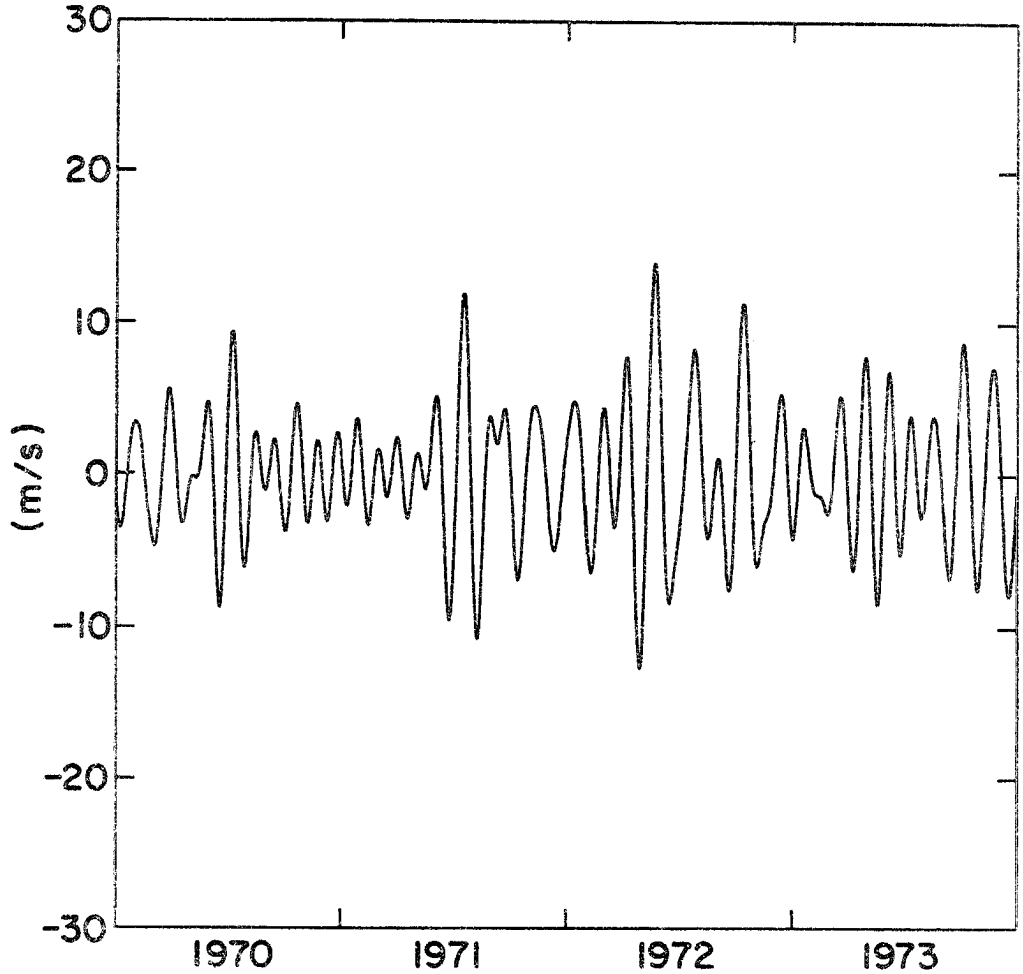

Fig. 5-11. Band-pass filtered Truk series for 1970-1973.

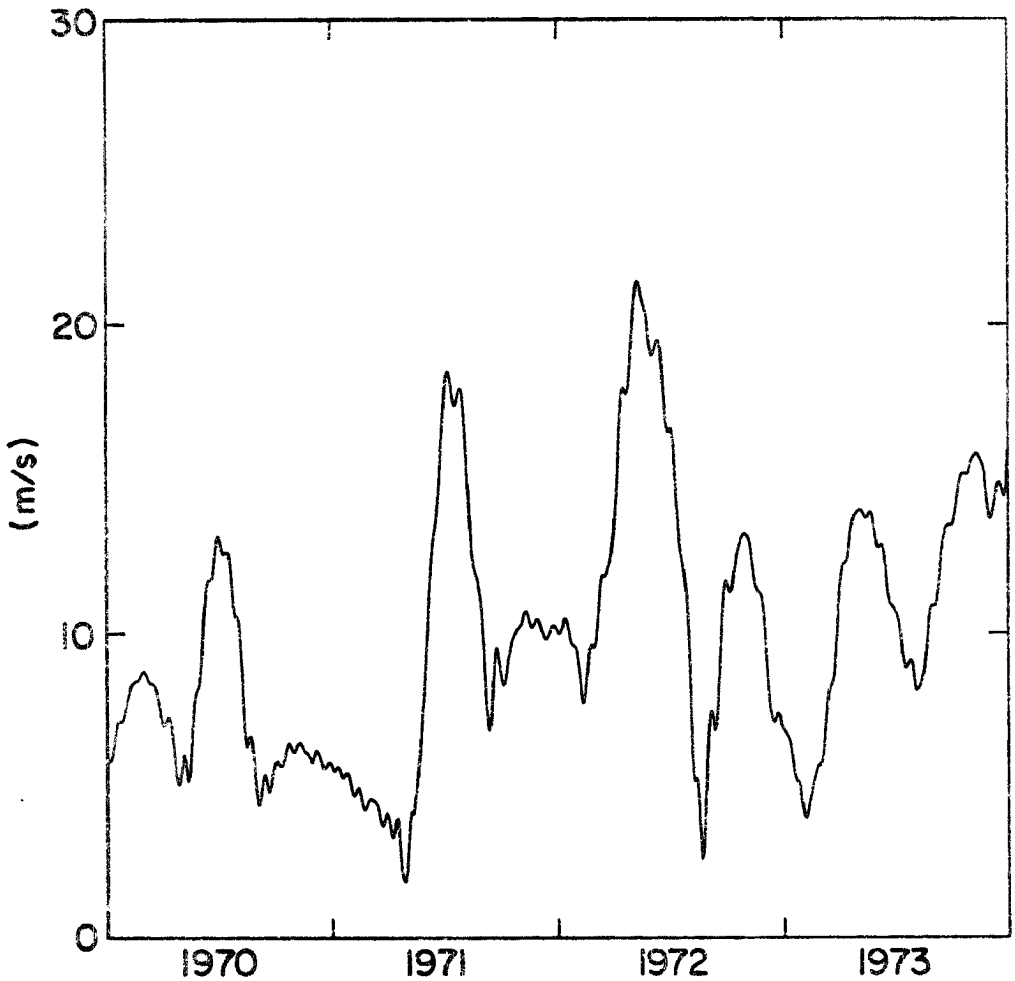

Fig. 5-12a. Amplitude estimate of series shown in Fig. 5-11.

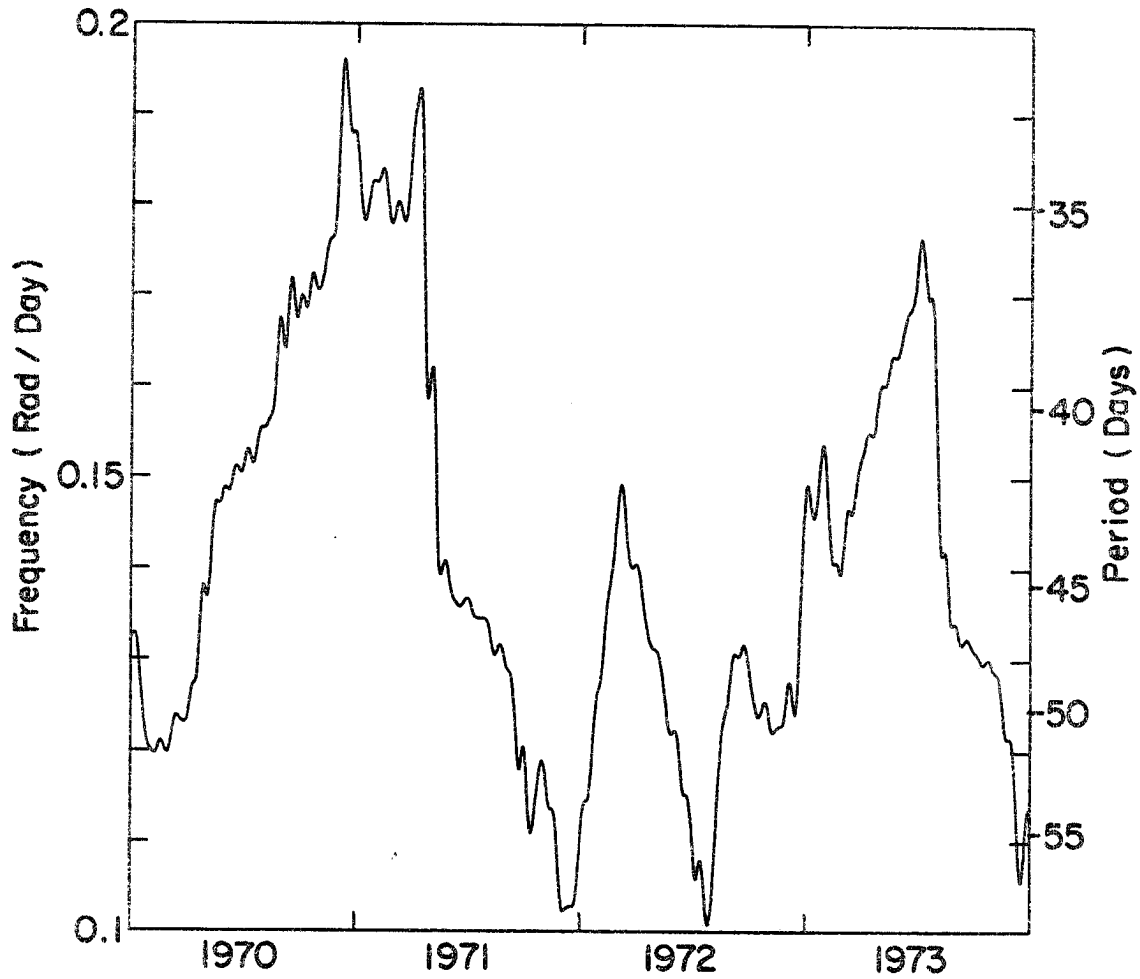

Fig. 5-12b. Frequency estimate of series shown in Fig. 5-11.

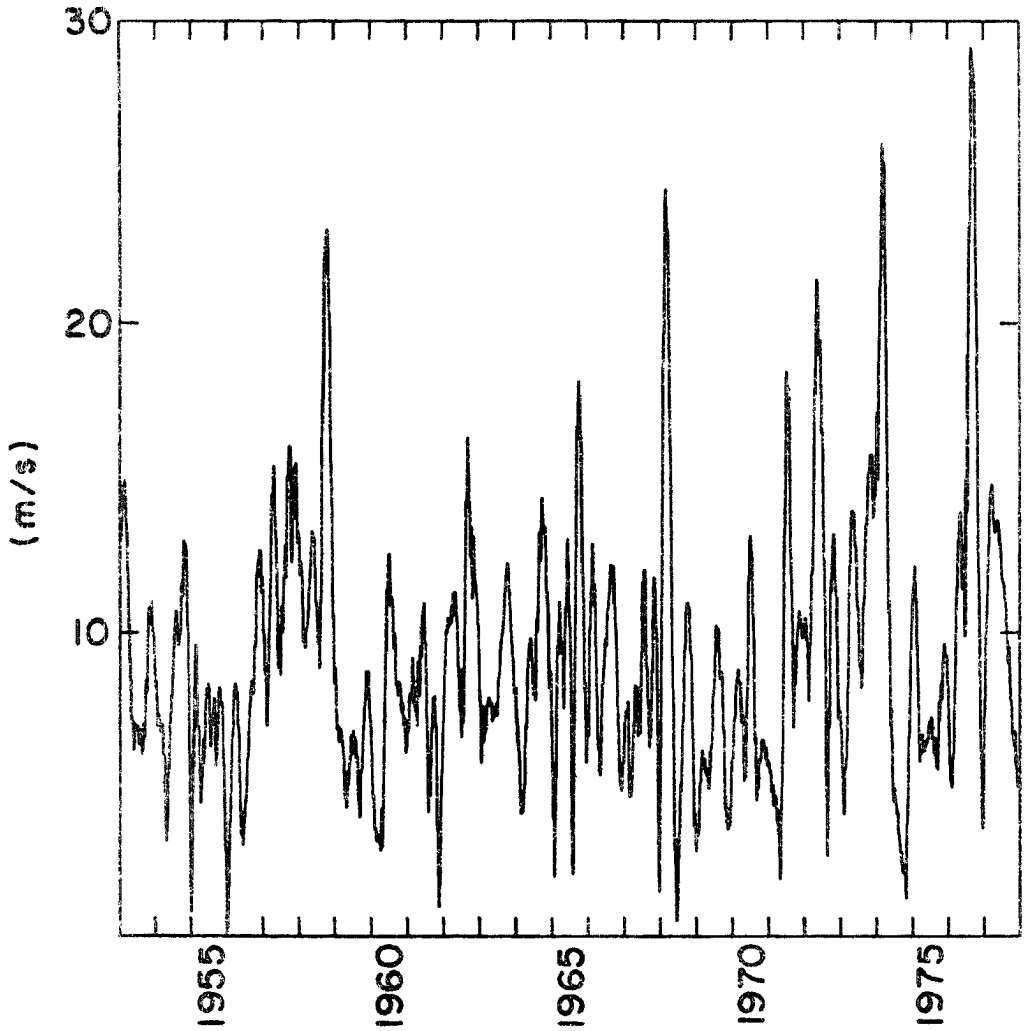

Fig. 5-13a. Amplitude estimate for Truk, 1953-1977.

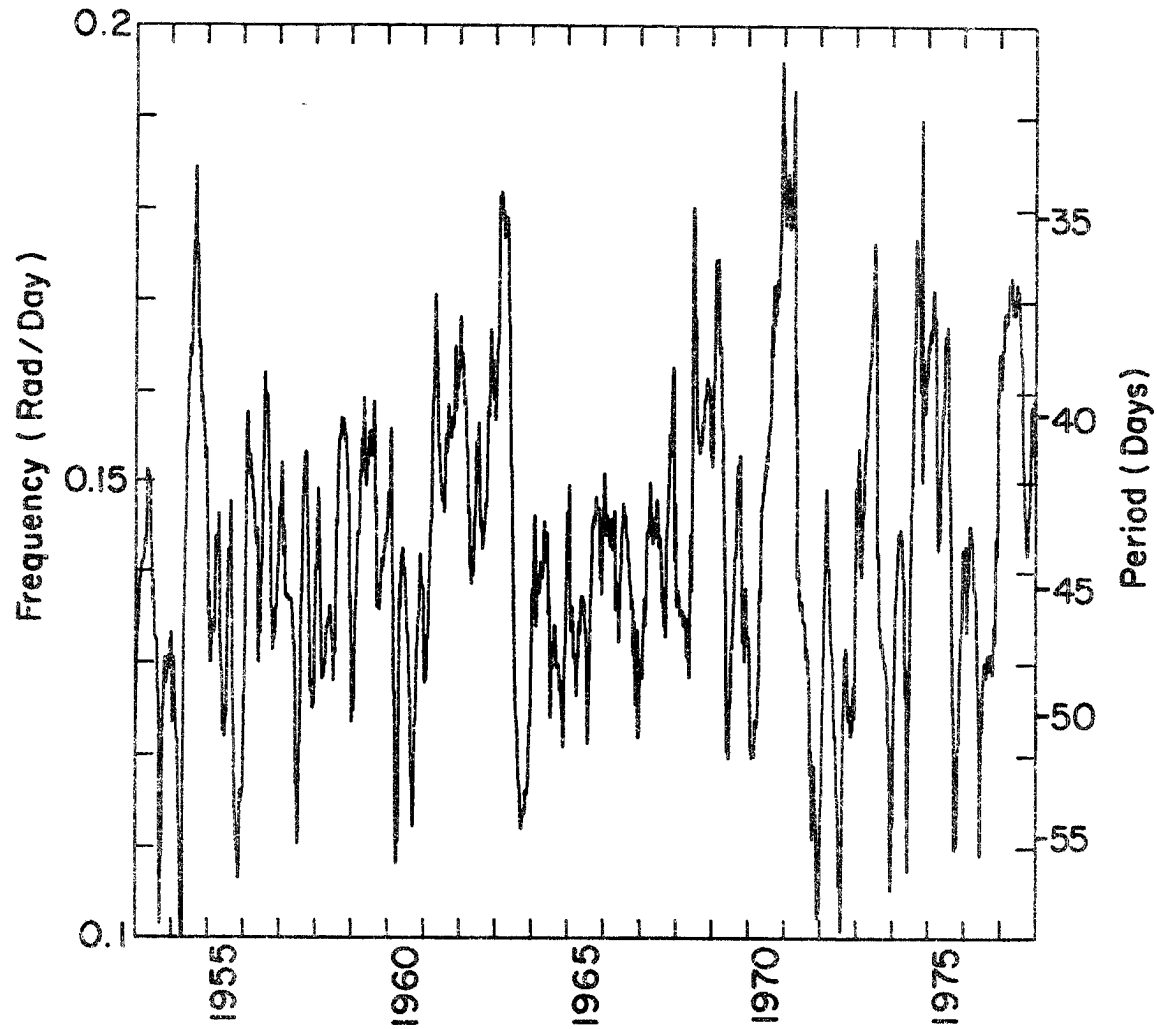

Fig. 5-13b. Frequency estimate for Truk, 1953-1977.

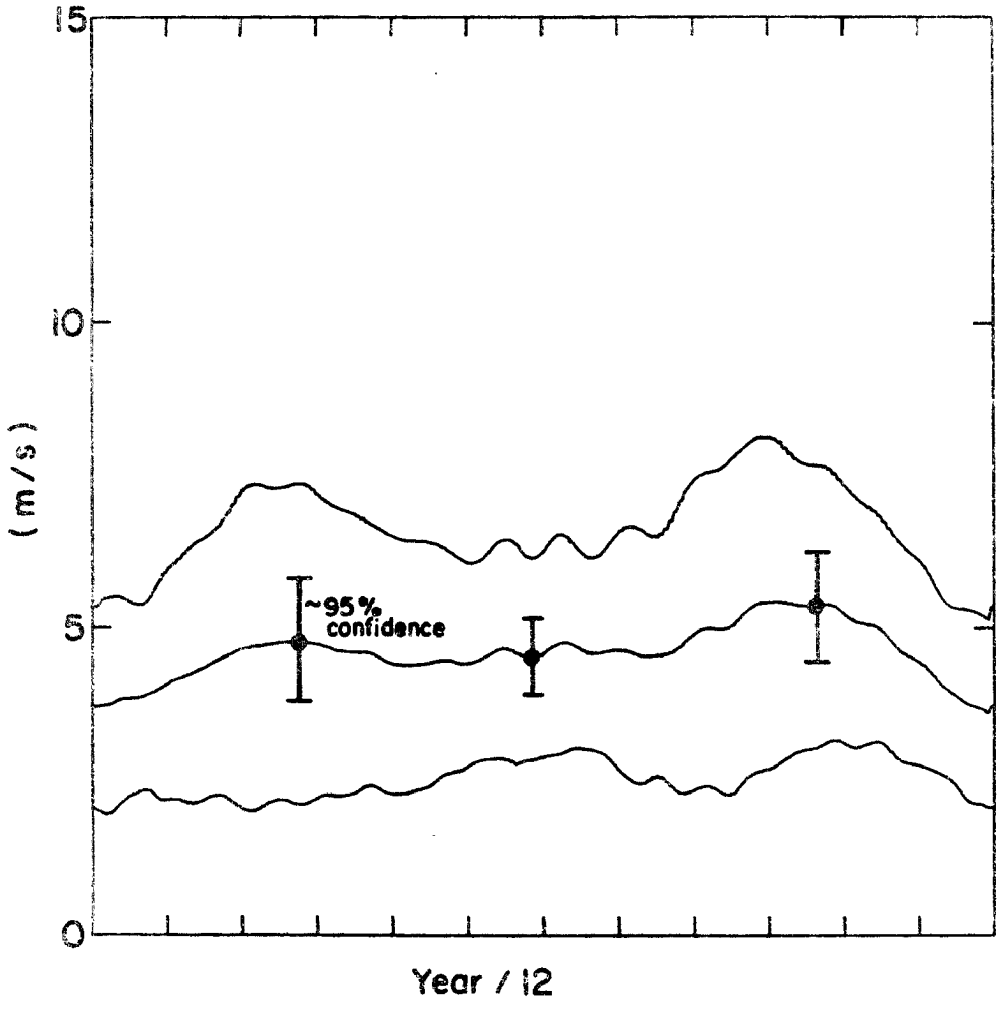

Fig. 5-14a. Mean seasonal cycle for Truk amplitude. Center line is mean, upper and lower lines are plus or minus one standard deviation. Error bars are 95% confidence limits on the mean.

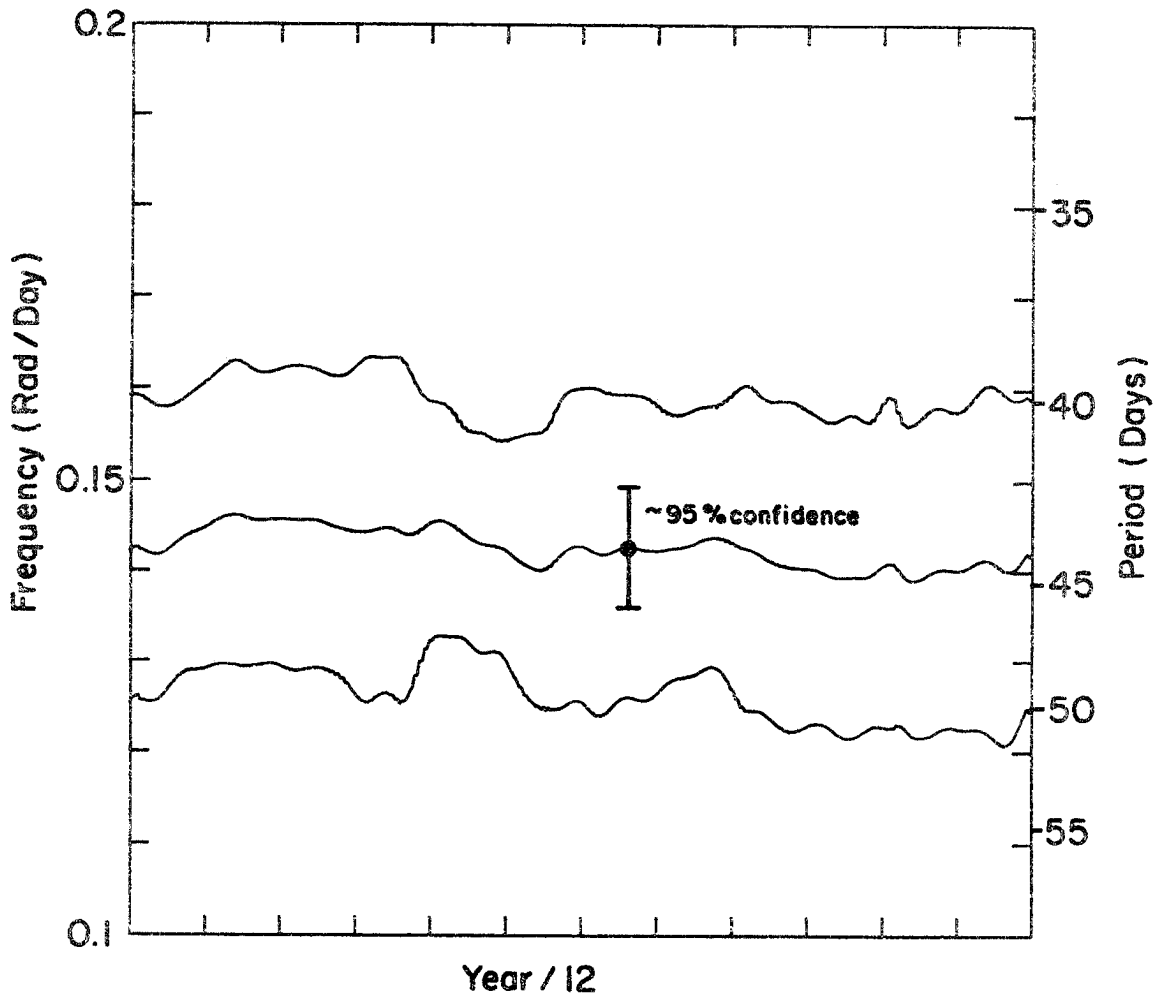

Fig. 5-14b. Mean seasonal cycle for Truk frequency.

These figures show that there appears to be a very small annual signal in the frequency and a semi-annual variation in the amplitude, although neither of these signals is significant at the 95% confidence level.

The frequency and amplitude of the tropical 40-50 day oscillation show large temporal variations; however, any regular seasonal cycle in the oscillation parameters appears to be very small. The presence of the oscillation during all parts of the year indicates that the 40-50 day variations exist independently of the monsoon circulations, although the relationship between the monsoon and the global oscillation remains undetermined. Of the possible sources for the time scales mentioned in the introduction, only the Doppler shifted wave mechanism proposed by Chang (1977) has an easily analyzed expected seasonal cycle. Chang suggested a wave with a Doppler shifted phase speed of ~15 m/s and a ground speed of ~10 m/s consistent with a 46 day period for the zonal wavenumber 1 wave. If we take an annual cycle amplitude for the Doppler shifting winds of 3 m/s following Newell et al. (1974), with the other oscillation parameters held constant, we would then expect to see a seasonal signal in the frequency of the oscillation varying the period from ~66 days to ~36 days corresponding to ground phase speeds of 7 m/s and 13 m/s respectively. Such a variation should be easily visible in the Truk data if it existed. The lack of a significant variation appears to indicate that the process proposed by Chang could not explain the time scale without the inclusion of some other physical process. It should be emphasized that the Chang description is still a viable explanation of the motion if there is external forcing which prescribes the 40-50 day period.

The expected seasonal dependence of the mechanism proposed by Webster (1983) and the time scale due to the Hadley cell advection are much less clear and will require further modeling work. It is hoped, however, that the description of the observed oscillation presented here will be of assistance in evaluating possible causes for the 40-50 day oscillation.

6. DISCUSSION OF RESULTS AND COMPARISON WITH OBSERVATIONS

In the introduction of this paper we discussed the observational history of the 40-50 day oscillation. It is perhaps surprising that a phenomenon which exhibits a near regular periodicity during all seasons and affects nearly every tropical meteorological parameter has eluded explanation for so long.

The first mechanism proposed as the basis of the oscillation time scale was presented by Chang (1977). Chang attempted to show that a possible cause of the time scale could be the time it takes a zonal wavenumber 1 Kelvin wave to travel around the planet when account had been taken of the effects of Doppler shifting by the mean zonal wind and the frictional effects of cumulus clouds. One consequence of this mechanism is that one would expect this time scale to change with season as the mean winds vary with the semi-annual and annual cycles. In Chapter 5 we present an analysis of the seasonal variation of the oscillation period and find it to change little, if any, with season. This would seem to cast doubt on the viability of this explanation for the period, although the mechanism which Chang proposed may well explain the eastward propagation of the observed motion if the oscillation period is externally forced.

Webster (1983) has proposed a mechanism by which fluctuations on this time scale in a simple zonally symmetric monsoon model result from the storage times for moisture in the soil. Webster does not say in

the paper if he feels that this mechanism could be responsible for the oscillation at times when there is not an active monsoon circulation and it seems unlikely that this effect could explain the phenomenon during the seasons when most of the precipitation occurs in oceanic areas.

In this work we present a third hypothesis, namely that the oscillation time scale results from the advective time scale associated with a basic state Hadley circulation. We investigate the effects of the Hadley circulation on equatorial wave modes in Chapter 3 and find that the thermal wind modes of the resting basic state now appear as modes which oscillate slowly. We also find that the modes which are the least damped tend to have periods in the 30-60 day range yielding a response spectrum to white noise forcing which has an enhanced amplitude at these frequencies. Comparisons with the observed spectra which appear in Chapter 5 still however show that the observed oscillation spectral peak is sharper than that which can be achieved with reasonable values of dissipation. To generate a peak as narrow as the observed spectra we would need a mode which is nearly neutral, probably requiring some energy source other than random forcing.

The presence of the response peak in the modes at periods of approximately 50 days can be explained in the relationship between the size and frequency of the "advective" modes. In general, approximately geostrophic modes which have lower frequencies tend to loose less energy to gravity waves when thermally forced than faster motions. When the advective effects are considered, however, the slower motions are forced to have large spatial scales. When the requirement that the mode contain some thermal gradient inside the domain is imposed so that

there will be an associated wind field, a low frequency limit is placed on the modes with u-wind fields at ~50 day periods. These modes have a single wind maximum between the equator and the poleward boundary. The poleward boundary is very dissipative, simulating the effects of the mid-latitude cyclones. The prognostic runs presented in Chapter 3 show that the least damped model motions tend to exhibit phase propagation of the zonal wind which is poleward and downward in agreement with the phase-amplitude eigenvector analysis of Anderson and Rosen (1983) This observational analysis is described in Chapter 1, and the primary result is reproduced here as Fig. 6-1.

One rather unsatisfying result of the calculation is that the model slow modes, due to their very small divergence, do not interact with cumulus cloud latent heat release as parameterized by a simple moisture convergence scheme (Stevens and Lindzen, 1978). This seems to indicate the necessity of a more elaborate parameterization, which is difficult to design in a strictly linear context, in order to appropriately describe and model the interaction between the slow modes and deep convection.

The inability of the model to couple the dynamical slow modes to cumulus convection represents a significant gap in an explanation of the 40-50 day oscillation. Simulation of the narrowness of the observed spectra requires either a coherent energy source or smaller than expected frictional dissipation. The energy source is probably supplied by a modulation of the tropical deep convection. This coupling may involve dynamical effects which we have not included - such as the effects of variations of tropical stability on the clouds - or it may result from physical processes such as the storage of soil moisture as described by Webster (1983).

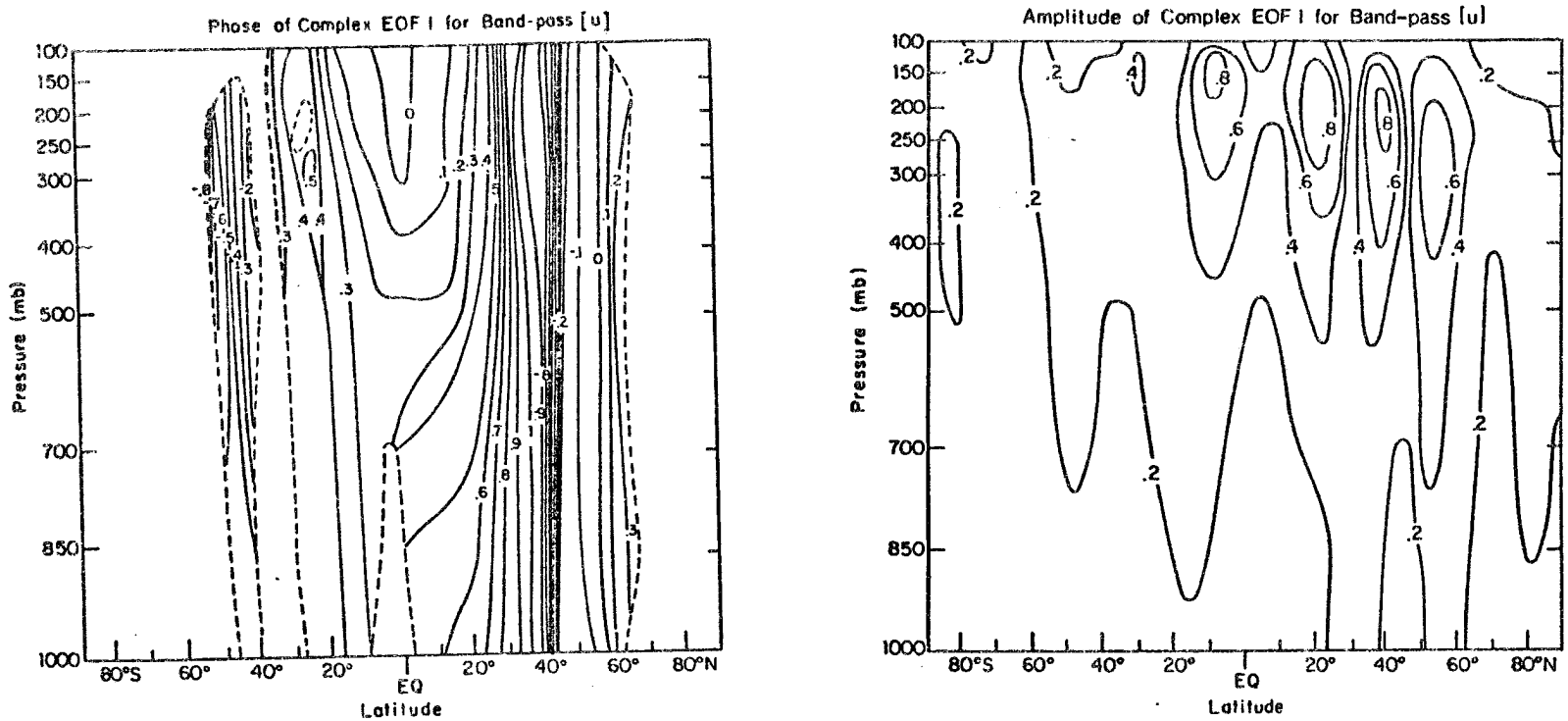

Fig. 6-1. Phase-amplitude analysis of the observed oscillation from Anderson and Rosen (1983). Phase convention is from -1 to 1 with propagation from smaller phase to larger.

In Chapter 4 we study the response of a tropical atmosphere to 40-50 day period thermal forcing with a number of models. The shallow water calculation of Yamagata and Hayashi (1984) was extended to a more general basic state and seems to give reasonably good agreement with observations for the oscillation structure in the tropical Pacific. The model indicates a geopotential response which is relatively smooth throughout the region and a u-wind field which exhibits a phase jump in the heating region at low latitudes. In Fig. 6-2 we present the results of an analysis of the surface pressure and the zonal wind fields by Madden and Julian (1972) which depicts these same features. These results indicate that the non-zonally symmetric part of the tropical u-response could be due to a spatially localized maximum in the heating field which could be modulated in some way by the zonally symmetric motions.

When the effects of the Hadley cell basic state are included in the forced calculation, the model shows a maximum u-wind response in the subtropical region east of the heating which propagates poleward and eastward. In Fig. 6-3 we present an analysis from Murakami et al. (1983) of the 40-day period, 200 mb zonal wind variations during the FGGE summer MONEX period. This analysis shows a zonal wind maximum in the northern hemisphere eastern Pacific subtropics with a well-defined eastward phase propagation, in agreement with the model results.

In Chapter 4 we also present the results of the zonally symmetric forced response for the Hadley cell basic state. This model response shows the formation of a wind anomaly which originates at the surface in the equatorial regions and then propagates poleward and eventually

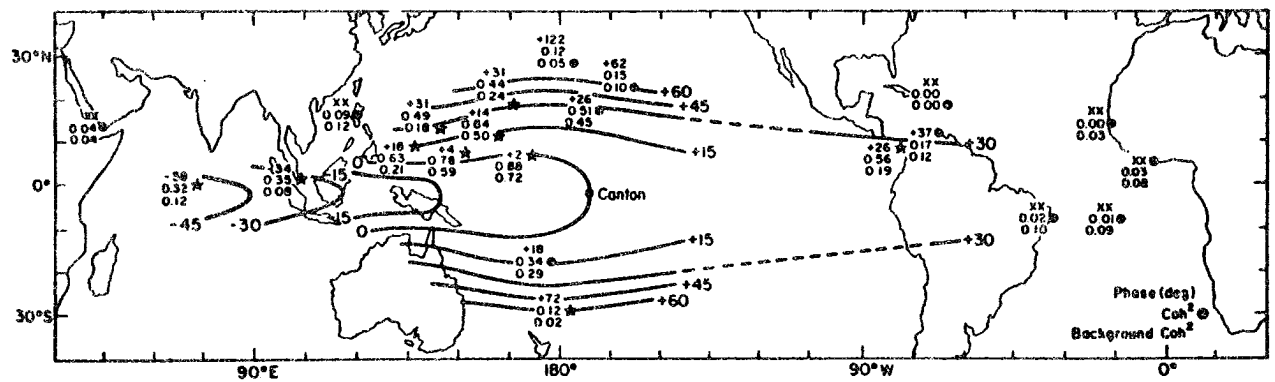

Fig. 6-2a. Mean phase angles, coherence-squares, and background coherence-squares for approximately the 36-50 day period range of cross spectra between all stations and Canton. The plotting model is given in lower right-hand corner. Positive phase angles at a station means the Canton series leads that of the station. Stations indicated by a star have coherence-squares above the background at the 95% level. Mean coherence-squares at Shemya (52°43'N, 174°6'E) and Campbell I (52°33'S, 169°9'E) (not shown) are 0.08 and 0.02, respectively. Both are below their average background coherence-squares (from Madden and Julian, 1972).

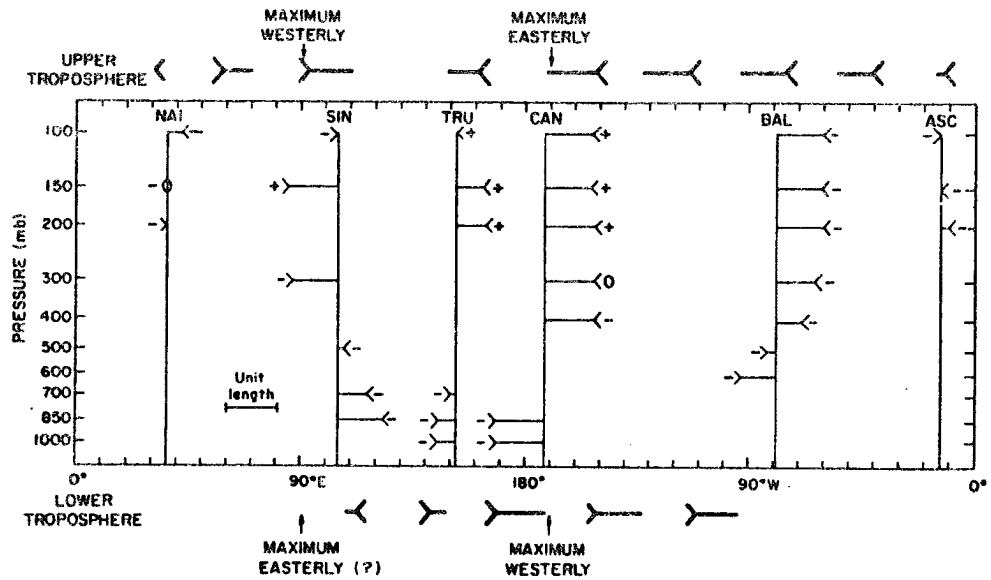

Fig. 6-2b. Zonal wind oscillation in the equatorial plane at the time when the station pressure is a maximum at Canton. The unit length represents the maximum excursion at each location. The +, -, or 0 at the tail of each wind arrow represents the sign of the instantaneous local change of the zonal wind. Arrows are plotted only at levels whose coherence squares are above their background coherence square, and whose spectra indicate a peak. Heavy arrows at the top and bottom represent a schematic of the upper and lower tropospheric wind disturbance that is consistent with the plotted wind arrows and that will satisfy the local changes if it propagates eastward (from Madden and Julian, 1972).

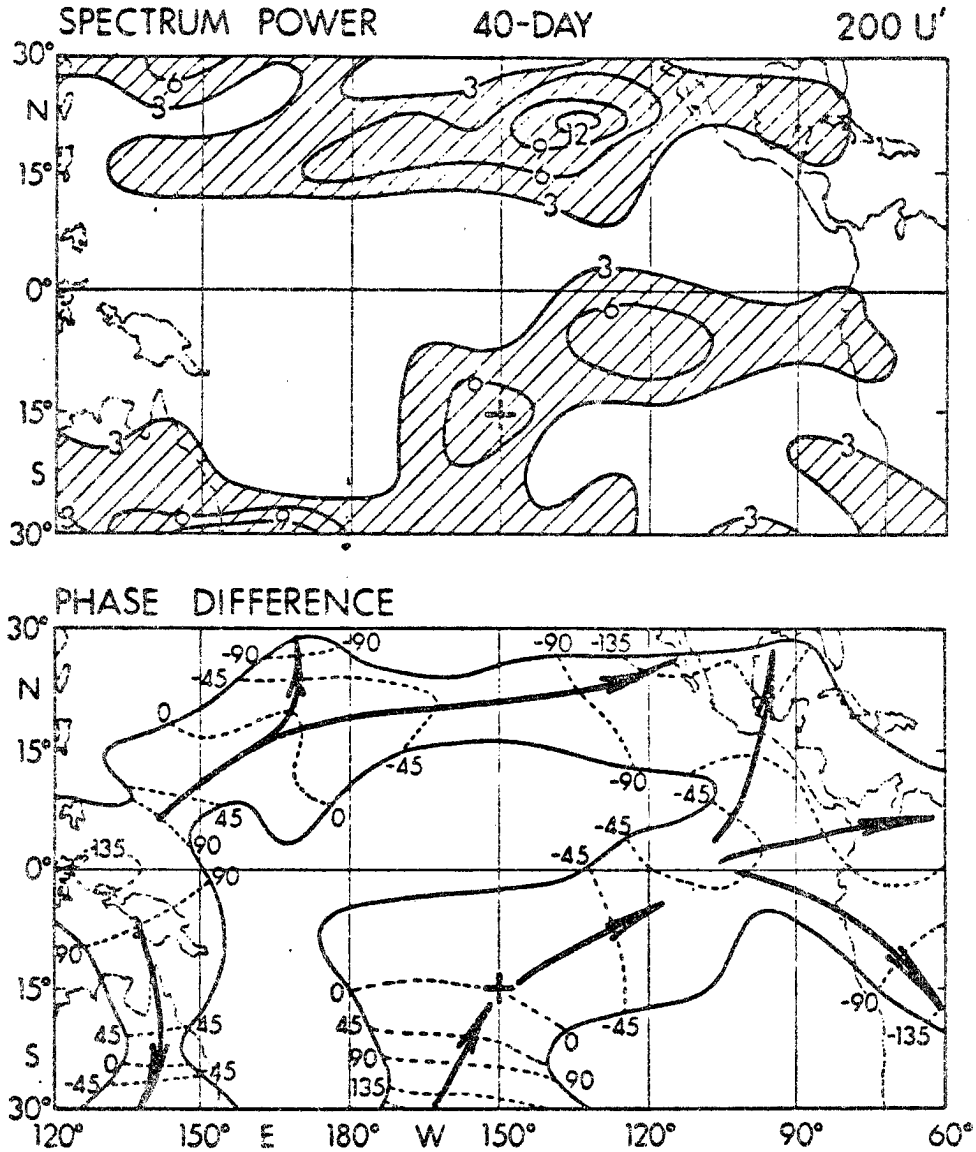

Fig. 6-3. Observed oscillation phase and amplitude for 200 mb u-winds (from Murakami et al., 1983).

downward under the influence of the Hadley circulation. This representation is in reasonable agreement with the Anderson and Rosen results for the region poleward of 15° North; however, the Anderson and Rosen results do not show the upward vertical propagation of the equatorial anomaly or the strong lower tropospheric winds. Observations by Murakami et al. (1983) of a partial zonal average taken over the monsoon region (60°E to 160°E), which is reproduced as Fig. 6-4, show a sequence almost exactly the same as the model forced motion during the summer monsoon. These results suggest that this feature of the oscillation may only occur in the regions where latent heat release is occurring.

An extremely interesting result of the forced symmetric calculation is that at the time of maximum heating the perturbation temperature field is such that it will tend to destabilize the troposphere. Thus the possibility exists that this destabilization may be the mechanism which gives size to the increased convective heating and provides the oscillation energy source. This effect is very difficult to parameterize in a purely linear model; however, in a non-linear, zonally symmetric model which uses a convective adjustment cumulus scheme which is sensitive to the local stability, Goswami and Shukla (1984) report similar low frequency oscillations which appear only when moisture is included.

In Chapter 5 we present an analysis of the "seasonality" of the observed oscillation. One result, which is mentioned above, is that the oscillation frequency appears to vary little, if any, with season. A second result is that the oscillation measured at Truk is certainly a year-round phenomenon, and there is no evidence that the oscillation is

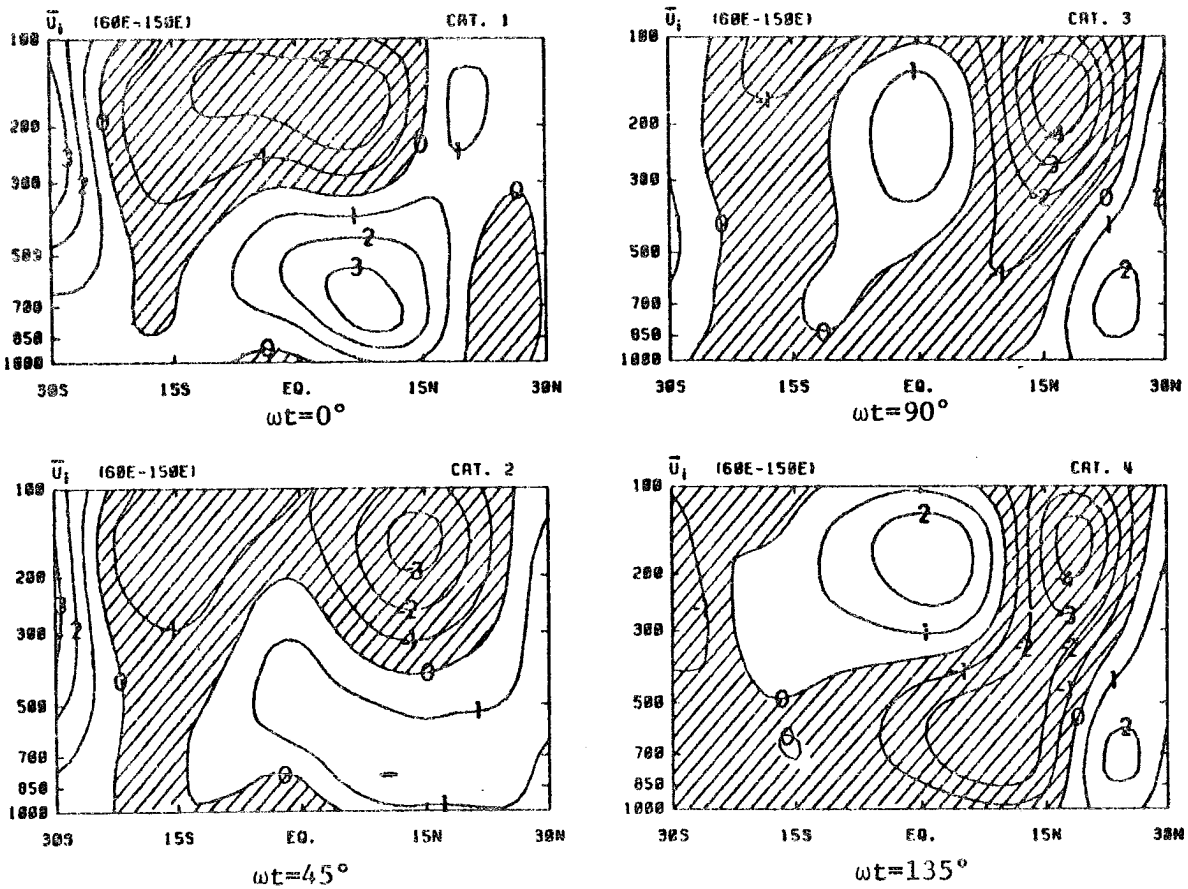

Fig. 6-4. Latitude-height structure of partial zonal average (60°E to 160°E) u-wind field (from Murakami et al, 1983).

stronger during the monsoon periods; in fact the oscillation amplitudes appear to be maximum during the equinoxial periods. Based on their study of the FGGE summer monsoon experiment, Murakami et al. state that "the monsoon region represents the major energy source for 40-50 day perturbations". The observations of the temporal variation indicate that while this may be true during the summer monsoon, the oscillation must have some other energy source during the seasons that the monsoon is not active. The results of this study suggest that the oscillation may be a natural variation of a direct Hadley-type circulation. During an active monsoon, when that region represents the major source of heating the motion could be due to a modulation of a monsoon circulation. When the monsoons are inactive this variation may result from a modulation of the other Hadley cell regions, particularly the west Pacific ITCZ.

In this study we have limited ourselves to the very simplest possible model which contains the effects of a Hadley cell type mean circulation. Important future work will involve considering the case of a Hadley cell which is not equatorially symmetric and the effects of the non-zonally symmetric "Walker" and monsoon circulations on the perturbation modes. In addition a full understanding of the energy source for the 40-50 day motions will not be possible until a better representation of the interactions between the large scale motions and deep convection is included, presumably through the solution of a non-linear system.

REFERENCES

Anderson, J.R., and R.D.Rosen, 1983: The latitude-height structure of 40-50 day variations in atmospheric angular momentum. J. Atmos. Sci., 40, 1584-1591.

Asselin, R.A., 1972: Frequency filter for time integrations. Mon. Wea. Rev., 100, 487-490.

Blackman, R.B., and J.W. Tukey, 1959: The Measurement of Power Spectra. Dover, 190 pp.

Chang, C.P., 1977: Viscous internal gravity waves and low-frequency oscillations in the tropics. J. Atmos. Sci., 38, 2254-2364.

Dunkerton, T.J., 1981: On the inertial stability of the equatorial middle atmosphere. J. Atmos. Sci., 38, 2354-2364.

Gill, A.E., 1980: Some simple solutions for heat induced tropical circulations, Quart. J. Roy. Meteor. Soc., 106, 447-462.

Goswami, B.N. and J. Shukla, 1984: Quasi-periodic oscillations in a symmetric general circulation model. J. Atmos. Sci., 41, 20-37.

Julian, P.R. and R.A. Madden, 1981: Comments on a paper by T. Yasumari. J. Meteor. Soc. Japan, 59, 435-437.

Kay, S.M., and S.L. Marple, Jr., 1981: Spectrum analysis - a modern perspective. Proc. of the IEEE, 69, 1380-1419.

Krishnamurti, T.N., and D. Subrahmanyan, 1982: The 30-50 day mode at 850 mb during MONEX. J. Atmos. Sci., 39, 2088-2095.

Langely, R.B., R.W. King, I.I. Shapiro, R.D. Rosen, and D.A. Salstein, 1981: Atmospheric angular momentum and the length of day: a common fluctuation with a period near 50 days. Nature, 294, 730-732.

Lindzen, R.S., 1967: Planetary waves on beta-planes. Mon. Wea. Rev., 95, 441-451.

Machenhaur, B. and E. Rasmussen, 1972: On the representation of the spectral hydrodynamical equation by a transform method. Rep. #4, Institut for Teoretisk Meteorolgi, Kobenhavens, Denmark.

Madden, R.A. and P.R. Julian, 1971: Detection of a 40-50 day oscillation in the zonal wind in the tropical Pacific. J. Atmos. Sci., 28, 702-708.

Madden, R.A. and P.R. Julian, 1972: Description of global-scale circulation cells in the tropics with a 40-50 day period. J. Atmos. Sci., 29, 1109-1123.

Matsuno, T., 1966: Quasi-geostrophic motions in the equatorial area. J. Meteor. Soc. Japan, 44, 24-42.

McWilliams, J.C., 1980: An application of equivalent modons to atmospheric blocking. Dyn. Atmos. Oceans, 5, 43-66.

Murakami, T., T. Nakazawa, and J. He, 1983: 40-50 day oscillations during the northern hemisphere summer. University of Hawaii Meteorological publication UHMET 83-02.

Newell, R.E., J.W. Kidson, D.G. Vincent, and G.J. Boer, 1974: The General Circulation of the Tropical Atmosphere and Interactions with Extratropical Latitudes, Volume 2. The MIT press, 371 pp.

Oppenheim, A.V., and R.W. Schafer, 1975: Digital Signal Processing. Prentice-Hall, 585 pp.

Orzag, S.A., 1970: Transform method for the calculation of vector-coupled sumes. J. Atmos. Sci., 27, 800-895.

Papoulis, A., 1973: Minimum-bias windows for high-resolution spectral estimates. IEEE Trans. Inform. Theory, IT-19, 9-12.

Parker, D.E., 1973: Equatorial Kelvin waves at 100 millibars. Quart. J. Roy. Meteor. Soc., 99, 116-129.

Rosen, R.D. and P.A. Salstein, 1983: Variations in atmospheric angular momentum on global and regional scales and the length of day. J. Geophys. Res., 88, 5451-5470.

Schneider, E.K., and R.S. Lindze, 1976: A discussion of the parameterization of momentum exchange by cumulus convection. J. Geophys. Res., 81, 3158-3160.

Silva Dias, M.F., 1979: Linear spectral model of tropical mesoscale systems. Ph.D. Dissertation, Colorado State University.

Stevens, D.E., 1983: On symmetric stability and instability of zonal mean flows near the equator. J. Atmos. Sci., 40, 882-893.

Stevens, D.E., R.S. Lindzen, and L.J. Shapiro, 1977: A new model of tropical waves incorporating momentum mixing by cumulus convection. Dyn. Atm. Oceans, 1, 365-425.

Stevens, D.E., and R.S. Lindzen, 1978: Tropical wave-CISK with a moisture budget and cumulus friction. J. Atmos. Sci., 35, 940-961.

Stevens, D.E. and G.H. White, 1979: Comments on "Viscous internal gravity waves and low-frequency oscillations in the tropics". J. Atmos. Sci., 36, 545-546.

Webster, P.J., 1983: Mechanisms of low-frequency variability: Surface hydrological effects. J. Atmos. Sci., 40, 2110-2124.

Weickman, K.M., 1983: Intraseasonal circulation and outgoing longwave radiation modes during northern hemisphere winter. Mon. Wea. Rev., 111, 1838-1858.

Yamagata, and Hayashi, 1984: A simple diagnostic model for the 30-50 day oscillation in the tropics. unpublished manuscript

Yasunari, T., 1980: A quasi-stationary appearance of 30 to 40 day period in the cloudiness fluctuations during the summer monsoon over India. J. Meteor. Soc. Japan, 58, 225-229.

APPENDIX I

LIST OF SYMBOLS

c_p specific heat of air at constant pressure

c_v specific heat of air at constant volume

F_{cx} contribution of cumulus momentum flux to x-momentum equation

F_{cy} contribution of cumulus momentum flux to y-momentum equation

g acceleration due to gravity

M_c vertical mass flux by cumulus clouds

p pressure departure from reference

$\tilde{p}$ reference pressure

Q Heat source due to radiation and condensation

u westerly wind

v southerly wind

w vertical wind

α Rayleigh friction coefficient

β y-derivative of Coriolis parameter

γ Newtonian cooling coefficient

θ potential temperature departure from reference

$\tilde{\theta}$ reference potential temperature

μ vertical mixing diffusivity

$\tilde{\rho}$ reference density

APPENDIX II

BAND-PASS FILTER DESIGN

The band-pass filter used in Chapter 5 is designed using the frequency sampling technique described by Oppenheim and Schaffer (1975). To design a filter using this technique one first chooses an impulse response length for the filter and then assigns an amplitude for each Fourier harmonic of the window defined by this length. For a band-pass filter we set the amplitude of the stop-band harmonics to 0 and the value of the pass-band harmonics to 1. To control the amplitude of the filter side-lobes we also include one transition harmonic on each side of the pass-band. For this filter the pass-band consists of window harmonics 3, 4, and 5 and the transition samples 2 and 6 are given the value 0.3409 which tends to produce flat side-lobes. This yields an impulse response given by

$$h(z) = \frac{1}{88}[\cos 3k\tau + \cos 4k\tau + \cos 5k\tau + 0.3409(\cos 2k\tau + \cos 6k\tau)] \quad \Big| \quad |\tau| \leq 88,$$

$$h(z) = 0 \text{ when } |\tau| > 88$$

$$k = \pi/89.$$

The frequency response of this filter is given by the continuous Fourier transform of h(z) and is plotted in Fig. 5-2. The frequency response has a flat (± 0.5 dB) pass-band and good (<-30 dB) side-lobe control.